432 P. Duangsuwan et al.

reticular fibers appeared as networks surrounding haemal sinuses and lymphoid tubules. The size of each reticular fiber was about 100–130 nm.

### Immunolabelling with antibodies against cytoskeletal proteins

Cytokeratin and vimentin are cytoskeletal proteins which are specific for epithelial [6] and mesodermal [7] cells, respectively. Hence, the distributions of cytokeratin and vimentin were used as markers for the two types of cells that may come together to constitute the wall of the tubules. Cytokeratin was not observed in any cell type of the lymphoid organ (Fig. 4C). In contrast, vimentin was localized as a reddish reaction product due to AEC, in the cytoplasm of stromal cells which were located in the middle layer of lymphoid tubules (Fig. 4D-F), and in some interstitial cells around haemal sinuses (Fig. 4D, inset). There was no staining in the endothelial and capsular cells in the lymphoid tubule. The negative control experiment using normal goat serum in place of the primary antibodies did not show any immunostaining (Fig. 4B). Immunostaining for cytokeratin and vimentin was not detected in haemocytes within the tubular (Fig. 4B) wall or in haemolymph smears (Fig. 4A).

### Visualization of the three dimensional structure of the vasculature in lymphoid organ

The three dimensional structure of the vascularization in the lymphoid organ was displayed by vascular corrosion cast and viewed by scanning electron microscopy (Fig. 5A-D). The two aorta arose anteriorly from the heart and each divided into subgastric and ophthalmic arteries (Fig. 5A). Each subgastric artery was further branched 4-5 times to form vascular plexuses in the lymphoid organ (Fig. 5B). Eventually, subgastric branches formed the highly convoluted and blind-ending terminal capillaries (Fig. 5C). Each capillary formed the lumen of a lymphoid tubule around which fixed and migratory cells form a cuff-like wall. This view was confirmed by the SEM micrograph of the cast whose soft tissues were not removed (Fig. 5D) and where lymphoid tubules exhibited a highly convoluted pattern matching the vascular network. However, the tubular wall was much thicker and not smooth as those appearing in the vascular cast (Fig. 5C). When the whole mounts of the lymphoid organ stained with anti-vimentin were viewed by confocal laser microscopy, the stromal cells that form part of the tubular wall showed an intense green fluorescent staining. This helped to trace the outline and branching pattern of the highly convoluted lymphoid tubules, and supports the notion that the lymphoid tubules were actually terminal branches of blood vessels (Fig. 5E, F).

### Discussion

The structural organizations of lymphoid organs of penaeid shrimp have been studied by many authors, i.e., in *P. orientalis* by Oka [1], in *S. ingentis* by Martin et al. [2], and in *Penaeus stylirostris* by Bell and Lightner [4]. These authors

described the lymphoid organ as being made up of lymphoid tubules which are the basic unit. It is believed that this organ plays a very important role against infection especially by viruses, as it is essentially a filtering organ that clears the haemolymph of viral particles [8-10]. However, it has not been made clear how lymphoid tubules are structurally related to each other, and how they appear in three dimension. This study is the first report that elucidates these points in the normal lymphoid organ of P. monodon that tested negative from WSSV and YHV which are the two major infections. The histology of these lymphoid organs was also judged to be normal. The detailed examination of the vascular cast of the lymphoid organ by SEM indicated clearly that this organ is actually the terminal part of subgastric arteries which branch off from the anterior aorta. The terminal branches of the subgastric artery are actually the blind-ending capillaries, each with a thick wall comprising endothelial cells, stromal cells and capsular cells which are the "fixed" cells. Together they formed the cellular scaffold that defined the structure of the lymphoid tubule, whereas haemocytes penetrated the endothelium to occupy the spaces between the stromal cells. In addition to these cellular components, elaborate connective tissue scaffolds were observed in and around lymphoid tubules. These scaffolds were formed by an extensive network of type 1 fibers which were embedded in an extracellular matrix (ECM). Both structures were PAS positive which implied that both were rich in carbohydrate content. This fiber-ECM network formed a thick layer at the capsular side of each tubule, where they appeared as "basket-like" in SEM. They, together with capsular cells, form a strong capsule around each tubule. From this capsular layer the fiber-ECM sheets permeated throughout the intercellular space in the tubular wall, and became less prominent only under the endothelial layer. The biochemical nature of this fiber-ECM structure needs to be studied further. However, by comparing with the vertebrate ECM, these combined structures appeared similar to the component of the basement membrane [11]. Moreover, the fibrous components appeared similar to protein fibers embedded in the basement membrane [11]. Interestingly, lymphoid tubules and haemal sinuses are circumscribed at their peripheries by argyrophilic filaments, whose affinity to silver staining and appearance are very much like "reticular" fibers in the vertebrate connective tissue [12]. In contrast, type 1 fiber-ECM components are not prevalent around the haemal sinuses and in the intertubular areas. Thus, we believe that this type 2 fiber (or reticular fibers) plays a major role in holding various structures of the lymphoid organ, particularly the lymphoid tubules, together.

Cytokeratin was not detected in any kind of cell, whereas vimentin was present in stromal cells but not in endothelial cells. Based on the vertebrate model of connective tissue, it is plausible that stromal cells, which are the "fixed" cells, could be derived from mesodermal origin like fibroblasts [13]. They may also act like fibroblasts in the sense that they provide the supporting scaffold for the lymphoid tubules, and they may even be responsible for the synthesis of type 1 fiber-ECM components, though this needs to be proven in further studies. Similarly, endothelial cells of lymphoid tubules, like endothelial cells of vertebrate capillaries and larger blood vessels, do not have cytokeratin [14,15].

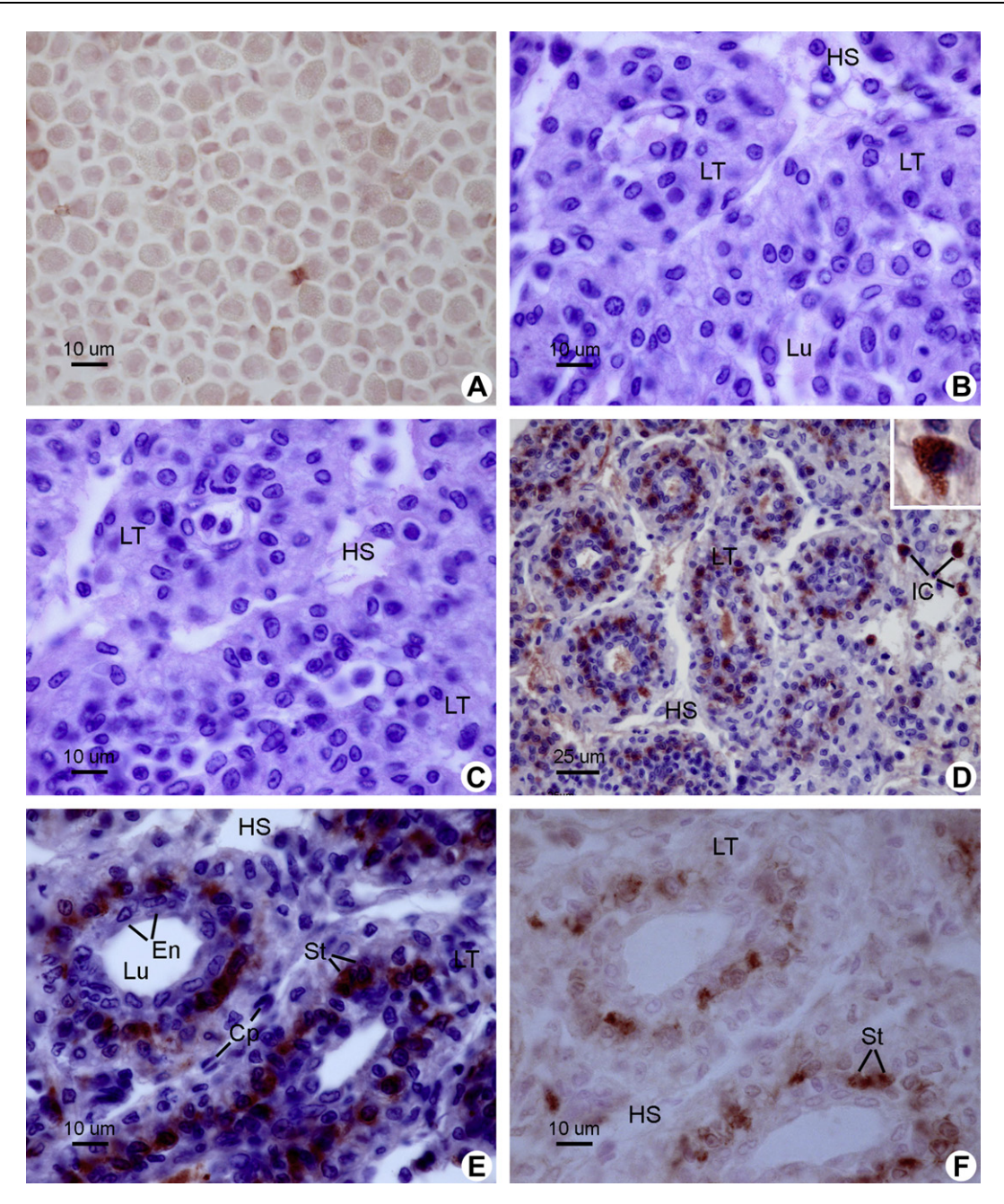


Figure 4 Light micrographs of haemolymph smear and the cross sections of normal lymphoid organ stained by immunoperoxidase technique using monoclonal antibodies (MoAb) against cytokeratin and vimentin as probes, and counterstained with Mayer's hematoxylin. (A) High magnification micrograph of haemolymph smear, showing no immunostaining in any type of haemocytes. (B) The control section of the normal lymphoid organ where the primary antibodies were omitted, showing no immunostaining while only Mayer's hematoxylin counterstaining was observed in the lymphoid tubules (LT) and haemal sinuses (HS). Lu: lumen. (C) High magnification micrograph of a normal lymphoid organ section stained by immunoperoxidase technique using MoAb against cytokeratin as a probe, showing no immunostaining while only Mayer's hematoxylin counterstaining was observed in the lymphoid tubules (LT) and haemal sinuses (HS). (D—F) Medium and high magnification micrographs of normal lymphoid organ sections stained by the immunoperoxidase technique using MoAb against vimentin as a probe and counterstained with Mayer's hematoxylin (in D and E) and uncounterstained (F), showing intense reddish immunostaining in the stromal cells (St) which were located in the middle layer of lymphoid tubules (LT), and some interstitial (IC) cells embedded around haemal sinuses (HS) (inset in D) were also stained. En: endothelial cell, Cp: capsular cell, Lu: lumen.

However, they have bundles of fine filamentous structure in their peripheral cytoplasm when viewed under TEM (data not shown), which could be actin-based microfilaments. Haemocytes, in both haemolymph smears and in sections of lymphoid tubules, do not exhibit either type of cytoskeletal filaments.

Haemal sinuses were described in penaeid shrimp's lymphoid organ by Oka [1], and Bell and Lightner [4], and

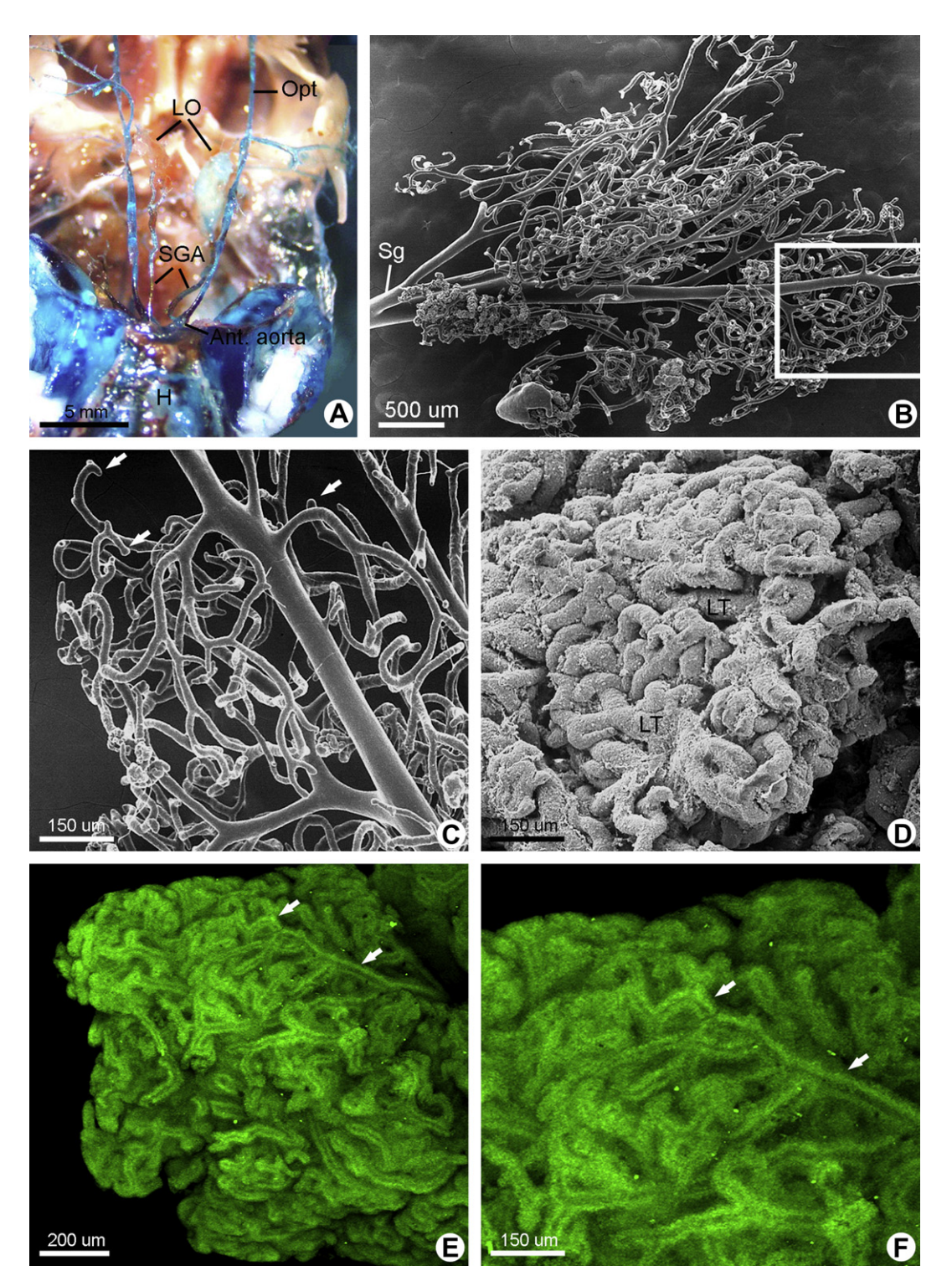


Figure 5 Light, SEM and confocal micrographs of subgastric artery which branched to form vascular plexus in the normal lymphoid organ of *Penaeus monodon*. (A) Overall view of a vascular cast of the cephalothorax region: anterior aorta (Ant. aorta) arose from the heart (H) and each divided into the ophthalmic (Opt) artery which gave off branches and terminated in eyestalk, and subgastric artery (SGA) which further branched to form vascular plexus in the lymphoid organ (LO). (B) Low and (C) medium magnification SEM micrograph taken from the boxed area in B of the normal lymphoid organ prepared by vascular cast technique, and viewed by SEM, showing the subgastric artery branched into highly convoluted and blind-ending terminal capillaries (arrows in C). Each capillary was the lumen of a lymphoid tubule which was surrounded by haemocytes and other cells aggregating to form a cuff-like wall. (D) Medium magnification SEM micrograph of the normal lymphoid organ, showing a large lymphoid tubule (LT) with thick wall branching into smaller highly convoluted tubules. (E, F) Low and medium magnification micrographs of the normal lymphoid organ prepared by staining the organ with anti-vimentin and observed by a confocal laser scanning microscope, showing intense fluorescence staining of stromal cells in the tubular wall (arrows), which could help to trace the outline and branching pattern of the highly convoluted lymphoid tubules comparable to the pattern in C.

these authors believed that they are the site where haemolymph is drained back to the circulation, and that they are actually the "open" part of the shrimp's open circulation. In addition to haemal sinuses we also observed the presence of an extensive branching system of "antennal tubules". This is a network of tubular structures that form part of the capsule of the lymphoid organs. They also branch extensively and permeate into the spaces between lymphoid tubules, sometimes, in close proximity to haemal sinuses. The antennal tubule is lined by cuboidal cells whose characteristics are quite similar to those found in the tubules of the antennal gland [4]. The aggregate of these tubules is observed at the antennal pole of the lymphoid organ (Fig. 1B). Since the lymphoid organ is physically quite close to the antennal gland, it is possible that this "tuft" of antennal tubules may be connected with the antennal gland. Since the latter is equivalent to the vertebrate kidney [16,17], it is plausible that these lymphoid associated-antennal tubules may function in controlling the electrolyte balance, osmotic regulation and disposal of wastes.

Taken together we agree with the "filtering function" of the lymphoid organ as proposed earlier by Oka [1], Bell and Lightner [4], and Kondo et al. [18]. However, we would like to propose more details to this concept as follows. The lymphoid tubules are essentially the blind-ending capillaries of the subgastric artery, where the haemolymph (blood) of the shrimp passes into, much like the blood circulating into the spleen of mammals. Once in the capillaries (lymphoid tubule lumens), the blood percolates through the endothelial cells and the tubular walls. Under normal situations, some haemocytes also routinely pass into the tubular wall and then traverse into the haemal sinuses with the filtrate. Judging from the extensive network of haemal sinuses, there must be a large volume of haemolymph flowing through the lymphoid organ at any one time. Because of this large amount of flow, part of this filtrate may pass into the antennal tubules which may exercise "homeostatic control" on the haemolymph filtered through the lymphoid organ. In other words, the lymphoid organ acts as a true filtering organ for the purposes of filtering and elimination of foreign materials and infectious agents from the haemolymph as well as for homeostatic improvement of the haemolymph filtrate.

### **Acknowledgements**

This research was supported by the Commission on Higher Education (PhD. Scholarship to P. Duangsuwan and Research Group Grant to P. Sobhon) and TRF (Senior Research Scholar Fellowship to P. Sobhon).

### References

[1] Oka M. Studies on *Penaeus orientalis* Kishinouye-VIII structure of the newly found lymphoid organ. Bull Jpn Soc Sci Fish 1969; 35:245—50.

- [2] Martin GG, Hose JE, Kim JJ. Structure of hematopoietic nodules in the ridgeback prawn, Sicyonia ingentis: light and electron microscopic observations. J Morphol 1987; 192:193–204.
- [3] Van de Braak CBT, Botterblom MHA, Taverne N, van Muiswinkel WB, Rombout JHWM, van der Knaap WPW. The roles of haemocytes and the lymphoid organ in the clearance of injected *Vibrio* bacteria in *Penaeus monodon* shrimp. Fish Shellfish Immunol 2002;13:293—309.
- [4] Bell TA, Lightner DV. A handbook of normal penaeid shrimp histology. Baton Rouge: World Aquaculture Society; 1996. p. 14, 70–3.
- [5] Chunhabundit P, Somana R. Scanning electron microscopic study on pineal vascularization of the common tree shrew (*Tupaia glis*). J Pineal Res 1991;10:59–64.
- [6] Kummar S, Fogarasi M, Canova A, Mota A, Ciesielski T. Cytokeratin 7 and 20 staining for the diagnosis of lung and colorectal adenocarcinoma. Br J Cancer 2002;86:1884—7.
- [7] Prelle K, Holtz W, Osborn M. Immunocytochemical analysis of vimentin expression patterns in porcine embryos suggests mesodermal differentiation from day 9 after conception. Anat Histol Embryol 2001;30:339—44.
- [8] Anggraeni MS, Owens L. The haemocytic origin of lymphoid organ spheroid cells in the penaeid prawn *Penaeus monodon*. Dis Aquat Org 2000;40:85–92.
- [9] Hasson KW, Lightner DV, Mohney LL, Redman RM, White BM. Role of lymphoid organ spheroids in chronic Taura syndrome virus (TSV) infections in *Penaeus vannamei*. Dis Aquat Org 1999;38:93–105.
- [10] Kanobdee K, Soowannayan C, Flegel TW, Ubol S, Withyachumnarnkul B. Evidence for apoptosis correlated with mortality in the giant black tiger shrimp *Penaeus mono-don* infected with yellow head virus. Dis Aquat Org 2002;48: 79–90.
- [11] Brown B, Lindberg K, Reing J, Stolz DB, Badylak SF. The basement membrane components of biological scaffolds derived from extracellular matrix. Tissue Eng 2006;12:519—26.
- [12] Montes GS, Kriszt RM, Shigihara KM, Tokoro R, Mourao PAS, Junqueira LCU. Histochemical and morphological characterization of reticular fibers. Histochemistry 1980;65:131–41.
- [13] Salvatori G, Lattanzi L, Coletta M, Aguanno S, Vivarelli E, Kelly R, et al. Myogenic conversion of mammalian fibroblasts induced by differentiating muscle cells. J Cell Sci 1995;108: 2733–9.
- [14] Mcdouall RM, Yacoub M, Rose ML. Isolation, culture, and characterisation of MHC class II-positive microvascular endothelial cells from the human heart. Microvasc Res 1996;51:137–52.
- [15] Watanabe Y. Microfilaments and intermediate filaments in the fetal capillary endothelial cells of the human chorionic villi—ultrastructural and immunohistochemical study. Nippon Sanka Fujinka Gakkai Zasshi 1989;41:257—64.
- [16] Lin S, Liou C, Chen J. The role of the antennal glands in ion and body volume regulation of cannulated *Penaeus monodon* reared in various salinity conditions. Comp Biochem Physiol A 2000;127:121–9.
- [17] Johnson PT. A review of fixed phagocytic and pinocytotic cells of decapod crustaceans, with remarks on hemocytes. Dev Comp Immunol 1987;11:679—704.
- [18] Kondo M, Itami T, Takahashi Y, Fujii R, Tomonaga S. Structure and function of the lymphoid organ in the kuruma prawn. Dev Comp Immunol 1994;18(Suppl. 1):S109.



### Contents lists available at ScienceDirect

### Fish & Shellfish Immunology

journal homepage: www.elsevier.com/locate/fsi



## Changes in the histological organization and spheroid formation in lymphoid organ of *Penaeus monodon* infected with yellow head virus

Pornsawan Duangsuwan <sup>a,b</sup>, Yotsawan Tinikul <sup>a</sup>, Charoonroj Chotwiwatthanakun <sup>c,d</sup>, Rapeepun Vanichviriyakit <sup>a,d</sup>, Prasert Sobhon <sup>a,\*</sup>

- <sup>a</sup> Department of Anatomy, Faculty of Science, Mahidol University, Rama VI Road, Bangkok 10400, Thailand
- <sup>b</sup> Department of Anatomy, Faculty of Science, Prince of Songkla University, Songkhla 90112, Thailand
- <sup>c</sup> Department of Biochemistry, Faculty of Science, Mahidol University, Rama VI Road, Bangkok 10400, Thailand

### ARTICLE INFO

#### Article history: Received 7 February 2008 Received in revised form 30 July 2008 Accepted 16 August 2008 Available online 29 August 2008

Keywords: Penaeus monodon Lymphoid organ Yellow head virus Histopathology Lymphoid spheroid

#### ABSTRACT

The changes in the histological and three dimensional organizations of lymphoid organ and characteristics of lymphoid cells after chronic infection with yellow head virus (YHV) in *Penaeus monodon* were investigated. The vascular cast of infected lymphoid organ showed less branching and dramatically shortened terminal capillaries that formed the lymphoid tubules, and only large stumps of these lymphoid tubules remained. This might occur because the terminal ends of the tubules were damaged from YHV infection, as stromal cells and hemocytes in the LT wall were infected and formed foci that could give rise to lymphoid spheroids that broke away from the original lymphoid tubules. Histologically, there was a decrease of PAS-stained connective tissue materials in lymphoid spheroids as well as a decrease of stromal cells as marked by anti-vimentin antibody. This indicated that stromal cells together with type 1 fibers and associated extracellular matrix degenerated in lymphoid spheroids, while type 2 or reticular fibers proliferated and encapsulated the spheroids.

© 2008 Elsevier Ltd. All rights reserved.

### 1. Introduction

The lymphoid organ of penaeid shrimp functions as a hemolymph filter [1–3] and plays a central role in the immune response [4]. It is a major target organ of viral infection [5] and responsible for viral and bacterial clearance [4,6], and elimination of foreign substances from hemolymph [2,7]. Following infection by certain types of viruses, the lymphoid organ forms spheroids [8] which have been reported in infections by vacuolization virus (LOVV) [11], lymphoid parvo-like virus (LPV) [12], lymphoid organ virus (LOV) [13], rhabdovirus of penaeid shrimp (RPS) [14], yellow head virus (YHV) [15], and Taura syndrome virus (TSV) [8].

Hasson et al. [8] classified lymphoid spheroids of white shrimp, *Penaeus vannamei*, infected with Taura syndrome virus into three types. Type A, believed to be the earliest type to appear during the host-viral interaction, is characterized by the presence of lightly basophilic, homogeneous cell masses containing few or no necrotic cells or cell debris. Type B is believed to evolve from type A, but differs in being more basophilic, having higher number of necrotic cells and higher amount of cell debris, with few to moderate

amounts of cytoplasmic vacuoles. Type C is believed to evolve from type B, and becomes the terminal lymphoid spheroid, which is characterized by intensely basophilic masses containing degenerating cells with numerous cytoplasmic vacuoles and highly basophilic nuclei [8]. Despite their common occurrence following infection, their origin, mode of formation and relationship to lymphoid tubules still remain unclear. In this study, we have addressed these questions by observing the three dimensional and histopathological changes that occurred in the lymphoid organ of *P. monodon* chronically infected with yellow head virus (YHV) by light microscopy with special stainings, confocal laser scanning (CLSM), scanning electron microscopy (SEM) using vascular cast technique, and transmission (TEM) electron microscopy.

### 2. Materials and methods

### 2.1. Shrimps

Thirty wild caught fully mature *Penaeus monodon* ( $\sim$  100–150 g) were obtained from the Gulf of Thailand. The shrimps were screened for white spot syndrome virus (WSSV), Taura syndrome virus (TSV), infectious hypodermal and hematopoietic necrosis virus (IHHNV), hepatopancreatic parvovirus (HPV), and yellow head virus (YHV) infections by RT-PCR using the IQ 2000 detection

<sup>&</sup>lt;sup>d</sup> Center of Excellence for Shrimp Biotechnology, Faculty of Science, Mahidol University, Rama VI Road, Bangkok 10400, Thailand

<sup>\*</sup> Corresponding author. Tel.: +66 2 201 5406; fax: +66 2 354 7168.

E-mail address: scpso@mahidol.ac.th (P. Sobhon).

kit (Farming IntelliGene Technology Corporation, Taipei, Taiwan). Only shrimp that tested positive with YHV were selected and maintained in 300 L aquarium tanks filled with filtered sea water with continuous aeration at room temperature for at least 21 days. Eight surviving shrimps were considered as chronically infected with YHV and used in this study.

### 2.2. Nested-RT-PCR detection of YHV using IQ2000 kit

#### 2.2.1. RNA extraction

Shrimp pleopods were excised and homogenized in 1 ml of TRI<sup>TM</sup> reagent (Pacific Science, USA). Chloroform (200  $\mu$ l) was then added to the homogenate and the mixture was centrifuged to separate the insoluble materials at 12,000  $\times$  g for 10 min. The aqueous phase was collected and then 200  $\mu$ l of chilled isopropanol was added to precipitate RNA. The RNA pellet was collected by centrifugation at 12,000  $\times$  g for 10 min, washed with cold 75% (v/v) ethanol, dried and re-suspended in 20  $\mu$ l diethyl pyrocarbonate (DEPC)-treated water.

#### 2.2.2. Nested-RT-PCR

Two microliters (50 ng) of extracted shrimp RNA were added to RT-PCR reaction consisting of 7 µl of RT-PCR premix, 0.50 µl of IQzyme DNA polymerase, and  $0.5\,\mu l$  RT Enzyme Mix. The RT-PCR reaction profile consisted of reverse transcription at 42 °C for 30 min, denaturation at 94 °C for 2 min, 15 cycles of denaturation at 94  $^{\circ}\text{C}$  for 20 s, annealing at 62  $^{\circ}\text{C}$  for 20 s, and extension at 72 °C for 30 s. The reaction was then extended at 72 °C for additional 30 s. The nested-PCR was carried out by adding 15 µl of nested-PCR mixture consisting of 14 µl Nested PCR premix and 1 µl IQzyme DNA Polymerase to the total RT-PCR reaction mixture, then the nested-PCR was performed by 30 cycles of denaturation at 94 °C for 20 s, annealing at 62 °C for 20 s and extension at 72 °C for 30 s. The reaction was then extended for completion at 72 °C for 30 s. A positive control was performed with standard YHV RNA 2000 copies. To the nested-RT-PCR reaction, 5 μl of 6× DNA loading dye was added and mixed. Ten µl of the mixture was fractionated by using 1.5% agarose gel electrophoresis. The bands at 277 and/or 777 base pairs indicated YHV infection (Fig. 1).

### 2.3. Localization of YHV Gp116 in YHV-infected lymphoid organ

To confirm that the shrimp were infected with YHV, their lymphoid organs were removed and fixed with Davison's fixative overnight. Subsequently, the samples were conventionally processed and embedded in paraffin blocks. The tissue sections (6-µm thick) were blocked with 4% BSA and 10% normal goat serum in Tris buffered saline containing 0.1% Tween 20 (TBST) and then incubated with the monoclonal antibody to YHV envelope glycoprotein 116 (gp116) (a kind gift from Dr. Paisarn Sithigorngul, Faculty of Science, Srinakharinwirot University, Bangkok, Thailand) at dilution of 1:500 for overnight at 4 °C.

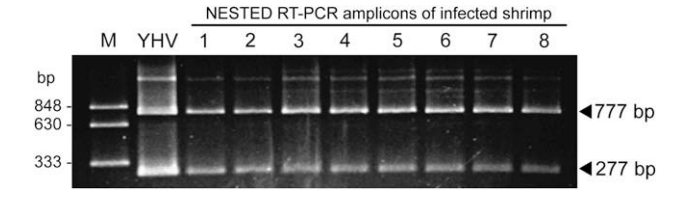


**Fig. 1.** Detection of YHV-infected shrimp used for the experiments: NESTED-RT-PCR detection of YHV from pleopods using IQ2000 detection kit. PCR amplicons at 277 and 777 bp indicated the specific YHV infection. Lane M: Standard DNA marker, Lane YHV: YHV positive control (2000 copies), lane 1–8; NESTED-RT-PCR product of the infected shrimp.

After washing, the sections were incubated with Alexa 594 conjugated goat anti-mouse IgG (Molecular Probe, Eugene, OR), at dilution 1:2000, for 1 h. The sections were then washed and observed under an Olympus FV1000 Laser Scanning Confocal Microscope (Fig. 2A–D). Exclusion of the primary antibody prior to incubation with secondary antibody was used as the negative control.

### 2.4. Reconstructing the three dimensional structure of the vascularization of lymphoid organ chronically infected with YHV

#### 2.4.1. Vascular cast of infected lymphoid organ

The modified method of Chunhabundit and Somana (1991) was used [16]. Briefly, vascular-corrosion casts of the subgastric arteries, which supply lymphoid organs of the shrimp were made by injecting the hearts with Batson's #17 Anatomical Corrosion Kit (Polysciences Inc., Warrington, PA). Soft tissues were removed by immersing in 40% sodium hydroxide for 24–48 h, followed by slow rinsing in running tap water for 6–8 h and washed in several changes of distilled water. The vascular casts were collected under a stereoscope, air-dried, coated with platinum and palladium in an ion sputtering apparatus, Hitachi E-120, before being observed under a Hitachi scanning electron microscope S-2500 set at the accelerating voltage of 15 kV.

### 2.4.2. Whole mount immunofluorescence for visualizing lymphoid tubules

Dissected lymphoid organs were fixed with 4% paraformaldehyde, dehydrated in ascending concentrations of ethanol (70–100%), permeabilized with Dent's solution (80% ethanol and 20% DMSO) and redehydrated in descending concentrations of ethanol (100–50%). Whole lymphoid organs were then incubated in monoclonal anti-vimentin antibody (Sigma Chemical Co., St. Louise, MO) at 4 °C for three days and Alexa 594 conjugated goat antimouse IgG (Zymed Laboratories, San Francisco, CA) for overnight, respectively. The nuclei were stained with Topro-3 (Zymed Laboratories, San Francisco, CA). The specimens were then cleared in methyl salicylate before being observed under a confocal laser scanning microscope (CLSM) Olympus FV1000.

### 2.5. Tissue preparation for observing histopathological changes by light microscopy

Dissected lymphoid organs were fixed in Davidson's fixative, dehydrated through ascending concentrations of ethanol, cleared with dioxane, and embedded in paraffin wax. Four to six micron thick sections were cut and stained with hematoxylin and eosin, Periodic Acid-Schiff (PAS) for extracellular matrix (ECM) [17], Gomori's stain for reticular fibers [18], and immunoperoxidase staining with anti-vimentin and anti-cytokeratin. All images were acquired by a Nikon microscope fitted with digital camera DXM 1200.

### 2.5.1. Immunolabeling with anti-vimentin and anti-cytokeratin

Hemolymph drawn from the ventral sinus was fixed with an equal volume of 4% paraformaldehyde for 1 h at 4 °C, smeared on the glass slides, and air-dried. The deparaffinized sections, as prepared in Section 2.3, and hemolymph smears were devoided of endogenous peroxidase by being incubated in 0.3% hydrogen peroxide in methanol for 30 min. Thereafter, free aldehydes were quenched with 1% glycine in PBS for 5 min, followed by incubation in blocking solution (4% BSA and 2% normal goat serum and 0.4% Triton X-100 in PBS) for 2 h. The sections were then incubated overnight at 4 °C in the mouse monoclonal antibody (MoAb) against vimentin and cytokeratin (Sigma Chemical Co., St. Louis, MO), and then goat anti-mouse IgG

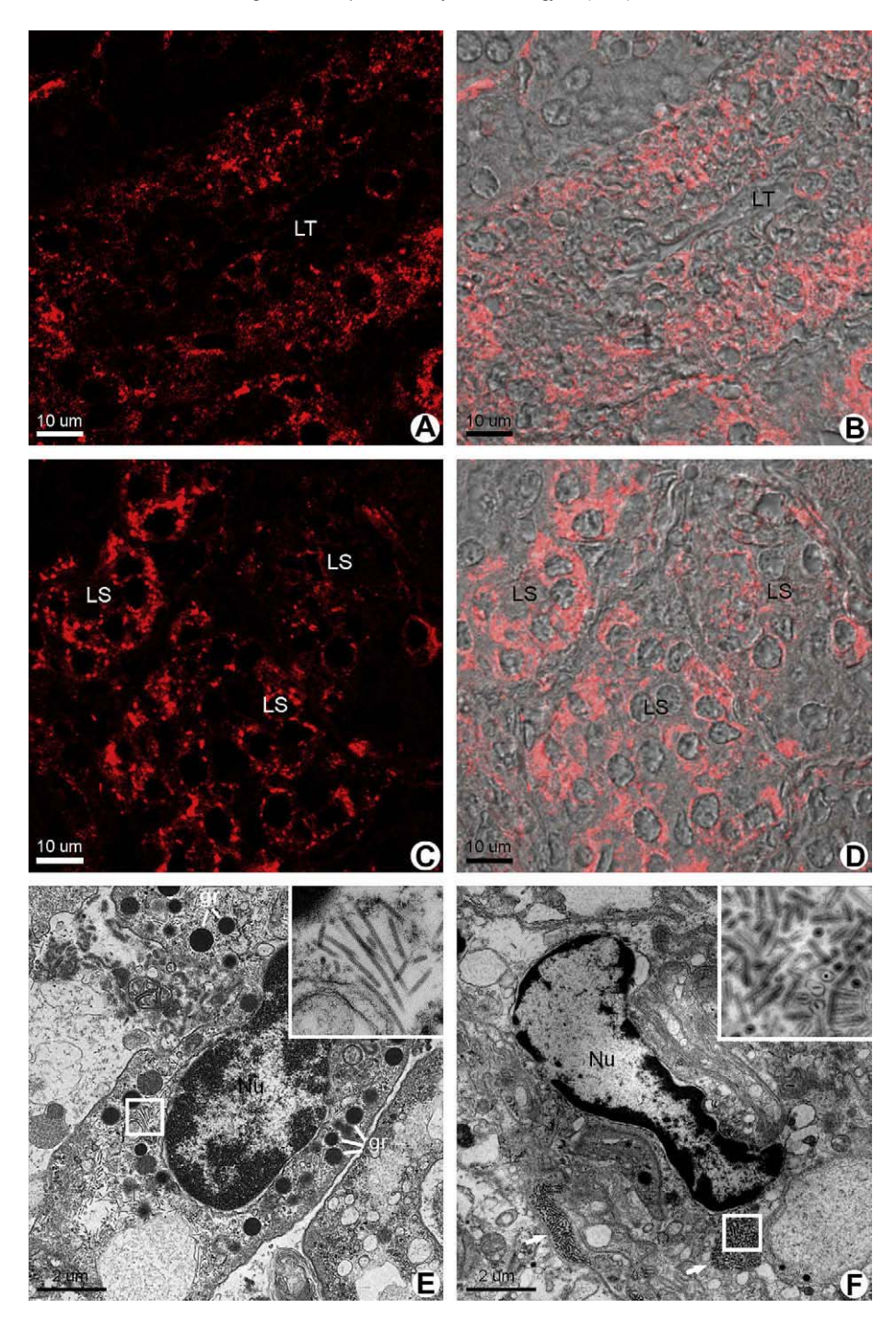


Fig. 2. Confocal laser scanning and TEM micrographs of YHV-infected lymphoid organ. (A–D) Confocal laser scanning micrographs of YHV-infected lymphoid organ sections immunostained with monoclonal antibody specific to YHV gp116 envelope glycoprotein. The immunoreactive fluorescence signal is present in cells of the lymphoid tubule with patent lumen (LT, in A), and cells of lymphoid spheroid (LS, in C). The superimposed fluorescence and phase-contrast images of immunostained sections, indicating the existence of YHV in the cytoplasm of cells in both LT (B) and LS (D). (E) Medium magnification micrograph of a granular hemocyte from the YHV-infected lymphoid tubule. Numerous unenveloped-YHV particles are observed in it's peripheral cytoplasm, an inset shows high magnification of YHV particles are observed in its cytoplasm (white arrows), and the inset shows high magnification of YHV particles from the boxed area. Nu: Nucleus, gr: granule.

conjugated to HRP, for 1 h. Sections with omitted primary antibodies or those treated with normal goat serum served as controls. Subsequently, the sections were immersed in the substrate containing AEC-red (Zymed Laboratories, San Francisco, CA) and counterstained with Mayer's hematoxylin. The sections were washed three times in PBS between each incubation step. All images were acquired by a Nikon microscope fitted with digital camera DXM 1200.

### 2.6. Tissue preparation for electron microscopy

Dissected lymphoid organs were fixed in 4.2% glutaraldehyde and 1% paraformaldehyde in 0.2 M cacodylate buffer, post-fixed in 1% OsO<sub>4</sub>, dehydrated through ascending concentrations of ethanol. For scanning electron microscopy, specimens were dried in a Hitachi HCP-2 critical point drying machine under liquid  $CO_2$ , coated with platinum and palladium in an ion sputtering apparatus,

Hitachi E-120, before being observed under Hitachi scanning electron microscope S-2500 at the accelerating voltage of 15 kV. For transmission electron microscopy, specimens were embedded in Araldite-502 resin. Ultrathin sections were cut and stained with uranyl acetate and lead citrate before being observed under a FEI Tecnai G<sup>2</sup> transmission electron microscope at 80 kV.

#### 3. Results

### 3.1. Nested-RT-PCR detection of YHV using IQ2000 kit

All the eight infected shrimps, used for vascular cast and histopathological studies were shown to be chronically infected with YHV by nested-RT-PCR as marked by PCR amplicons at 277 and 777 bp, which are specific for YHV infection (Fig. 1). Furthermore, the YHV infection was confirmed by detecting the presence of YHVgp116 envelope glycoprotein in the cells within the wall of intact lymphoid tubules with still patent lumen (Fig. 2A,B). Cells within a lymphoid spheroid without lumen also exhibited the presence of YHVgp116 (Fig. 2C,D). The intensity of fluorescence in the spheroid was more than in the tubule. Furthermore, YHV particles were detected in the hemocytes as well as stromal cells of the infected lymphoid tubule (Fig. 2E,F).

### 3.2. Changes of the three dimensional structure of lymphoid organ chronically infected with YHV

The vascular cast of a lymphoid organ chronically infected with YHV, viewed by SEM, showed subgastric artery branching into shorter, larger, less convoluted, blind-ending terminals (Fig. 3C,D) in comparison to those of the uninfected shrimp (Fig. 3A,B) (see ref. [23] for description of three dimensional organization of the normal lymphoid organ). It is possible that this occurred as the result of the breaking away of the terminal parts of the lymphoid tubules, some of which might become the lymphoid spheroids. As a result, only short stumps of the original tubules with blind endings remained (Fig. 3D).

When the chronically YHV-infected lymphoid organ was studied by confocal laser microscopy using MoAb against vimentin as a stromal cell marker [23], intense green fluorescence appeared in the lymphoid tubule wall (Fig. 3E) whereas this fluorescence was much less intense in the lymphoid organ spheroid (Fig. 3E,H). In contrast, nuclei stained by ToPro-3, showed intense red fluorescence in both lymphoid tubule and lymphoid spheroid (Fig. 3F,I). Merged pictures, showing orange color (Fig. 3G,J) in lymphoid tubule due to the combination of green and red colors from the presence of vimentin in stromal cells and nuclei of the same cells, whereas lymphoid spheroid exhibited more red staining (Fig. 3G,J) due to the lack of vimentin which implied a lower number of the stromal cells.

### 3.3. Histopathological changes in lymphoid organ chronically infected with YHV $\,$

Chronically YHV-infected lymphoid organ was still covered by a complete capsule bearing the antennal tubules (Fig. 4C). Within the lobules, lymphoid tubules were disorganized and had lost the normal appearance, and parts of the tubules were lymphoid spheroids that lacked a lumen (Fig. 4D–F) when compared to the normal lymphoid organ (Fig. 6A,B). The lymphoid spheroids could be classified into three types as described earlier by Hasson et al. in Taura syndrome virus infection in *P. vanamei* [8]. Spheroid type 1 (Fig. 4G) was a lightly basophilic, homogeneous mass. Cells in the spheroid contained hypertrophic nuclei with few or no cytoplasmic vacuoles. Spheroid type 2 (Fig. 4H), considered to develop from type 1, appeared more basophilic in staining, and was fully

encapsulated with a fibrous connective sheet and a layer of cells with flat nuclei. There were increased numbers of apoptotic cells that contained intensely basophilic nuclei and a moderate number of cytoplasmic vacuoles. Spheroid type 3 (Fig. 4I) contained the most basophilic cells and was encapsulated by thick fibrous connective tissue. Most cells in this type of spheroid appeared highly vacuolated with apoptotic nuclei with dense and marginalized chromatin.

### 3.4. Ultrastructural changes of lymphoid organ chronically infected with YHV

Prior to the examination by TEM, the semithin plastic sections of the same tissue blocks were studied. In the methylene blue-stained semithin plastic sections, infected lymphoid tubules were still lined by endothelial cells (Fig. 5A). In a tubular wall, large numbers of small granular hemocytes surrounded a group of apoptotic cells (Fig. 5A), which were identified as stromal cells at TEM level (Fig. 5C,D). Lymphoid spheroids might form from these focal changes and sequentially transform into the 3 types as mentioned. Spheroid type 1, considered to be the first to develop from lymphoid tubule, appeared as a blue, homogeneous mass in methylene blue staining (Fig. 5B). At the ultrastructural level, spheroid type 1 contained degranulated small granular hemocytes surrounding stromal cells (Fig. 5E,F). No type 1 fiber and PASpositive ECM were found in the spheroid (see ref. [23] for detailed description of type 1 fiber and ECM). Spheroid type 2 was paler blue when compared to spheroid type 1 (Fig. 5B). There were increasing numbers of hypertrophic and apoptotic cells in spheroid type 2 (Fig. 5B,G). Spheroid type 3 was a degenerating blue-staining mass with mostly vacuolated apoptotic cells (Fig. 5B). At TEM level, it became clear that most cells in this type of spheroid were highly vacuolated and contained apoptotic nuclei (Fig. 5H).

### 3.5. Change of fibrous scaffold in YHV-infected lymphoid organ

In general, both fibrous components exhibited similar patterns to those of normal lymphoid tubule where PAS-intensely stained extracellular matrix (ECM) were associated with type 1 fibers, and Gomori's stained type 2 (reticular) fibers (see ref. [23] for complete description). However, the staining of ECM and associated type 1 fibers within spheroids appeared much less intense, and less organized than in normal tubules (Fig. 6A,B). In contrast, intensely-stained argyrophilic fibers surrounding lymphoid spheroids became more prominent when compared to those around lymphoid tubules (Fig. 6C). When observed by SEM, spheroids showed a smooth surface (Fig. 6D-F) perhaps due to the loss or lower amount of ECM and type 1 fibers that formed the outer zone of the lymphoid tubules. In comparison, the surface of normal lymphoid tubules appeared rough and basket-like due to the presence of networks of numerous type 1 fibers and ECM (Fig. 6D-F).

### 3.6. Immunolabeling with anti-vimentin and anti-cytokeratin

No cytokeratin (Fig. 7B) and vimentin (Fig. 7C,D) immunostainings were detected in lymphoid spheroids. In contrast, intact lymphoid tubules in chronically YHV-infected lymphoid organ still showed positive immunostaining of vimentin in stromal cells. The negative control experiment using normal goat serum showed no staining (data not shown). Immunostaining for both cytokeratin and vimentin was not detected in hemocytes in tubular walls (Fig. 7B–D) or in the hemolymph smears (Fig. 7A) as in the case of uninfected shrimp.

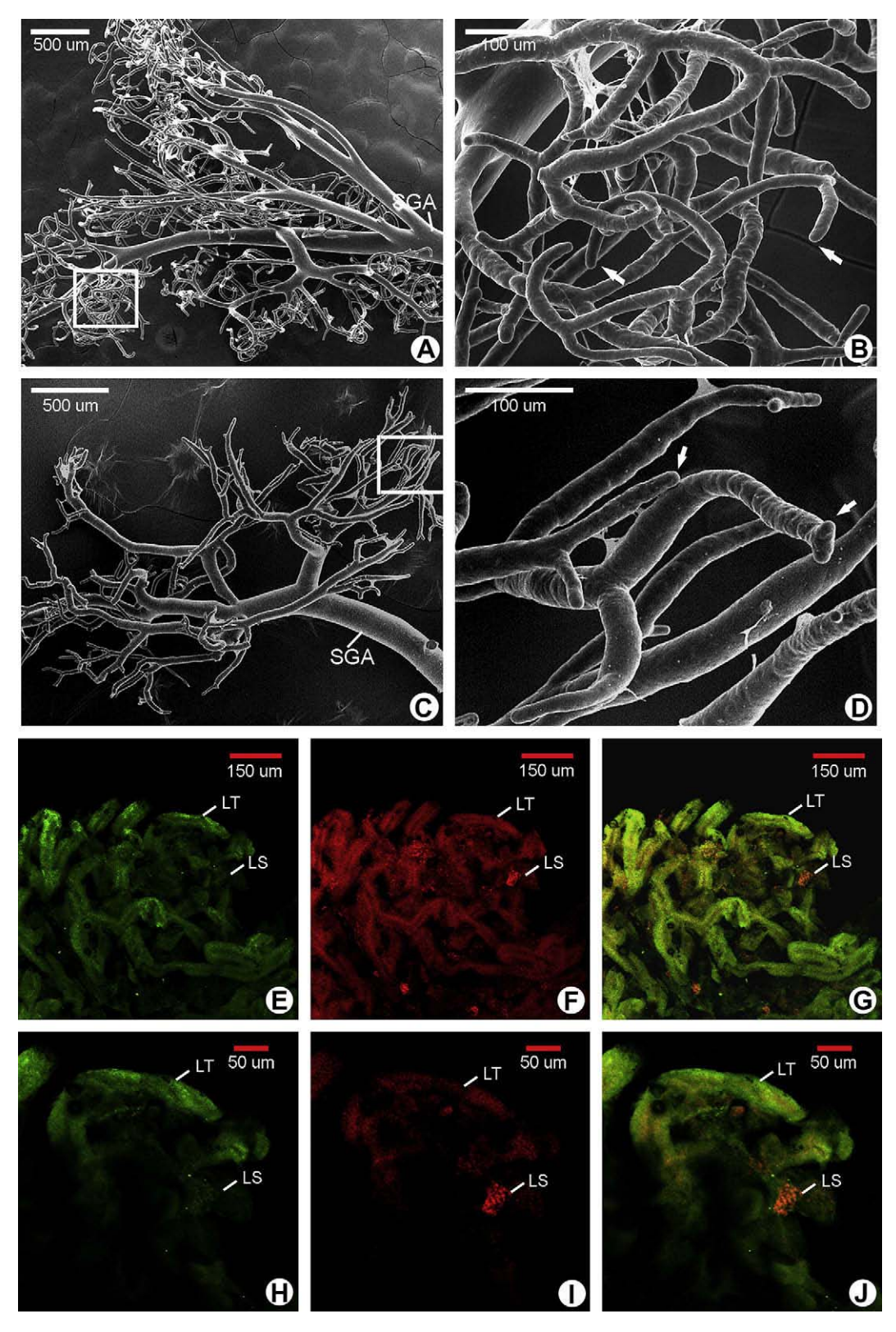


**Fig. 3.** Scanning electron (SEM) micrographs and confocal (CF) micrographs of normal and chronically YHV-infected lymphoid organs of *P. monodon*. **(A)** Low and **(B)** medium magnification SEM micrograph (taken from boxed area in A) of a normal lymphoid organ prepared by vascular cast technique and viewed by SEM, showing subgastric artery (SGA) branching into highly convoluted and blind-ending terminal capillaries (arrows in B). **(C)** Low and **(D)** medium magnification SEM micrograph (taken from boxed area in C) of chronically YHV-infected lymphoid organ prepared by vascular cast technique and viewed by SEM, showing the subgastric (SGA) artery branching into shorter, more limited number of branches that lead to the blind-ending stumps (arrows in D). It is believed that lymphoid spheroids lack a lumen, hence injected plastic would not fill them and consequently, most lymphoid organ spheroids might be disconnected from lymphoid tubules and washed out during the casting process. **(E-J)** Low and medium magnification CF micrographs of chronically YHV-infected lymphoid organ prepared by staining the whole-mounted lymphoid organ with MoAb against vimentin and viewed by confocal laser scanning microscopy, showing intense green fluorescence in lymphoid tubule (LT) but less intense fluorescence in lymphoid spheroid (LS) in E, H. Nuclei stained by ToPro 3 in F and I, show intense red fluorescence in both lymphoid tubule (LT) and lymphoid spheroid (LS). Merged pictures in G and J show orange color in lymphoid tubule (LT) due to the merged green fluorescence of vimentin and red fluorescence of nuclei in the same cells, whereas lymphoid spheroid (LS) was more red due to the lack of vimentin in stromal cells.

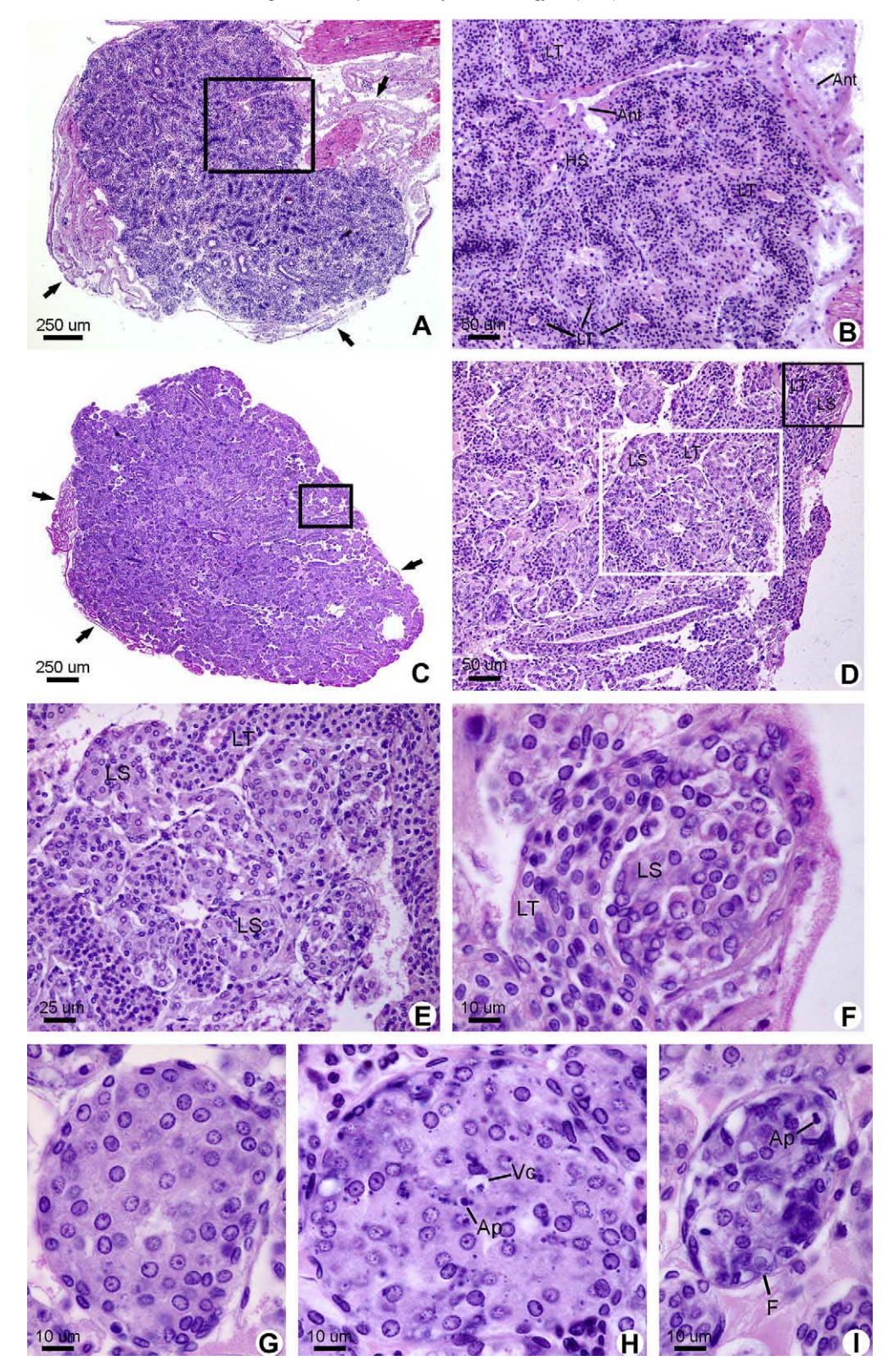


**Fig. 4.** Light micrographs (LM) of paraffin sections of normal and chronically YHV-infected lymphoid organs of *P. monodon* stained with hematoxylin and eosin. **(A, C)** Low magnification LM micrographs, showing the general features of normal (in A) and YHV-infected (in C) lymphoid organs surrounded by capsules containing antennal tubules embedded in the connective tissue (arrows in A and C). **(B)** A medium magnification LM micrograph taken from boxed area in A, showing antennal tubules (Ant) which are the invaginated parts from the antennal capsules that project inwards and partitioned the lymphoid organ into lymphoid tubules, each showing patent lumen. LT: lymphoid tubule, HS: hemal sinus. **(D)** A medium magnification LM micrograph taken from boxed area in C, showing lymphoid tubule (LT) transformed into lymphoid spheroid (LS) with occluded lumen. **(E, F)** High magnification micrographs, showing in E (taken from white-boxed area in D) the transitional zone from lymphoid tubule (LT) to the more disorganized lymphoid spheroid (LS), and in F (taken from black boxed area in D) long section of LS that lacked lumen. **(G)** A high magnification micrograph of a lymphoid spheroid type 1, showing light basophilic homogenous spheroid. The spheroid contained cells with hypertrophic nuclei with marginating heterochromatin along the nuclear periphery but no cytoplasmic vacuoles. **(H)** A high magnification micrograph of a lymphoid spheroid type 2, showing more intense basophilic spheroid. Prominent fibrous connective tissue capsule surrounded the spheroid. Increasing numbers of apoptotic (Ap) cells with fragmented nuclei with densely stained chromatin and cytoplasmic vacuoles (Vc) were observed. **(I)** A high magnification micrograph of a lymphoid spheroid type 3, showing the smallest and most basophilic spheroid clearly encapsulated by fibrous tissue (F). Vacuolized apoptotic (Ap) cells are present over the entire spheroid.

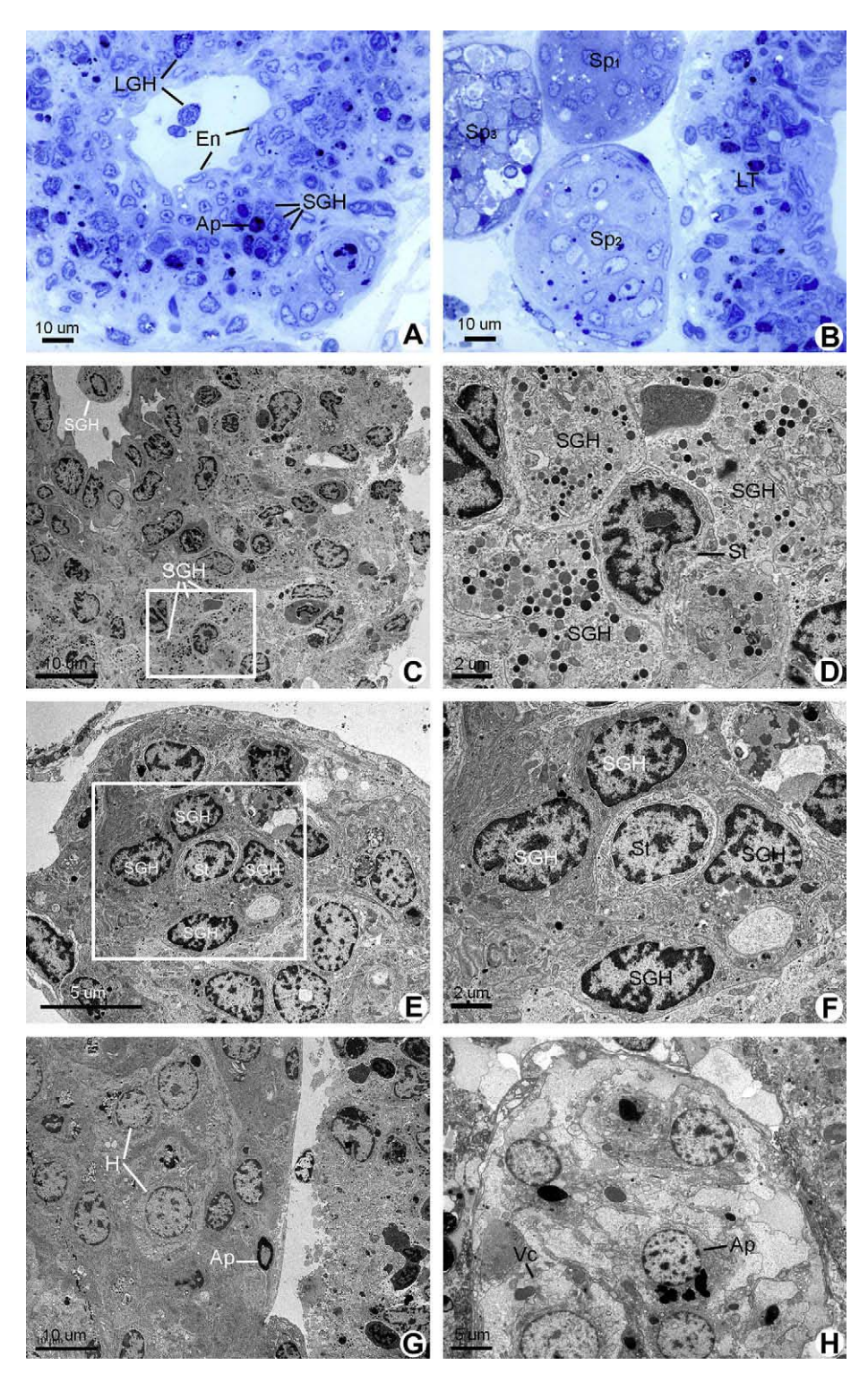


**Fig. 5.** Light (LM) and transmission electron (TEM) micrographs of chronically YHV-infected lymphoid organs of *P. monodon.* (**A, C, D**) High magnification LM micrographs of semi-thin sections of chronically YHV-infected lymphoid organ stained with methylene blue (in A) and TEM micrographs (in C and D), showing a large number of small granular hemocytes (SGH) surrounding apoptotic (Ap) cells (in A), which were identified as stromal cell (St). En: Endothelial cell. (**B**) A high magnification LM micrograph of semi-thin section of chronically YHV-infected lymphoid organ stained with methylene blue, showing infected lymphoid tubule (LT) and three types of spheroids: type 1 (Sp<sub>1</sub>), type 2 (Sp<sub>2</sub>) and type 3 (Sp<sub>3</sub>). (**E**) Low and (**F**) medium magnification TEM micrograph (taken from boxed area in E) of lymphoid spheroid type 1, showing a group of degranulated small granular hemocytes (SGH) surrounding a stromal cell (St). (**G**) A low magnification TEM micrograph of lymphoid spheroid type 2, showing increasing number of hypertrophic (H) and apoptotic cells (Ap) in the spheroid. (**H**) A low magnification TEM micrograph of lymphoid spheroid type 3, showing vacuolized apoptotic (Ap) cells in the entire spheroid.

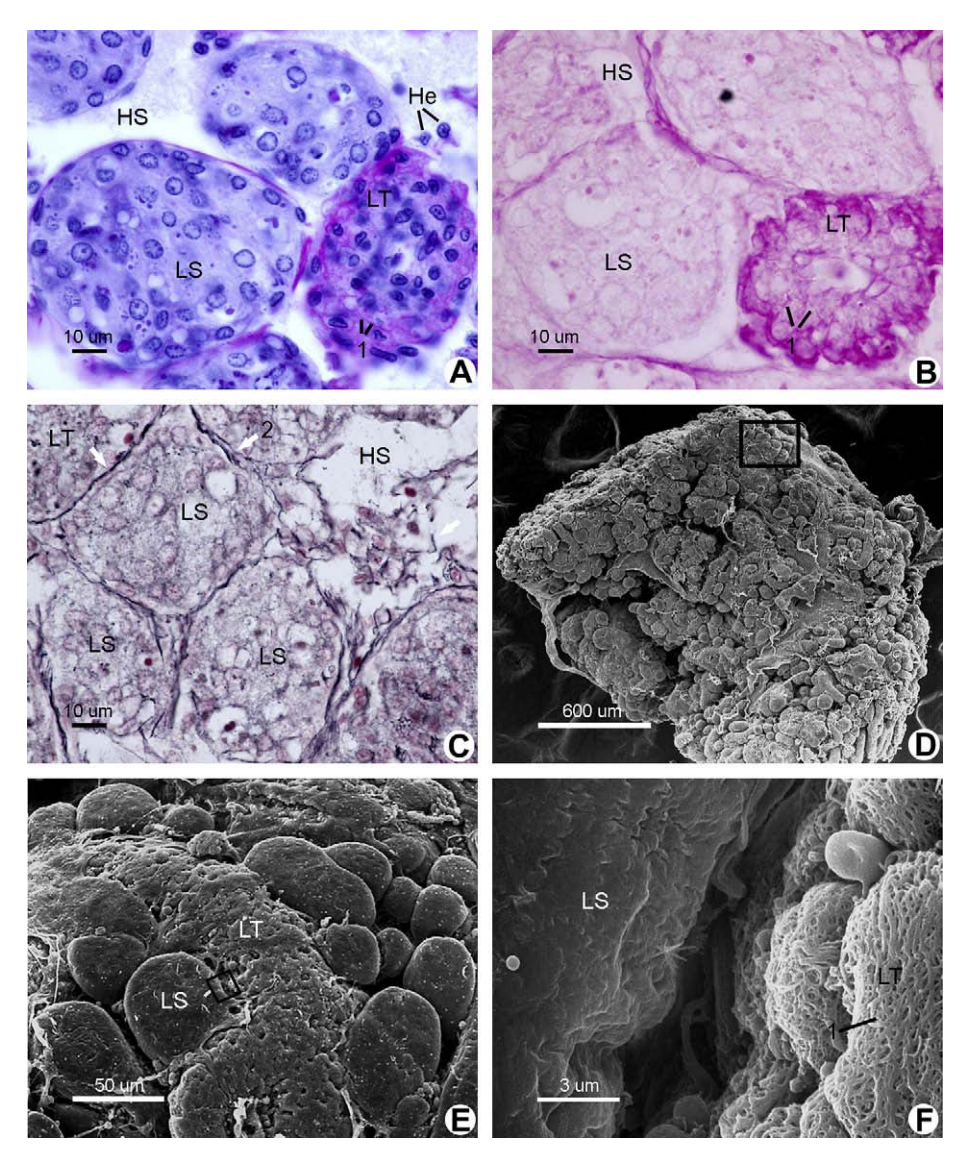


**Fig. 6.** Light and SEM micrographs of chronically YHV-infected lymphoid organs of *P. monodon*. **(A, B)** High magnification LM micrographs of lymphoid organ sections stained with PAS and counterstained with Mayer's hematoxylin (in A) and uncounterstained (in B), showing intense PAS staining of fibrous scaffold of type 1 fibers and extracellular matrix (ECM) at the capsular layer of lymphoid tubules (LT), and light staining of type 1 fibers running in ECM between stromal cells. However, the staining of ECM and associated type 1 fibers within the spheroid (LS) appeared much less intense and less organized. There was no staining in hemal sinuses (HS). He: Hemocyte, 1: type 1 fibers. **(C)** A high magnification LM micrograph of a lymphoid organ section stained with Gomori's stain for reticular fibers (type 2 fibers), showing black lines (arrows) around hemal sinuses (HS), and lymphoid spheroids (LS) and lymphoid tubules (LT). 2: type 2 fibers. **(D-F)** SEM micrographs, showing the surface of chronically YHV-infected lymphoid organ. Spheroids (LS) exhibited smooth surface due to the lack of type 1 fibers and ECM (in E-which was taken from the boxed area in D), whereas there were still numerous networks of type 1 fibers and ECM surrounding lymphoid tubule (LT), which make it's surface appearing rough and basket-like (in F which was taken from boxed area in E). 1: type 1 fibers.

### 4. Discussion

In this report, only the YHV-infected shrimp were selected for the histopathological study in order to make sure that any changes that occurred would be in response to a single species of virus. This was ascertained by the rigorous diagnosis of YHV infection with nested-RT-PCR. Furthermore, YHVgp116 envelope glycoprotein was detected specifically in cells within the wall of lymphoid tubules as well as lymphoid spheroids. The most obvious changes in the organization of lymphoid organ of the chronically YHV-infected shrimp were the presence of numerous lymphoid spheroids (LS) that were formed during the course of infection. Vascular casts of the infected lymphoid organ showed that the terminal lymphoid tubules (LT) were drastically shortened and the branching of LT was not as elaborate as normal LT. In many instances only the relatively large "stumps" of the terminal LT remained. Furthermore,

observation by light microscopy of a large area and labeling of spheroid stromal cells by vimentin indicated that the lumen in the distal end of LT was obliterated and this end might breakdown thus shortening the original LT. The formation of LS in penaeid shrimp has been previously studied in P. vannamei [8] and in P. monodon [10]. These authors observed the presence of three types of spheroidal masses after infection with taura syndrome virus and proposed that they played roles in sequestering and finally eliminating viruses. The morphological transformation of lymphoid spheroid type 1-3 represented the viral sequestering stages largely by hemocytes, most of which became apoptotic in stage 3 spheroid. As a result, the viruses were prevented from spreading and were eliminated. However, in chronic infection a certain amount of viral particles remained, thus LT were re-infected and the cycle of LS formation was repeated and resulted in the abundance of LS in the lymphoid organ as observed in the present study. As for the

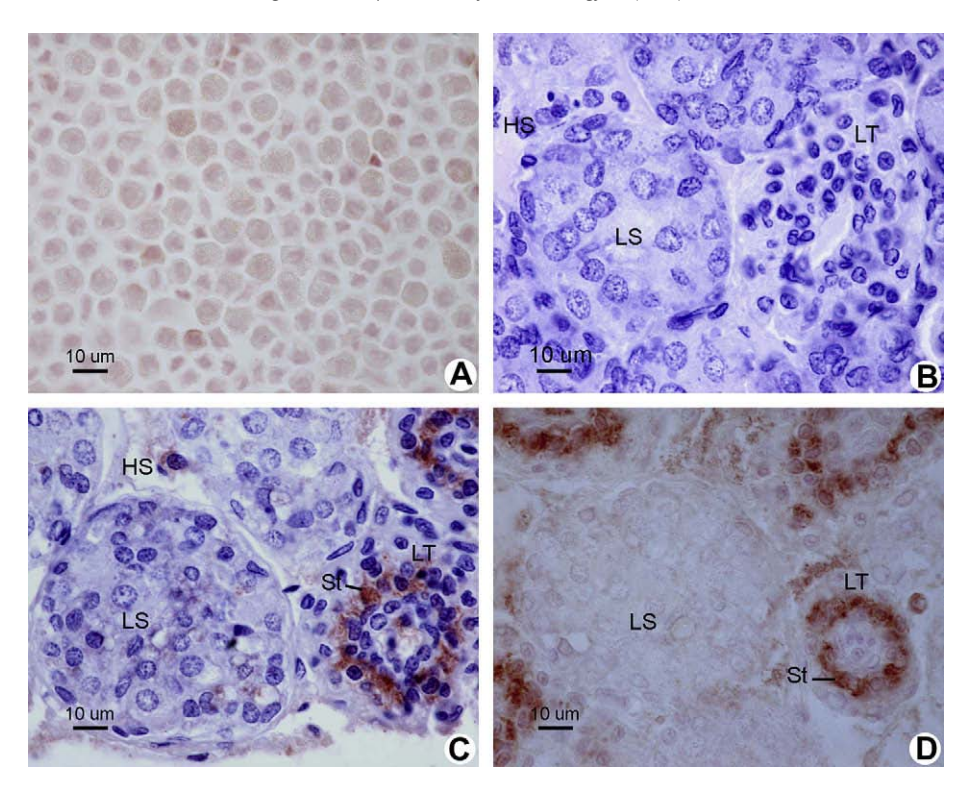


Fig. 7. Light micrographs of hemolymph smear and the cross sections of chronically YHV-infected lymphoid organ stained by immunoperoxidase technique using MoAb against cytokeratin and vimentin as probes. (A) A high magnification micrograph of hemolymph smear, showed no immunostaining in all types of hemocytes. (B) A high magnification micrograph of chronically YHV-infected lymphoid organ sections stained by immunoperoxidase technique using MoAb against cytokeratin as probe, showing no immunostaining while only Mayer's hematoxylin staining was observed in the lymphoid spheroid (LS), lymphoid tubules (LT) and hemal sinuses (HS). (C, D) High magnification micrographs of chronically YHV-infected lymphoid organ section stained by immunoperoxidase technique using MoAb against vimentin as probe (in D) and counterstained with Mayer's hematoxylin (in C), showing no immunostaining in lymphoid spheroid (LS), in contrast there was intense reddish immunostaining in the stromal cells (St) which was located in the middle layer of the wall of lymphoid tubules (LT).

relationship between LS and LT, Hasson et al. [8] reported that during acute infection with TSV, there is an increase of type 1 LS and a decrease of TSV-positive LT suggesting that LT might transform to LS. However, the authors were influenced by Anggraeni and Owen's suggestion [9,10] that LS were purely of hemocytic origin. According to this hypothesis LS may occur when resident LT phagocytes that sequestered TSV migrate into the intertubular hemal sinuses and hemocytes aggregate around them to form LS. In the present study, the decrease in number and shortening, possibly by breaking of the terminal parts of LT, were demonstrated by SEM and vascular cast, which could portray LT in three dimensions and covered a larger area than that which could be viewed in histological sections. This certainly demonstrated that LTs are structurally affected by YHV. Whether the broken-up terminal parts of LT became LS is still debatable. We believe that at least some parts of damaged LT became the seeding site for LS formation as in the present study we have also observed the dynamics of changes in LT cellular components and connective tissue scaffold in chronically YHV-infected lymphoid organ. There appeared to be more extravasation of hemocytes into the LT wall during YHV infection. So much that hemocytes were the major population of the LT wall. Viral particles were found in both stromal cells and hemocytes that aggregated together in the lymphoid tubule's wall (LTW). It is quite remarkable that the stromal cells and surrounding hemocyte's apoptosis occur before the degeneration of LTW. The role of stromal cells in processing antigens and in attracting hemocytes to LT needs to be verified in further studies. It is also interesting to note that most hemocytes in these foci were undergoing exocytosis of their granules, as in LS type 2 and 3 where granules were hardly visible in the hemocytes, which were similar to the spheroidal hemocytes reported by Anggraeni and Owen [10]. It is interesting to note that these authors also reported the presence of stromal cells like those in LTW in the LS even though they were not stained for phenol oxidase like hemocytes [10]. Since stromal cells are an intrinsic population of the LT wall, this suggested that part of LS cells were derived from LT cells. Therefore, even though it was suggested [10] that all LS may be formed de novo from hemocytes aggregating in the hemal sinuses, we believe that the LT origin of LS formation could not be ruled out. The compositions and possible functions of the released granular materials from hemocytes could partly be enzymes that break down viruses, while the rest could be proteins that were involved in the coagulation [19-22] and walling off (encapsulating) the spheroids, thus preventing viral particles and debris from the infected apoptotic cells from spreading. To ensure that this is the case, spheroids were surrounded by a thickened capsule which was made up of argyrophilic type 2 fibers (Fig. 6C). In contrast it was observed that type 1 fibers with associated ECM drastically decreased (Fig. 6A,B), as there was no more basket-like network (Fig. 6F) around LS as appearing around LT, resulting in the smooth appearance of LS when viewed under SEM. Labeling with vimentin also demonstrated there were much fewer stromal cells remaining in the LS (Fig. 7C,D), indicating their decreased number together with fiber type 1 and associated-EMC. Finally, LS were reduced in size after the apoptotic cells and their debris had been absorbed.

### Acknowledgements

This research was supported by Commission on Higher Education (Ph.D. Scholarship to P. Duangsuwan and Research Group Development Grant to P. Sobhon) and TRF (Senior Research Scholar Fellowship to P. Sobhon). We would like to thank Dr. Paisarn

Sithigorngul, Department of Biology, Faculty of Science, Srinakharinwirot University, Bangkok, Thailand for generously providing the monoclonal antibody to YHV envelope glycoprotein 116 (gp116). We also thank Ms. Jaruwan Poljaroen for assistance with graphics.

#### References

- [1] Oka M. Studies on Penaeus orientalis Kishinuoye-VIII structure of the newly found lymphoid organ. Bull Jpn Soc Sci Fish 1969;35:245-50.
- Kondo M, Itami T, Takahashi Y, Fujii R, Tomonaga S. Structure and function of the lymphoid organ in the Kuruma prawn, Dev Comp Immunol 1994;18, S109.
- Bell TA, Lightner DV. A Handbook of normal penaeid shrimp histology. Baton Rouge: World Aquaculture Society; 1996. p. 70-73.
- Van de Braak CBT, Botterblom MHA, Taverne N, van Muiswinkel WB, Rombout JHWM, van der Knaap WPW. The roles of the haemocytes and the lymphoid organ in the clearance of injected Vibrio bacteria in Penaeus monodon shrimp. Fish Shellfish Immunol 2002;13:293–309.
- [5] Kanobdee K, Soowannayan C, Flegel TW, Ubol S, Withyachumnarnkul B. Evidence for apoptosis correlated with mortality in the giant black tiger shrimp Penaeus monodon infected with yellow head virus. Dis Aquat Org 2002;48:79-90.
- [6] Martin GG, Hose JE, Minka G, Rosenberg S. Clearance of bacteria injected into hemolymph of Ridgeback prawn, Sicyonia ingentis (Crustacia: Decapoda): role of hematopoietic tissue. J Morphol 1996;227:227-33.
- Takahashi Y, Itami T, Kondo M. Immune system of crustacean. Fish Pathol 1995;30:141-50.
- [8] Hasson KW, Lightner DV, Mohney LL, Redman RM, White BM. Role of lymphoid organ spheroids in chronic Taura syndrome virus (TSV) infections in Penaeus vanamei. Dis Aquat Org 1999;38:93-105.
- Anggraeni MS, Owen L. Evidence for the haemocytic origin of lymphoidal spheroids in Penaeus monodon. In: Flegel TW, editor. Advances in shrimp biotechnology. Bangkok: National Center for Genetic Engineering and Biotechnology; 1998. p. 137.
- [10] Anggraeni MS, Owen L. The haemocytic origin of lymphoid organ spheroid cells in the penaeid prawn Penaeus monodon. Dis Aquat Org 2000;40:85-92.

- [11] Bonami JR, Lightner DV, Redman RM, Poulos BT. Partial characterization of togavirus (LOVV) associated with histopathological changes of the lymphoid organ of penaeid shrimps. Dis Aquat Org 1992;14:145–52.
- [12] Owens L, De Beer S, Smith J. Lymphoidal parvovirus-like particles in Australian penaeid prawns. Dis Aquat Org 1991;11:129-34.
- [13] Spann KM, Vickers JE, Lester RJ. Lymphoid organ virus of Penaeus monodon from Australia. Dis Aquat Org 1995;23:127–34.
  [14] Nadala ECB, Tapay LM, Loh PC. Yellow-head virus: a rhabdovirus-like pathogen
- of penaeid shrimp. Dis Aquat Org 1997;31:141-6.
- [15] Flegel TW, Fegan DF, Kongsom S, Vuthikornudomkit S, Sriurairatana S, Boonyaratpalin S, et al. Occurrence, diagnosis and treatment of shrimp diseases in Thailand. In: Fulks W, Main KL, editors. Diseases of cultured penaeid shrimp in Asia and the United States. Honolulu: The Oceanic Institute; 1992. p. 57-112.
- [16] Chunhabundit P, Somana R. Scanning electron microscopic study on pineal vascularization of the common tree shrew (Tupaia glis). J Pineal Res 1991;10:59-64.
- McManus JFA. Histological demonstration of mucin after periodic acid. Nature 1946:158:202.
- Jones Lamar. Connective tissues and stains. In: Bancroft JD, Gamble M, editors. Theory and practice of histological techniques. New York: Churchill Livingstone; 2002. p. 159-60.
- Huang CC, Sritunyalucksana K, Soderhall K, Song YL. Molecular cloning and characterization of tiger shrimp (*Penaeus monodon*) transglutaminase. Dev Comp Immunol 2004;28:279–94.
- Chen MY, Hu KY, Huang CC, Song YL. More than one type of transglutaminase in invertebrates? A second type of transglutaminase is involved in shrimp coagulation. Dev Comp Immunol 2005;29:1003-16.
- [21] Yeh MS, Kao LR, Huang CJ, Tsai IH. Biochemical characterization and cloning of transglutaminases responsible for hemolymph clotting in Penaeus monodon
- and *Marsupenaeus japonicus*. Biochim Biophys Acta 2006;1764:1167–78. [22] Yeh MS, Huang CJ, Cheng JH, Tsai IH. Tissue-specific expression and regulation of the haemolymph clottable protein of tiger shrimp (Penaeus monodon). Fish Shellfish Immunol 2007;23:272-9.
- Duangsuwan P, Phoungpetchara I, Tinikul Y, Poljaroen J, Wanichanon C, Sobhon P. Histological and three dimensional organizations of lymphoid tubules in normal lymphoid organ of *Penaeus monodon*. Fish Shellfish Immunol 2008:24:426-35.

EFFECTS OF SEROTONIN, DOPAMINE, OCTOPAMINE, AND SPIPERONE ON OVARIAN MATURATION AND EMBRYONIC DEVELOPMENT IN THE GIANT FRESHWATER PRAWN, MACROBRACHIUM ROSENBERGII (DE MAN, 1879)

BY

YOTSAWAN TINIKUL<sup>1</sup>), BOWORN SOONTHORNSUMRITH<sup>1</sup>), ITTIPON

PHOUNGPETCHARA<sup>1</sup>), PRASERT MEERATANA<sup>2</sup>), JARUWAN POLJAROEN<sup>1</sup>), PORNSAWAN

DUANGSUWAN<sup>3</sup>), NANTAWAN SOONKLANG<sup>1</sup>), A. JOFFRE MERCIER<sup>4</sup>), and

PRASERT SOBHON <sup>1,5</sup>)

<sup>1</sup>)Department of Anatomy, Faculty of Science, Mahidol University, Rama VI Road, Ratchathewi, Bangkok 10400, Thailand

<sup>2</sup>)Department of Medical Science, Faculty of Science, Burapha University, Chonburi 20131, Thailand

<sup>3</sup>)Department of Anatomy, Faculty of Science, Prince of Songkla University, Songkhla 90112, Thailand

<sup>4</sup>)Department of Biological Sciences, Brock University, St. Catharines, Ontario L2S 3A1, Canada

### ABSTRACT

Mature female, <u>Macrobrachium rosenbergii</u> in stage I of their ovarian cycle were divided into 17 groups (14 experimental groups and 3 control groups) of 28 animals each. Animals in each experimental group were injected intramuscularly with 2-3 doses of serotonin (5-HT), dopamine (DA), octopamine (OA), spiperone (SP), or 5-HT plus SP, at four-day intervals from day 1 to 49. Five animals each in every group were sacrificed,

<sup>&</sup>lt;sup>5</sup>) e-mail: Hscpso@mahidol.ac.thH or: Hanatch2002@yahoo.com

respectively, at day 14, 25, and 49 to evaluate the gonadosomatic index (GSI) and oocyte diameters. The experimental groups that received the doses of 2.5 x 10<sup>-5</sup>, 2.5 x 10<sup>-6</sup> mol of 5-HT/prawn,  $2.5 \times 10^{-5}$ ,  $2.5 \times 10^{-6}$ ,  $2.5 \times 10^{-7}$  mol of 5-HT/prawn plus  $2.7 \times 10^{-7}$  mol of SP/prawn, as well as SP alone at the dose of 5.4 x 10<sup>-7</sup> mol of SP/prawn, exhibited significantly shorter periods of ovarian maturation and embryonic development, as well as increased GSI values and oocyte diameters, when compared with vehicle-injected and untreated control groups. In contrast, groups injected with DA and OA at similar doses showed decreased ovarian maturation, oocyte diameters, and embryonic periods, but no differences in GSI, when compared with control groups. For the number of eggs per spawn, the groups of animals that received 5-HT at doses of 2.5 x 10<sup>-5</sup> and 2.5 x 10<sup>-6</sup> mol/prawn, 5-HT at doses of  $2.5 \times 10^{-5}$  mol plus SP at  $2.7 \times 10^{-7}$  mol/prawn, 5-HT at  $2.5 \times 10^{-6}$  mol plus SP at 2.7 x 10<sup>-7</sup> mol/prawn, and SP at a dose of 2.7 x 10<sup>-7</sup> mol/prawn, yielded higher numbers than the control groups, and with a significant difference (P<0.05). All DA and OA injected groups showed lower numbers of eggs when compared to the control groups. Eggs from all these experimental groups exhibited equally good quality both among each other and in comparison with control groups, as judged from the percentage of fertilized eggs.

### INTRODUCTION

The giant freshwater prawn, <u>Macrobrachium rosenbergii</u> (De Man, 1879), is an important food source that is cultured worldwide (Sandifer & Smith, 1985). Also, it is a highly valued aquatic animal in Thailand and other Asian countries. Hormonal regulation of the reproductive process of this decapod crustacean is not as well understood as in the crayfish, <u>Procambarus clarkii</u> (Girard, 1852), or the lobster, <u>Homarus americanus</u> (Milne-Edwards, 1837), in which a number of hormones from the eyestalk and other endocrine organs play roles in controlling the development of the gonads and of secondary sexual

characteristics (Fingerman, 1997; Herp & Soyez, 1997). Furthermore, in the crayfish, major neurotransmitters that could control ovarian maturation include serotonin (5-HT) and dopamine (DA): 5-HT has a stimulating effect on gonadal maturation, perhaps by inhibiting the release of gonad inhibiting hormone (GIH), and/or by stimulating the release of gonad stimulating hormone (GSH), whereas DA plays the opposite role (Sarojini et al., 1995b; Fingerman, 1997). Additionally, it was reported that female crayfish, given 5-HT, exhibit a significant increase in the ovarian index and in the size of the oocytes (Sarojini et al., 1995d). DA inhibits gonadal maturation in both sexes, apparently by inhibiting the release of GSH and possibly also by triggering the release of GIH. Interestingly, a DA antagonist, spiperone (SP), increases the gonadosomatic (GSI) index in P. clarkii when injected during early vitellogenesis (Rodríguez et al., 2002). SP also stimulates ovarian growth in the crab, Chasmagnathus granulatus (Dana, 1851) (cf. Zapata et al., 2003) and induces testicular maturation in the crayfish, P. clarkii (cf. Sarojini et al., 1995e). 5-HT induces ovarian maturation and spawning in Litopenaeus vannamei (Boone, 1931) (cf. Vaca & Alfaro, 2000). The aim of this study was to investigate whether these neurotransmitters and a DA antagonist have similar effects on ovarian maturation, embryonic development, and spawning in the giant freshwater prawn, Macrobrachium rosenbergii.

### MATERIAL AND METHODS

### Experimental animals

Mature female, Macrobrachium rosenbergii (giant freshwater prawns) (weighing on average  $42.71 \pm 5.8$  g each) were obtained from commercial farms in Chonburi Province, Thailand. The animals were kept in outdoor concrete circular tanks, each with 1.50 m diameter and a water depth of 0.80 m; about 30% of the water was changed every 2 days. The prawns were fed commercial food pellets (Charoen Pokphand Group, Thailand) twice per

day. Aeration was given all day. To allow mating, blue-claw males and females were stocked at a ratio of 1:5, respectively, in the same tank. Thirty plastic cages were added into every tank for molting animals to hide in and avoid being killed as a result of the cannibalistic behaviour of this species. The prawns were acclimatized under a photoperiod of 12:12 h light: dark for two weeks before the beginning of the experiments. Female prawns were selected and used in the experiments to test the effects of 5-HT, DA, OA, and SP on the length of the ovarian cycle and embryonic development, as soon as they exhibited stage I of the ovarian cycle.

# Effects of 5-HT, DA, OA, SP, and 5-HT plus SP on ovarian maturation, embryonic development, and spawning

Female prawns at ovarian stage I were divided into 17 groups, each with 28 animals. The prawns in the 14 treatment groups were injected with 5-HT at doses of 2.5 x 10<sup>-5</sup>, 2.5 x 10<sup>-6</sup>, and 2.5 x 10<sup>-7</sup> mol of 5-HT/prawn, DA at doses of 2.5 x 10<sup>-5</sup>, 2.5 x 10<sup>-6</sup>, and 2.5 x 10<sup>-7</sup> mol of DA/prawn, OA at doses of 2.5 x 10<sup>-5</sup>, 2.5 x 10<sup>-6</sup>, and 2.5 x 10<sup>-7</sup> mol of OA/prawn, SP at doses of 2.7 x 10<sup>-7</sup>, and 5.4 x 10<sup>-7</sup>, mol of SP/prawn, and 5-HT plus SP at doses of 2.5 x 10<sup>-5</sup> mol of 5-HT/prawn plus 2.7 x 10<sup>-7</sup> mol of SP/prawn, 2.5 x 10<sup>-6</sup> mol of 5-HT/prawn plus 2.7 x 10<sup>-7</sup> mol of SP/prawn, and 2.5 x 10<sup>-7</sup> mol of 5-HT/prawn plus 2.7 x 10<sup>-7</sup> mol of SP/prawn. 5-HT, DA, and OA were dissolved in crustacean physiological saline (CPS, containing NaCl 29 g, KCl 0.71 g, CaCl<sub>2</sub>.2H<sub>2</sub>O 2.38 g, MgSO<sub>4</sub>.7H<sub>2</sub>O 3.16 g, NaHCO<sub>3</sub> 0.5 g, MgCl<sub>2</sub>.6H<sub>2</sub>O 0.17 g, and HEPES 4.76 g in 1 liter of distilled water), whereas SP was dissolved in 95% ethanol. The injected volumes of 5-HT, DA, and OA were 0.10 ml, whereas SP was 0.05 ml. The females treated with 5-HT plus SP received 0.10 ml of 5-HT solution and 0.05 ml of SP solution, in separate injections. The doses of the chemicals used in this study were based on their positive effects as shown by Chen et al. (2003) for 5-HT and DA, and Alfaro et al.

(2004) for SP. All prawns could tolerate the injected doses of neurotransmitters without showing any abnormal behaviour. All injections were performed at 4-day intervals, covering a period of 49 days. The effects on the neurotransmitter-treated groups were compared with three control groups of 28 animals each: in the first group, each animal was injected with 0.1 ml of crustacean physiological saline (CPS), in the second each animal was injected with 0.1 ml CPS plus 0.05 ml 95% ethanol (CPSE), and the third group was an untreated negative control (NC) group. Animals in each group were identified by tying plastic loops of different colours around the eyestalk. The injections were performed via an intramuscular route at the lateral aspect of the second abdominal somite using a 1 ml syringe (NIPRO) fitted with 26 G x  $\frac{1}{2}$ " (0.45 x 12 mm) thin-wall needles (NIPRO).

The weight and total length of the prawns were measured on every treatment day, before injection. Total length was taken from the base of the eyestalk to the telson (Eyestalk base-telson length, EBTL). Five animals in each group were randomly selected and sacrificed at days 14, 25, and 49 to evaluate the gonado-somatic index (GSI) and oocyte diameter. The GSI was calculated using the formula [ovarian weight (g) / body weight (g)] x 100. The rest of the prawns were allowed to proceed until they ovulated. The experiment was done in triplicate. All GSI values and oocytes diameters were then compared between the treated groups and the control groups. Pieces of ovary were subsequently fixed in Bouin's solution, and prepared by the paraffin technique for light microscopic observations to determine the ovarian stages and oocyte diameters.

Percentage of spawning prawn, and the quantity and quality of the spawned eggs

Percentage of spawning was determined from the number of spawning prawn in each group at the end of the experiment. The quality and quantity of spawned eggs were evaluated from the number of eggs per spawn and the percentage of fertilized eggs. The abdomen of

each spawning prawn was carefully scraped to obtain all the light yellow eggs from the brood chamber. All spawned eggs were mixed with 3% sodium hypochlorite (NaClO) in distilled water to thoroughly disperse the eggs. At least 300 eggs were observed under a compound or stereo-microscope for determining the morphology and percentage of developing embryos (successfully fertilized eggs). For evaluating the quantity of spawned eggs, the eggs were placed in 15 ml of 3% NaClO and mixed thoroughly. After that, 3 times aliquots of 10 µl of the egg suspension were randomly drawn from the 15 ml tube into a 0.6 ml tube to count the total number of eggs under a stereo-microscope. Counting was always triplicated, and the total number of eggs per spawn was calculated from the total volume of each egg suspension.

### Determination of ovarian stages and embryonic stages

The ovarian cycle in female broodstocks was classified into five stages, based on ovarian size and colour as reported by Chang & Shih (1995). Fig. 1A shows stages 0 or I, which are spawned and spent phases, respectively. These ovarian stages appear white and when observed through the carapace, they do not seem to be different. However, after spawning, the ovary appears loose and empty, as it contains collapsed ovarian pouches with only strands of follicular cells and connective tissue remaining; thus this is called stage 0 (Meeratana and Sobhon, 2007). In stage II (Fig. 1B, C) (proliferative) a small yellow mass of ovary could be observed dorsally under the carapace. In stage III (Fig. 1D, E) (premature), the ovary became orange. In stage IV (Fig. 1F, G) (mature), the reddish-orange ovary extended from behind the eye posteriorly to the first abdominal somite. These ovarian stages were confirmed by histological study (Fig. 2) based on the criteria described by Meeratana & Sobhon (2007). Fig. 3 shows embryonic stages: the newly spawned eggs were characterized into 3 stages by their colour, i.e., the light yellow to orange stage, which gradually changed to the brown stage, and finally to the black stage just before hatching.

### Determination of the mean oocyte diameters

Five stages of developing oocytes (Oc1, Oc2, Oc3, Oc4, and mOc) were classified according to Meeratana & Sobhon (2007). Fifty randomly selected oocytes at each stage in three widely separated ovarian sections from each animal were observed under the light microscope (LM). Diameters of the oocytes that contained full nuclear profiles were measured, and the data were expressed as the average diameters ± standard deviations.

### Statistical analysis

Statistical significance was analysed with an SPSS program using one-way analysis of variance (ANOVA) and Duncan's multiple range test. A probability value less than 0.05 ( $\underline{P}$ <0.05) indicated a significant difference. Data were presented as means  $\pm$  standard deviations.

### **RESULTS**

Effects of 5-HT, DA, and DA-antagonist on the ovary (Fig. 4A)

The ovarian maturation period (OMP) is defined as the time needed for the ovary to develop from stage I through stage II, III, and IV to spawning. The OMP of experimental subgroups that received 5-HT at doses of  $2.5 \times 10^{-5}$ ,  $2.5 \times 10^{-6}$  mol/prawn (~34 and ~29 days, respectively), all groups of 5-HT plus SP (~24, ~25, and ~31 days, respectively), as well as the group treated with SP at a dose of  $5.4 \times 10^{-7}$  mol/prawn (~34 days), were all significantly shorter (P<0.05) than those of CPS (~41 days), CPSE (~41 days), and NC (~39 days). All DA treated groups (~70, ~64, ~67 days, respectively), and OA treated groups (~63, ~60, ~60 days, respectively) exhibited significantly longer OMP (P<0.05) than those of the control groups.

### Effects on the embryonic development period (Fig. 4B)

The embryonic development period (EDP) is defined as the time needed from spawning to the appearance of the next black egg stage. The EDP of experimental groups that received 5-HT at doses of 2.5 x 10<sup>-5</sup> and 2.5 x 10<sup>-6</sup> mol/prawn (~20 and ~19 days, respectively), 5-HT plus SP at doses of 2.5 x 10<sup>-5</sup> mol of 5-HT/prawn plus 2.7 x 10<sup>-7</sup> mol of SP /prawn (~16 days), and SP alone at a dose of 2.7 x 10<sup>-7</sup> mol/prawn (~20 days), were all significantly shorter (P<0.05) than the EDP of CPS (~28 days), CPSE (~26 days), and NC (~25 days). All DA-treated (~49, ~47, ~48 days, respectively), and OA-treated groups (~46, ~42 days, respectively), exhibited a significantly longer EDP (P<0.05) than those of the control groups.

### Effects on GSI and oocyte diameters

Gonado-somatic index (GSI) (Fig. 5A)

When measured at days 14, 25, and 49, treatment with all doses of 5-HT, 5-HT plus SP, as well as SP alone, caused significantly higher GSI compared to those of the control groups. In contrast, treatment with all doses of DA and OA showed no significant difference in GSI compared to the control groups.

### Mean oocyte diameter (Fig. 5B)

Mean oocyte diameter of vitellogenic oocytes (Oc3, Oc4) and mature oocytes (mOc) of all groups of prawns treated with those of 5-HT, 5-HT plus SP, and SP alone, exhibited significant increases when compared with the control groups. In contrast, all groups of prawns treated with DA and OA showed significantly decreased diameters of these last three steps of oocytes when compared with the control groups.

### Effects on spawning

Number of spawned eggs (Fig. 6)

The number of eggs per spawn, after injection with 5-HT at doses of 2.5 x  $10^{-5}$ , 2.5 x  $10^{-6}$  mol/prawn (~92240 and 94,683 eggs, respectively), 5-HT plus SP at doses of 2.5 x  $10^{-5}$  mol/prawn plus 2.7 x  $10^{-7}$  mol/prawn, 2.5 x  $10^{-6}$  mol/prawn plus 2.7 x  $10^{-7}$  mol/prawn (~93,390 and ~93,270 eggs, respectively), and SP at a dose of 2.7 x  $10^{-7}$  mol/prawn (~91,163 eggs) were significantly higher (P<0.05) than the control groups (~68,826, ~69,554, and 70,053, for NC, CPS, and CPSE, respectively). In contrast, DA injected groups at the doses of 2.5 x  $10^{-5}$  and 2.5 x  $10^{-6}$  mol/prawn (~46,112 and ~49,756, respectively), and OA injected group at the dose of 2.5 x  $10^{-6}$  mol/prawn (~51,440 eggs) showed a lower number of eggs per spawn when compared to the control groups with significantly different (P<0.05). However, for other DA and OA injected groups, the data suggest that the number of eggs might be lower, but that the differences were not statistically significant (P>0.05).

Percentage of fertilized eggs (Fig. 7)

The number of fertilized eggs obtained after all of the treatments showed an equally good quality both among each other and in comparison with control groups as judged from the percentages of fertilized eggs, which were not statistically different.

### **DISCUSSION**

Injection of 5-HT in mature <u>Macrobrachium rosenbergii</u> females shortened the ovarian maturation period by about 10 days compared to control groups (~29 days for 5-HT vs ~41 days for CPSE, ~39 days for NC). 5-HT injection also shortened the embryonic development period by about 6-9 days compared to the control groups (~19

days for 5-HT vs ~28 days for CPS, ~26 days for CPSE, ~25 days for NC). Both results were significantly different ( $\underline{P}$ <0.05). 5-HT also caused significant increases in GSI index and mean oocyte diameter of vitellogenic and mature oocytes (from Oc3 to mOc), when compared with the control groups ( $\underline{P}$ <0.05).

There have been several previous studies of the effect of 5-HT on gonadal maturation in other decapods. It was suggested that in the crayfish, Procambarus clarkii, and the lobster, Homarus americanus, 5-HT may act indirectly on the gonads by stimulating the release of a putative gonadotropic factor, gonad stimulating hormone (GSH), from the thoracic ganglia, and/or by inhibiting the release of gonad inhibiting hormone (GIH) from the optic lobe in the eyestalk (Kulkarni et al., 1992; Fingerman 1997). GSH activity in the thoracic ganglia was increased by 5-HT administration in the crab, Uca pugilator (Bosc, 1802) (cf. Richardson et al., 1991) and the freshwater crayfish, P. clarkii (cf. Kulkarni et al., 1991). The crayfish, P. clarkii, treated with 5-HT also showed significant increases in ovarian index and oocyte diameter (Kulkarni et al., 1992). In the white shrimp, Litopenaeus vannamei, 5-HT at doses of 15 and 50 µg g<sup>-1</sup> BW induced ovarian maturation and spawning (Vaca & Alfaro, 2000). In the later report, it was demonstrated that 5-HT raised haemolymph vitellogenin 15-26 times over the normal level within 16 days in eyestalk-ablated M. rosenbergii female broodstock (Chen et al., 2003). Recently, it was also shown that the ovaries of Macrobrachium rosenbergii treated with the medium from 5-HT-primed thoracic ganglia exhibited higher numbers of oocytes that developed into the vitellogenic and the mature stage, despite pretreatment of the broodstocks with cyproheptadine (CYP), a 5-HT antagonist. This finding strongly suggested that 5-HT did not induce ovarian maturation directly, but through its action on the thoracic ganglia (Meeratana et al., 2006). As for the exact target and mechanism of action of 5-HT, Sáenz et al. (1997) reported that 5-HT could induce the bursting of action potentials and associated slow inward current in the intact X-organ axons as well as in the X-

organ neurons kept in culture. This bursting electrical activity by the X-organ neurons could mediate the release of CHH in the crayfish Orconectes limosus (Rafinesque, 1817) (Keller and Beyer, 1968). Similarly, 5-HT has been reported to elicit changes in the electrical activity of X-organ cells in the crabs Cardisoma carnifex (Herbst, 1794) and Podophthalmus vigil (Fabricius, 1798) (Nagano and Cooke, 1981). It was also reported that 5-HT could stimulate the release of molt-inhibit hormone (MIH) from the isolated eyestalks of crab, Cancer antennarius (Stimpson, 1856) by providing an excitatory input to MIH-containing neurosecretory cells (Mattson and Spaziani, 1985). Hence the primary target of 5-HT seems to be at the X-organ neurons. Whether it also affects the thoracic ganglion neurons directly remained to be studied.

SP, the DA antagonist, could also induce shorter ovarian maturation period (~34 days for SP vs ~41 days for CPS, ~41 days for CPSE, ~39 days for NC) and embryonic development periods (~ 20 days for SP vs ~28 days for CPS, ~26 days for CPSE, ~25 days for NC) than the control groups. Both results were statistically significant (P<0.05). The combined treatment, 5-HT plus SP, shortened the ovarian maturation period (~24 days) and embryonic development period (~16 days) even more than 5-HT-treated, SP-treated, and control groups. In vitro, SP has been shown to inhibit the secretion of a GIH-like factor from the eyestalks in Chasmagnathus granulata, which could explain its effect on the induction of ovarian growth (Zapata et al., 2003). In the penaeid shrimp, Litopenaeus stylirostris (Stimpson, 1874) and L. vannamei, combined treatment of 5-HT and SP not only induced ovarian maturation and spawning, but also stimulated the release of maturation promoting pheromones into the water (Alfaro et al., 2004). Our study is the first to report on the positive effects of 5-HT and SP alone, and in combination, on the development of ovaries and embryos of M. rosenbergii. The two chemicals appeared to be synergistic, and they might act

through the inhibition of GIH release and/or the stimulation of GSH release. This hypothesis needs, however, to be tested further.

Unlike 5-HT and SP, no dose of DA and OA shortened the ovarian maturation or embryonic development period. In the fiddler crab, <u>Uca pugilator</u>, it was shown that DA inhibits vitellogenin synthesis, either by inhibiting the release of GSH or by stimulating the release of GIH from the eyestalks, or through a combination of these two mechanisms (Sarojini et al., 1995e). Using HPLC, DA was detected in the brain and thoracic ganglia but not in the eyestalk of <u>M. rosenbergii</u> (cf. Chen et al., 2003). Taken together with the fact that DA was able to exert its effect in eyestalk-ablated prawns, it has been suggested that the action of DA on GIH release was unlikely in this species, and the most likely site of the action of DA could be at the thoracic ganglia through the inhibition of GSH release (Chen et al., 2003). It is presumed that DA exerts its inhibitory effect on vitellogenesis by acting indirectly via GSH, rather than directly on the target organ, the hepatopancreas (Chen et al., 1999). The action of OA on the gonads had not been studied previously. Our study is the first to show that this neurotransmitter exerts effects similar to those of DA, and that these effects may be mediated via the same mechanism as for DA.

Regarding the quantity and quality of the eggs, treatment with 5-HT, SP, and 5-HT plus SP resulted in significantly higher numbers of eggs per spawn than in the control groups (P<0.05). In contrast, DA and OA injected groups showed lower numbers of eggs per spawn than the control groups. The number of fertilized eggs obtained after all of the injections also showed equally good quality both among each other and in comparison with control groups. The number of eggs produced by each female was found to be directly proportional to the animal's size. A fully mature female might lay between 80,000 and 100,000 eggs per spawning, which is similar to that reported earlier (New, 2002). The fertilized eggs remained attached to the brood chamber between the pleopods for about 18–23 days after spawning.

The newly spawned eggs are characterized by a bright yellow to orange colour, which gradually changes to brown, and finally grey and black about 2–3 days before hatching. The quality of the spawned and fertilized eggs was equally good in all treatments, as the percentage of successfully developed zygotes was similar to those of the controls.

In summary, the present study shows that in <u>Macrobrachium rosenbergii</u>, 5-HT and SP exert a positive control, while DA and OA exert a negative control on ovarian maturation, oocyte development, and embryonic maturation, but these chemicals have no effect on spawning induction. In future, this knowledge could be adapted for improving prawn productivity.

### **ACKNOWLEDGEMENTS**

This research was supported by the Thailand Research Fund (Royal Golden Jubilee Ph.D. Program (Grant No. PHD/0171/2547) to Yotsawan Tinikul and Prasert Sobhon, Senior Research Scholar Fellowship to Prasert Sobhon), and the Commission on Higher Education (Research Group Development Grant to Prasert Sobhon). For technical assistance, we thank Ms. Ratchanok Cheotacha and Mr. Anurak Prabyai.

### REFERENCES

- ALFARO, J., G. ZUNIGA & J. KOMEN, 2004. Induction of ovarian maturation and spawning by combined treatment of serotonin and a dopamine antagonist, spiperone in Litopenaeus stylirostris and Litopenaeus vannamei. Aquaculture, **236**: 511 –522.
- BAUCHAU, A.G. & J. C. MANGEOT, 1966. Sérotonine et glycémie chez les crustacés. Experientia, 22: 238–239.
- CHANG, C.F. & T. W. Shih, 1995. Reproductive cycle of ovarian development and vitellogenin profiles in the freshwater prawn, <u>Macrobrachium rosenbergii</u>. Invertebr. Reprod. Dev., **27**: 11-20.
- CHANG, E.S., 1985. Hormonal control of molting in decapod crustacea. American Zool., **25**: 179–185.
- CHEN, Y.N., H.F. FAN, S.L. HAIEH & C. M. KUO, 2003. Physiological involvement of DA in ovarian development of the freshwater giant prawn, <u>Macrobrachium rosenbergii</u>. Aquaculture, **228**: 383–395.
- CHEN, Y.N., D.Y. TSENG, P.Y. HO & C.M. KUO, 1999. Site of vitellogenin synthesis determined from a cDNA encoding a vitellogenin fragment in the freshwater giant prawn, Macrobrachium rosenbergii. Mol. Reprod. Dev., 54: 215–222.
- FINGERMAN, M., 1997. Roles of neurotransmitters in regulating the reproductive hormone release and gonadal maturation in decapod crustaceans. Invertebr. Reprod. Dev., 31: 47-54.
- HERP, F. VAN. & D. SOYEZ, 1997. Arthropoda-Crustacea. In: R.G. Adiyodi, K.G. Adiyodi, T.S. Adams, (eds.), Reproductive biology of invertebrates, 3: 247-275. (John Wiley & Sons, New York).
- KELLER, R. & J. BEYER, 1968. Zur hyperglykämischen Wirkung von Serotonin und Augenstielextrakt beim Flusskrebs Orconectes limosus. Z. vergl. Physiol. **59**: 78–85.

- KULKARNI, G.K., L. GLADE & M. FINGERMAN, 1991. Oogenesis and effects of neuroendocrine tissues on in vitro synthesis of protein by the ovary of the red swamp crayfish <a href="Procambarus clarkii">Procambarus clarkii</a> (Girard). Journ. Crust. Biol., 11: 513–522.
- KULKARNI, G.K., R. NAGABHUSHANAM, G. AMALDOSS, R.G. JAISWAL & M. FINGERMAN, 1992. In vitro stimulation of ovarian development in the red swamp crayfish, <a href="Procambarus clarkii">Procambarus clarkii</a> (Girard), by 5-hydroxytryptamine. Invertebr. Reprod. Dev., 21: 231–240.
- MATTSON, M.P. & E. SPAZIANI, 1985. 5-hydroxytryptamine mediates release of molt inhibiting hormone activity from isolated crab eyestalk ganglia. Biol. Bull., **169**: 246–255.
- MEERATANA, P. & P. SOBHON, 2007. Classification of differentiating oocytes during ovarian cycle in the giant freshwater prawn, <u>Macrobrachium rosenbergii</u> De Man. Aquaculture, **270**: 249-258.
- MEERATANA, P., B. WITHYACHUMNARNKUL, P. DAMRONGPHOL, K. WONGPRASERT, A. SUSEANGTHAM & P. SOBHON, 2006. Serotonin induces ovarian maturation in giant freshwater prawn broodstock, <u>Macrobrachium rosenbergii</u> De Man. Aquaculture, **260**: 315–325.
- NAGANO, M. & I. M. COOKE, 1981. Electrical activity in the crab X-organ sinus gland system: site of initiation, ionic bases and pharmacology. In: Neurosecretion, molecules, cells, systems (eds): 504–505. (Plenum Press, New York).
- NEW, M.B., 2002. Farming freshwater prawns: a manual for the culture of the giant river prawn (Macrobrachium rosenbergii). FAO Fisheries Technical Paper, **428**: 1–10.
- RICHARDSON, H.G.D., M. DECARAMAN & M. FINGERMAN, 1991. The effect of biogenic amines on ovarian development in fiddler crab, <u>Uca pugilator</u>. Comp. Biochem. Physiol., (C) **99:** 53–56.

- RODRÍGUEZ, E.M., D.A. MEDESANI, L.S. LOPEZ GRECO & M. FINGERMAN, 2002. Effects of some steroids and other compounds on ovarian growth of the red swamp crayfish, <a href="Procambarus clarkii">Procambarus clarkii</a>, during early vitellogenesis. Journ. exp. Zool., 292: 82–87.
- SANDIFER, P.A. & T.J. SMITH, 1985. Freshwater prawn: crustacean and mollusk aquaculture in the United States: 1–15. (A Publishing Company Inc., West Port, Connecticut, USA).
- SÁENZ, F., U. GARCÍA & H. ARÉCHIGA, 1997. Modulation of electrical activity by 5-hydroxytryptamine in crayfish neurosecretory cells. Journ. Exp. Biol. **200**: 3079–3090.
- SAROJINI, R., R. NAGABHUSHANAM & M. FINGERMAN, 1995a. In vivo effects of DA and DArgic antagonists on testicular maturation in the red swamp crayfish, <u>Procambarus clarkii</u>. Biol. Bull., .........**189**: 340–346.
- neurotransmitter 5-hydroxytryptamine in stimulating ovarian maturation in the red swamp crayfish, <u>Procambarus clarkii</u>: an in vivo and in vitro study. Journ. exp. Zool., **271:** 395–400.
- SAROJINI, R., R. NAGABHUSHANAM, M. DEVI & M. FINGERMAN, 1995c. DArgic inhibition of 5-hydroxytryptamine-stimulated testicular maturation in the fiddler crab, <u>Uca</u> pugilator. Comp. Biochem. Physiol., (C) **111**: 287–292.
- VACA, A.A. & J. ALFARO, 2000. Ovarian maturation and spawning in the white shrimp, Penaeus vannamei, by serotonin injection. Aquaculture, 182: 373-385.
- ZAPATA, V., L.S. LOPEZ GRECO, D. MEDESENI & E.M. RODRIGEZ, 2003. Ovarian growth in the crab <u>Chasmagnathus granulata</u> induced by hormones and neuroregulators throughout the year. In vivo and in vitro studies. Aquaculture, **224**: 339-352.

### **CAPTIONS**

Fig. 1. Top views of females of the giant freshwater prawn, <u>Macrobrachium rosenbergii</u> (De Man, 1979), whose bodies were in both unflexed and flexed positions to show various ovarian stages: A, stage 0 or I appears grossly as there is no yellow mass of ovary under the carapace; B and C, stage II shows small yellow mass; D and E, stage III shows enlarged yellow mass; F and G, stage IV shows full yellow mass.

Fig. 2. Light micrographs of H&E-stained ovarian sections showing various steps of oocyte development in Macrobrachium rosenbergii (De Man, 1979): A, ovarian stage I; B, stage II; C, stage III; and D, stage IV. Oog, oogonia; Oc1, early previtellogenic oocyte; Oc2, late previtellogenic oocytes; Oc3, early vitellogenic oocytes; Oc4, late vitellogenic oocytes; mOc, mature oocytes (classified according to Meeratana & Sobhon, 2007). Scale bars, 50 μm.

Fig. 3. Various stages of developing embryos of <u>Macrobrachium rosenbergii</u> (De Man, 1979): A, yellow egg stage; B, orange egg stage; C, brown egg stage; and D, black egg stage.

Fig. 4. A, Ovarian maturation period (defined as the time for ovarian development from ovarian stage I to spawning); and B, Embryonic developmental period (defined as the time for egg development from spawning to black egg stage), after injections with various doses of 5-HT, DA, OA, SP, and 5-HT plus SP, when compared with the control groups (NC, CPS, CPSE). The numbers indicate doses of chemicals in various groups in mol/prawn for 5-HT, DA, OA, 5-HT plus SP, and SP alone. Asterisks indicate significant differences (P<0.05) with respect to the control groups; one asterisk indicates significantly shorter/longer OMP and EMP periods than control groups.

Fig. 5. A, Mean gonadosomatic index (GSI) determined at days 14, 25, and 49 after the prawns were injected with various doses of 5-HT, DA, OA, 5-HT plus SP, and SP alone when compared with the control groups (NC, CPS, CPSE); B, Mean oocyte diameters of vitellogenic oocytes (Oc3, Oc4, and mOc), after the prawns were injected with various doses of 5-HT, DA, OA, 5-HT plus SP, and SP alone, when compared with the control groups. The numbers indicate doses of chemicals in various groups in mol/prawn for 5-HT, DA, OA, 5-HT plus SP, and SP alone. Asterisks indicate significant differences (P<0.05) with respect to the control groups; one asterisk indicated significant increase/decrease of GSI and oocyte diameters, when compared with control groups.

Fig. 6. Number of eggs per spawn, after injection with various doses of 5-HT, DA, OA, SP, and 5-HT plus SP, when compared to the control groups. Asterisks indicate significant differences (P<0.05) when compared to the control groups.

Fig. 7. Percentage of fertilized eggs of all experimental groups, after injection with various doses of 5-HT, DA, OA, SP, and 5-HT plus SP when compared to the control groups.

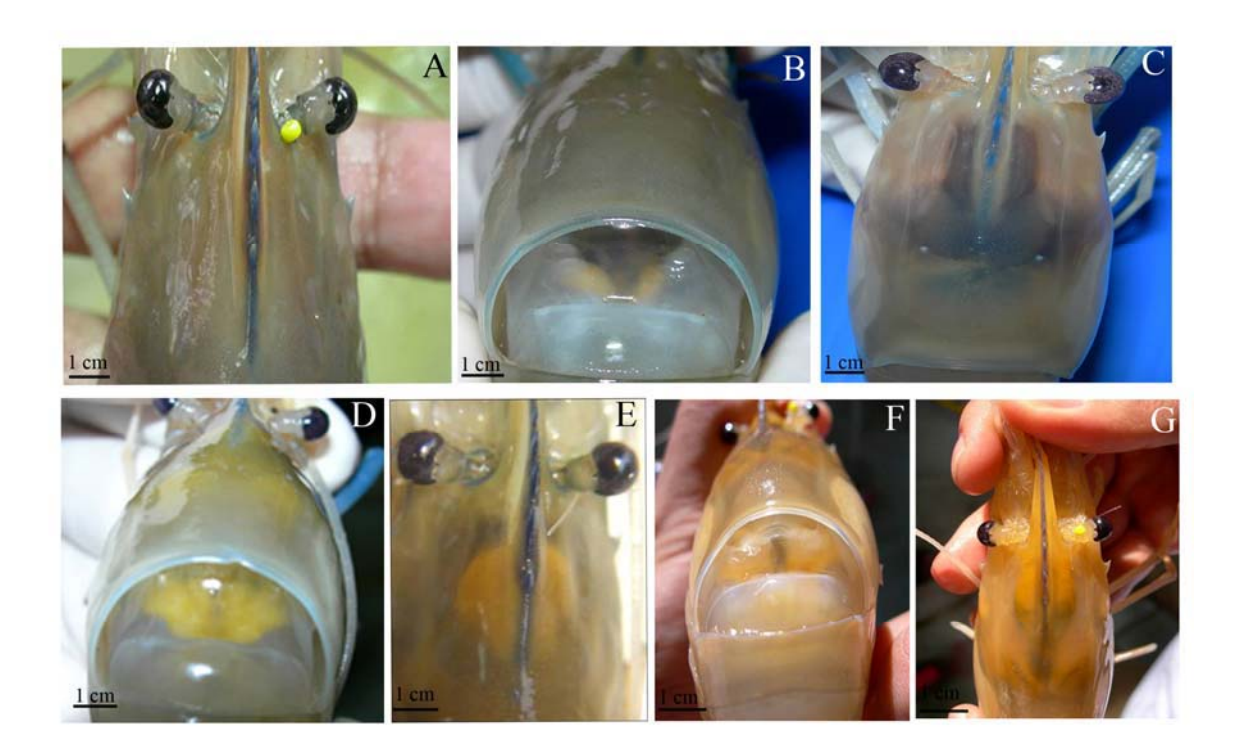


Figure 1

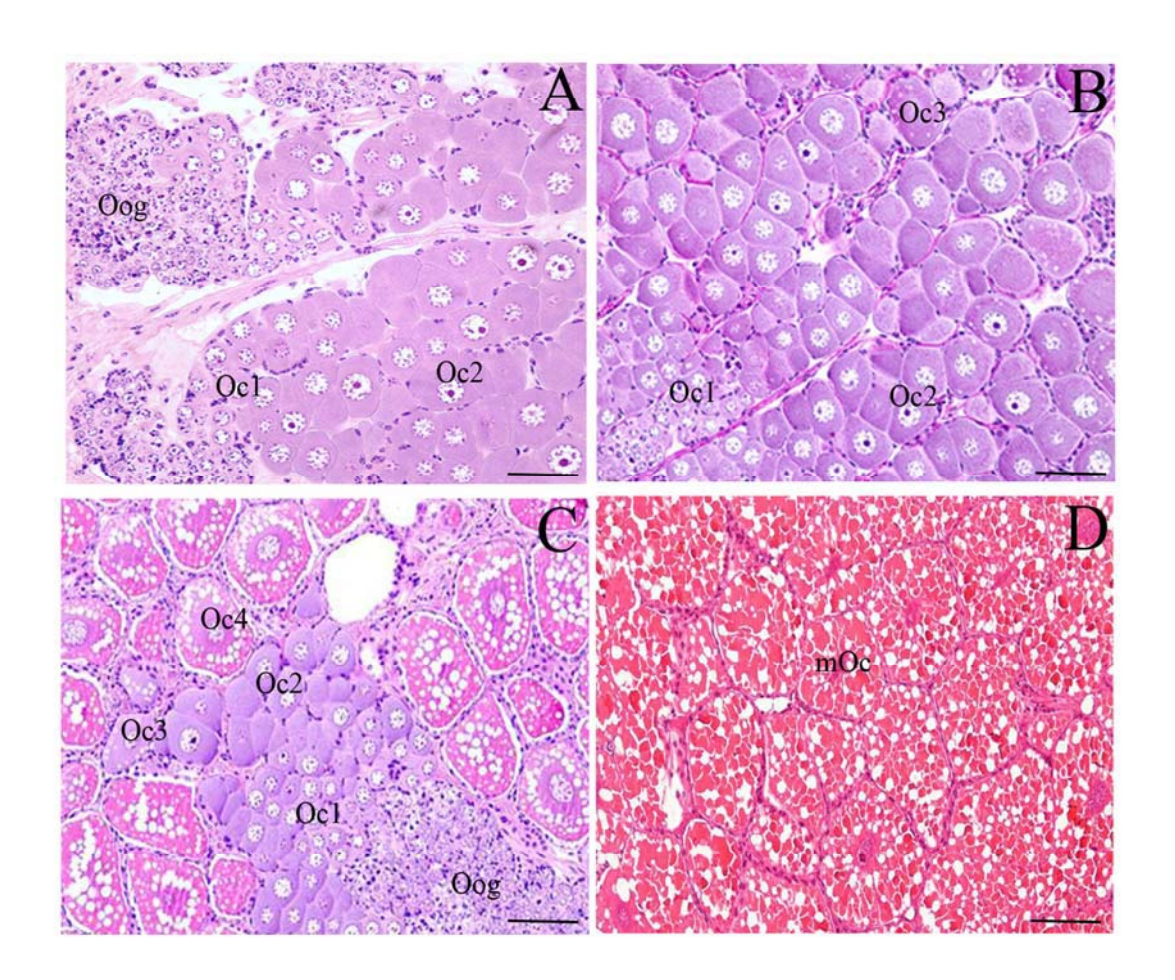


Figure 2

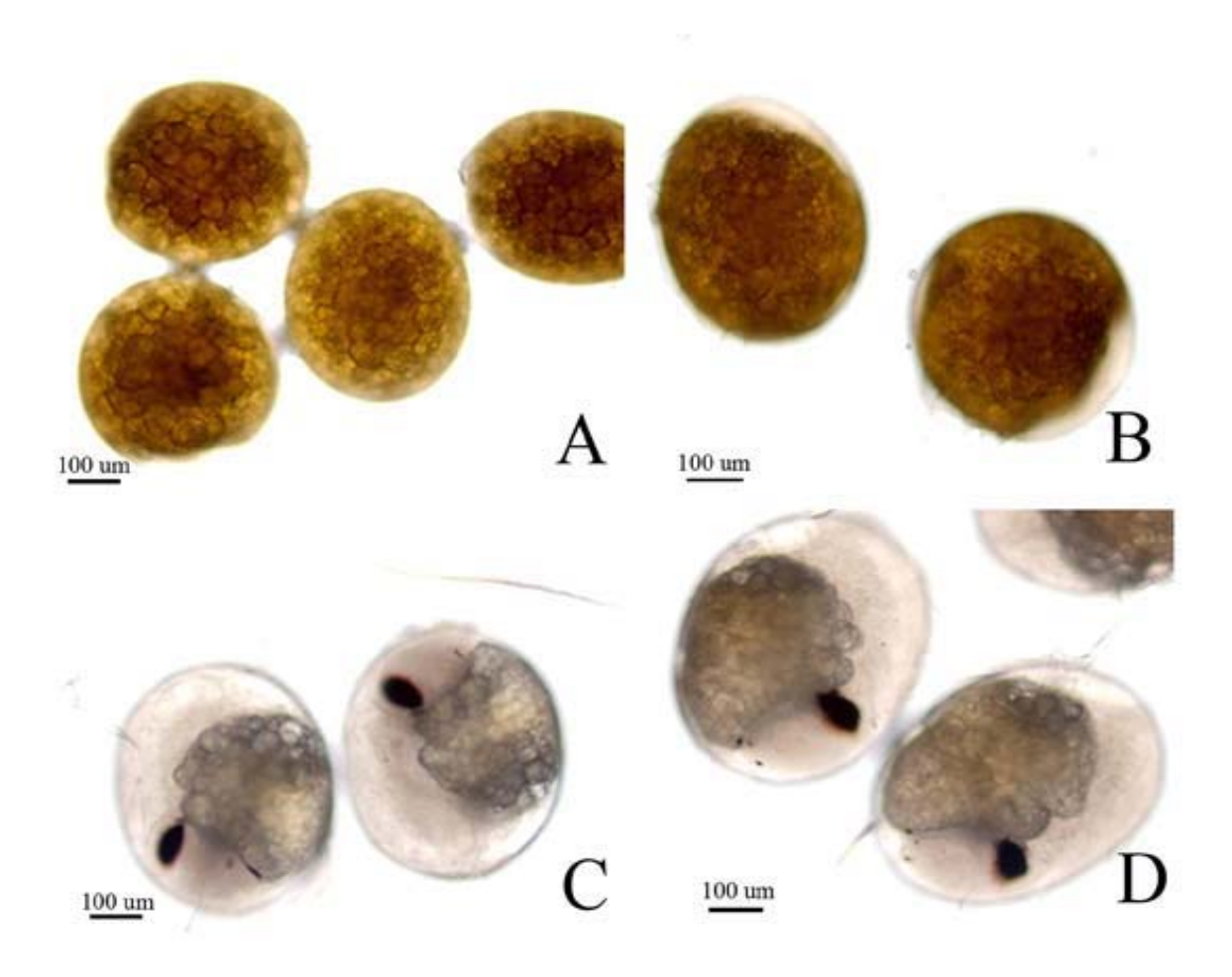
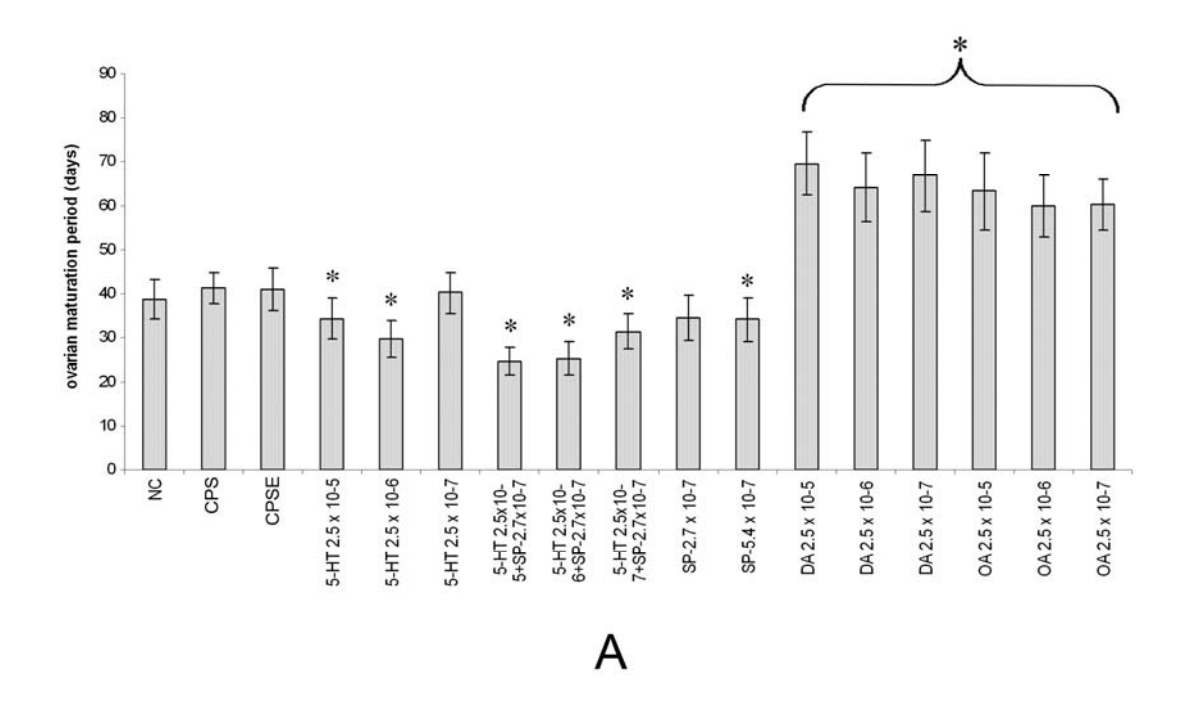
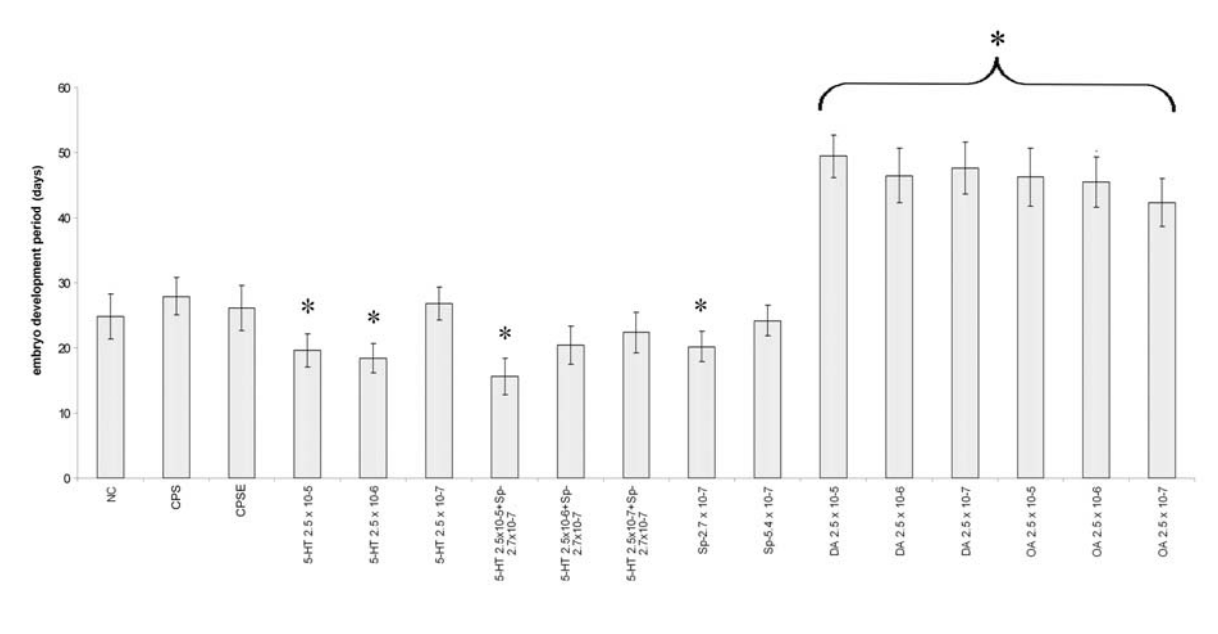


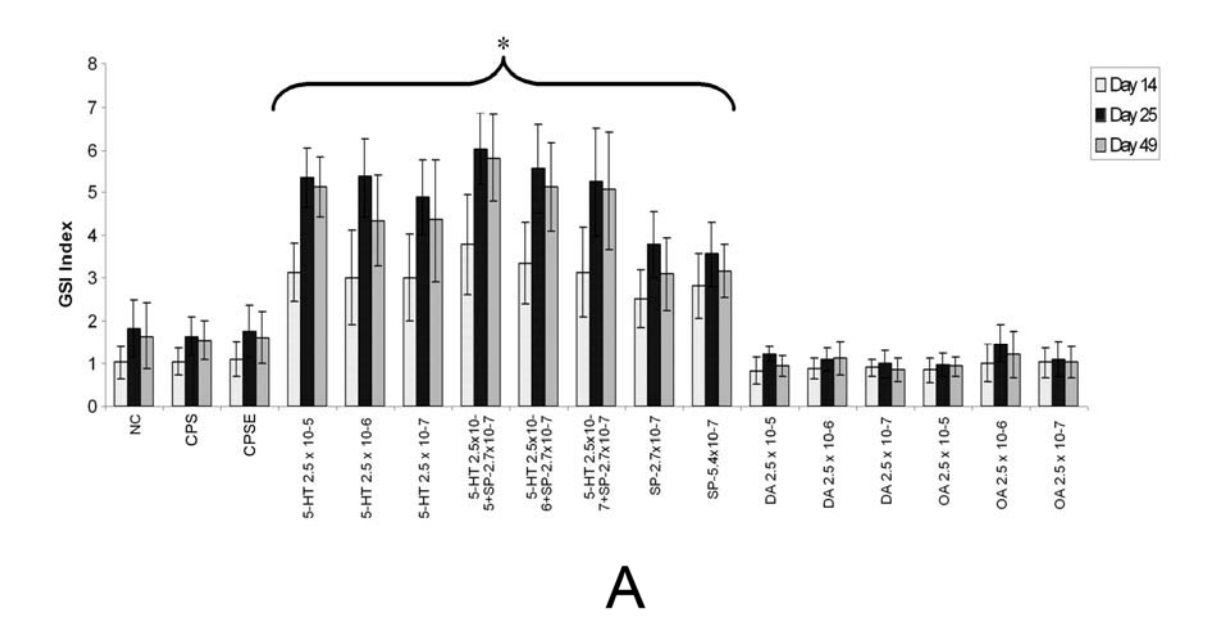
Figure 3.





В

Figure 4



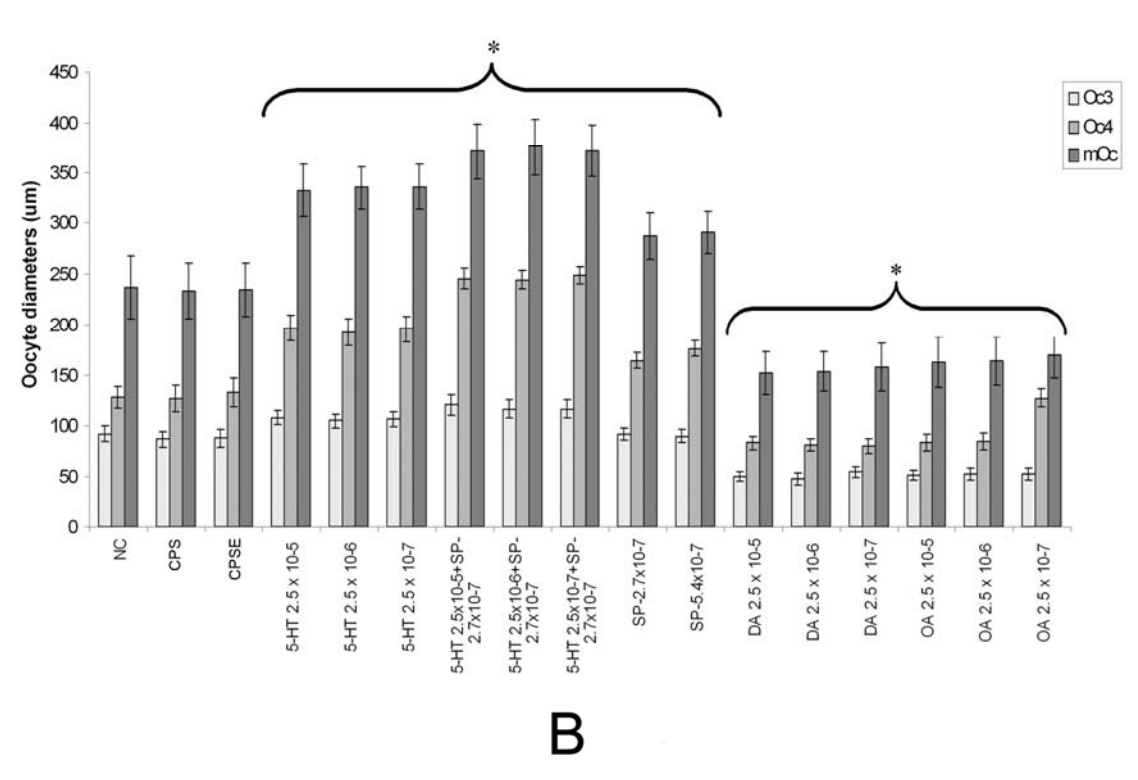


Figure 5

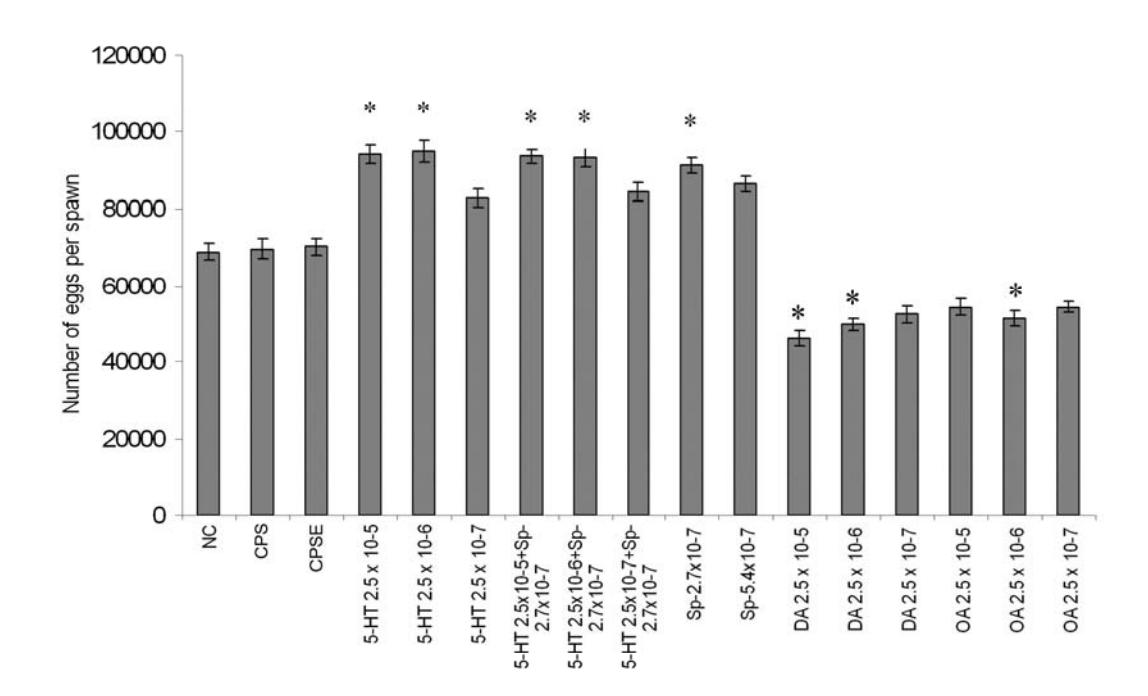


Figure 6

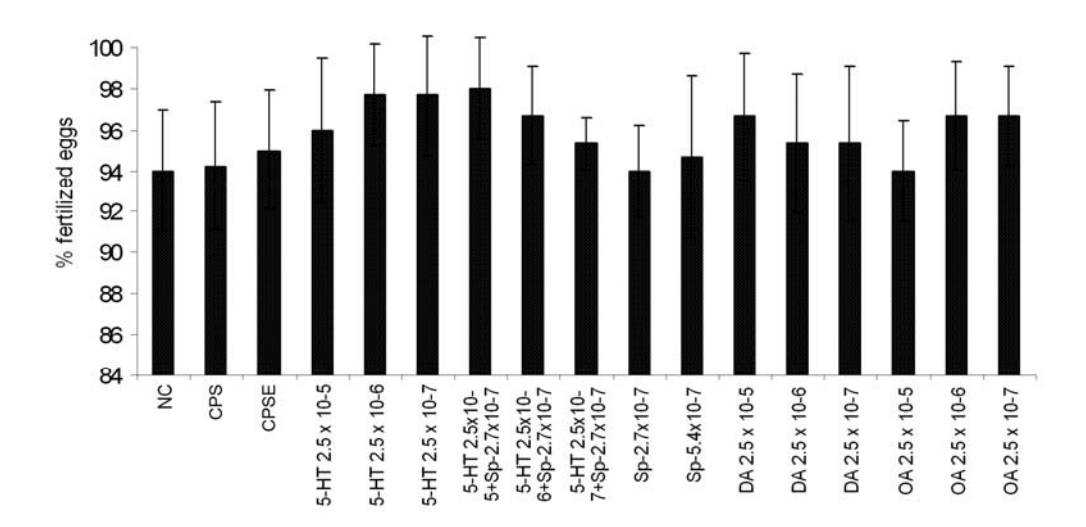


Figure 7.

1

Comparative distribution of a putative egg-laying hormone in neural

and reproductive tissues of four Decapoda crustaceans

Zhipeng Liu<sup>1</sup>, John Donald<sup>1</sup>, Peter Hanna<sup>1,2</sup>, Parinyaphon Nuurai<sup>2</sup>, Prasert Sobhon<sup>2</sup>

<sup>1.</sup> School of Life & Environmental Sciences, Deakin University, Geelong, VIC 3217

Australia

<sup>2.</sup> Department of Anatomy, Faculty of Science, Mahidol University, Bangkok 10400,

Thailand

**Corresponding author:** 

**Prof. Prasert Sobhon** 

**Department of Anatomy** 

**Faculty of Science** 

**Mahidol University** 

Bangkok 10400

Thailand

+66 - 2 - 2015406 Tel:

Email: scpso@mahidol.ac.th, anatch2002@yahoo.com

Abstract Evidence for the presence of a putative egg-laying (ELH) hormone has been previously described in the Black Tiger shrimp, *Penaeus monodon*, so a further investigation was carried out to detect its presence in a range of *Decapoda* crustaceans prior to a full molecular analysis. The crustaceans were represented by the Australian fresh water yabbie, Cherax destructor, the Australian southern rock lobster, Jasus edwardsii, the snow crab, Chionoecetes opilio, and the blue swimmer crab, Portunus pelagicus. Female cerebral ganglia, ventral nerve cords and gonads were investigated in a comparative study of the distribution of the immunoreactive hormone using immunoenzyme and immunofluorescence techniques. Immunoreactivity was detected in all tissues of interest, and the distribution patterns showed similarity within the four species, as well as that of P. monodon reported in the earlier study. There were minor variations. These data indicate that a putative ELH-like neuropeptide is widespread in crustaceans, and supports its previous identification in a range of molluscs and other invertebrates. Elucidation of the molecular structure of the peptide hormone and its encoding gene, as well as its involvement in spawning behaviour of crustaceans, is now fully under investigation.

**Keywords** Egg-laying like hormone – Decapoda crustaceans – Immunohistochemistry – Neurosecretory cells – Ovary – Oocytes

### Introduction

There is limited success in the natural spawning of cultured crustaceans, such as the black tiger shrimp, *Penaeus monodon*, and therefore the artificial spawning of these crustacean species relies primarily on the collection of eggs from wild broodstock (Hoang et al., 2002). This has raised further problems which include the depletion of wild stocks, unknown disease status, and genetic unreliability (Liu et al., 2006). Spawning of wild and cultured broodstock is usually achieved by eyestalk ablation of females, such as with the white Pacific shrimp, *P. vannamei* (Palacios et al., 1999), the black tiger shrimp, *P. monodon* (Primavera, 1978), and the Kuruma prawn, *P. japonicus* (Tsutsui et al., 2005).

Eye ablation is generally practiced by most commercial hatcheries, and is known to function by decreasing the amount of gonad-inhibiting hormone (GIH), also known as vitellogenesis-inhibiting hormone (VIH). This loss of hormone is due to the removal of a neuroendocrine secretory tissue called the X-organ which is located in the terminal medulla, as well as the associated sinus gland, all within the eye stalk (Desai and Achuthankutty, 2000). The GIH inhibits female reproduction, i.e. ovarian development, and especially vitellogenesis (Keller, 1992). However, after eyestalk ablation, subsequent spawning and larval survival are markedly reduced, necessitating the replacement of broodstock a few weeks after eyestalk ablation (Palacios et al., 1999).

An approach to obviate eye ablation in crustacean farming could be the use of techniques that increase reproductive hormone(s), such as the egg-laying hormone (ELH) identified in the sea hare, *Aplysia californica* (Scheller et al., 1982; Nambu and Scheller, 1986). This may be achieved by supplying excitatory hormone(s) in sufficient quantities to override the inhibitory hormones, such as GIH in crustaceans (Lacombe et al., 1999). It has been reported that spawning

of female molluscs can be achieved by injection of neural tissue homogenates from sexually mature females; examples include the sea hare, *Aplysia californica* (Kupferman, 1967), and the disk abalone, *Haliotis discus* (Yahata, 1973). As well, injection of a recombinant abalone ELH from *H. discus hannai* has been used to spawn ripe females of the California red abalone, *H. rufescens*, and the blacklip abalone, *H. rubra* (unpublished data). Therefore, a means to activate crustacean spawning could be through the characterisation and application of spawning inducing hormone(s). This method could lead to a convenient crustacean farming practice, compared with the current high cost of using wild spawners and relative lack of control in all species (Primavera, 1978).

Immunocytochemical studies have identified an ELH type of immunoreactivity in a range These include gastropod molluscs, such as the sea hare, A. californica of invertebrates. (Shyamala et al., 1986), the great pond snail, Lymnaea stagnalis (Vreugdenhil et al., 1988), the brown garden snail, Helix aspersa (Van Minnen et al., 1992), the Australian blacklip abalone, H. rubra (Cummins et al., 2001), the tropical abalone, H. asinina (Saitongdee et al., 2005), the giant garden slug, Limax maximus (Van Minnen et al., 1992), a few basommatophoran snails, including Bulinus truncates, B. glabrata, Listera ovata, Planorbarius corneus, P. planoribis and P. vortex (Roubos and van de Ven, 1987); the bloodfluke planorb, Biomphalaria glabrata; annelids, including the rhyonobdellid leech, Theromyzon tessulatum (Salzet et al., 1997); and arthropods, including the Colorado potato beetle, Leptinotarsa decemlineata, the flesh fly, Sarcophaga bullata, the migratory locust Locusta migratoria, the American cockroach Periplaneta Americana (Theunis et al., 1990), the fruit fly, Drosophila melanogaster (Herndon and Wolfner, 1995), and the black tiger shrimp, P. monodon (Liu et al., 2006). A sequence alignment of T. tessulatum LELH, A. californica ELH, A. parvula ELH and L. stagnalis CDCH, has shown conserved regions within the 36 amino acid peptides which could act as cross-reactive epitopes (Salzet et al., 1997). The *H. rubra* aELH peptide [LSITNDLRAIADSYLYDQHKLRERQEENLRRRFLRL], which is identical with CDCH except for Arg rather than Glu in residue 35 (Wang and Hanna, 1998), was used as the peptide to make antisera.

Although a putative ELH was recently identified in *P. monodon* (Liu et al., 2006), there has been no evidence for the putative neuropeptide being present in other crustaceans. Therefore, we carried out a comparative immunocytochemical study to investigate the presence of a putative ELH in four crustacean species, namely the Australian fresh water yabbie, *Cherax destructor*, the Australian southern rock lobster, *Jasus edwardsii*, the snow crab, *Chionoecetes opilio*, and the blue swimmer crab, *Portunus pelagicus*.

### Materials and methods

#### Animals and tissue preparations

*C. destructor* (n=5) were captured in a local reservoir at Deakin University, Waurn Ponds, Victoria, Australia; live *J. edwardsii* (n=3) and *C. opilio* (n=3) were obtained from a commercial seafood supplier in Melbourne, Australia. Paraffin embedded blocks of tissues of *P. pelagicus* (n=3) were produced at the Anatomy Department, Faculty of Science, Mahidol University, Bangkok, Thailand, from live animals obtained at a local seafood supplier. Only females were investigated in this research. Target tissues, i.e. cerebral ganglia, ventral nerve cords and ovaries, were dissected and fixed immediately in 20 volumes of 4% paraformaldehyde in phosphate-buffered saline (PBS), pH 7.4. The fixation was carried out at 4°C for 24 h, after which tissue samples were dehydrated in an ascending ethanol series (70%, 80% and 90%) and three final changes of 100% ethanol for 30 min each at room temperature. The ethanol in the tissue samples

was cleared using three changes of dioxane for 30 min each at room temperature, and the tissues were then embedded in melted Paraplastic Plus (Kendall) at 65°C with three changes of 30 min each. Serial sections of prepared blocks were cut with a Reichert-Jung microtome and mounted onto silane-coated slides. Before immunostaining, the tissue sections were dewaxed in three change of xylene for 2 min each, rehydrated in a descending ethanol series (100%, 90%, 80% and 70% for 2 min each), then running tap water for 5 min. The tissue sections were then stored in a moist chamber prior to immunostaining. Twenty sections of each tissue were used to confirm immunostaining.

#### **Immunostaining**

The primary polyclonal antibody was produced in mouse against expressed recombinant abalone (*H. rubra*) egg-laying hormone (aELH; Sequence is given in the Introduction section), at Mahidol University. Immunoenzyme studies utilised horse radish peroxidase (HRP) with an avidin-biotin amplification step. Rehydrated tissue sections were treated with 10% v/v H<sub>2</sub>O<sub>2</sub> in 80% v/v methanol to quench potential endogenous HRP activity. They were rinsed in PBS, and underwent a microwave treatment to nearly boiling in PBS for 15 min. The sections were blocked with 1% w/v gelatin in PBS for 30 min, and then 4% bovine serum albumin (BSA) and 2% goat serum w/v in PBS for another 30 min. Following this, the blocking solution was removed and primary antibody was applied. Sections were incubated at 4°C overnight, and then washed three times in PBS. Secondary antibody (i.e. biotinylated polyclonal goat anti-mouse IgG (Sigma), was applied and the sections were then incubated at room temperature for 45 min. Following another series of washes in PBS, as above, the sections were incubated with HRP-avidin conjugate (Sigma) for a further 45 min. This was followed by another series of washes in PBS, and a freshly prepared NovaRED<sup>TM</sup> (Vector Laboratory) substrate was then applied to

develop a colour reaction, which was stopped by rinsing in dH<sub>2</sub>O. The sections were then counterstained in 0.1% haematoxylin (Mayer), rinsed in dH<sub>2</sub>O, soaked in formulated tap water (i.e. 0.35% w/v NaHCO<sub>3</sub>, 2% w/v MgSO<sub>4</sub>) for 30 s and rinsed again in dH<sub>2</sub>O. Sections were finally mounted in aqueous mounting medium (DAKO) and examined under a Zeiss Axioskop MC 80 microscope. Images were captured with a Spot cooled CCD camera.

In immunofluorescence studies, and prior to the application of secondary antibody, sections were treated the same as for immunoenzyme preparations, except that the enzyme quenching step was omitted. After the washes in PBS, the sections were incubated in secondary antibody, a polyclonal sheep anti-mouse IgG-FITC conjugate (Sigma), in the dark for 45 min. Following further washes in PBS, in the dark, the sections were mounted in FITC-mounting medium (50% glycerol in PBS), and images were captured under a fluorescence microscope (Leica).

Positive controls for the two methods were performed using the primary antibody on sections of known immunoreactive abalone tissues, i.e. cerebral ganglia, pleuropedal ganglia, and gonads, of reproductively mature *H. asinina* and *H. rubra* female as used by Saitongdee et al. (2005) and Cummins et al. (2001). Negative controls were made by substituting the primary antibody incubation step with pre-immune mouse serum. As well, preabsorption controls were used to show specificity of the antiserum to ELH epitopes.

#### Results

ELH-immunoreactivity (ELH-ir) was observed in neural and ovarian tissues of the Decapods, *Cherax destructor*, *Jasus edwardsii*, *Chionoecetes opilio*, and *Portunus pelagicus*, and with similar distribution patterns to that previously observed in *Penaeus monodon*. All tissues

studied showed ELH-ir, viz the cerebral ganglia, ventral nerve cords connecting thoracic and abdominal ganglia, and gonads. However, there were some minor variations. Positive controls using *Haliotis rubra* and *H. asinina* sections all showed ELH-ir in the expected tissues and cells. In all negative controls using both immunoperoxidase and immunofluorescence, there was no detection of any positive ELH-ir (data not shown).

### Australian fresh water yabbie, Cherax destructor

ELH-ir was identified in the cerebral ganglion and the ventral nerve cord. In the cerebral ganglion region (Fig. 1A), dense ELH-ir was observed in the dorsal giant neurons (DGN), the olfactory lobe (OL), and in the neurons of the ventral paired lateral cluster (VPLC) or cluster 9 (LI-C9). It was also found in the interneuron cell cluster 11 (DCI-C11) of the central body (CB), in which the ELH-like peptide was located around the nuclei. In the ventral nerve cord (Fig. 1B, Fig. 5A), the ELH-ir was localised around the nuclei of small neural cells that were densely distributed along the nerve fibers of the cord (Fig. 1B).

In the ovary (Fig. 1C), ELH-ir was detected in the cells of ovarian capsule (OC) and the follicular cells which surround mature oocytes (Ocy). The ELH-ir were identified in most, but not all, follicular cells. Early previtellogenic oocyte stages were not detected in these ovarian sections and these lacked the sheath of follicular cells.

#### Australian southern rock lobster, Jasus edwardsii

ELH-ir was found to have an almost identical distribution to that observed in *C*. *destructor*. In the cerebral ganglion (Fig. 2A), ELH-ir was detected in the CB with highest staining density observed near the nuclei of the DCI-C9, and within the DCI-C11. However, there was low staining density in the OL and VPLC (data not shown). ELH-ir was also found in

the olfactory globular tract neuropil (OGTN), in which the staining was located around the nuclei of DGN. In the ventral nerve cord (Fig. 2B, Fig. 5B), ELH-ir was observed around nuclei in some small neurons within the nerve bundle, and these neurons also had positive granules in their axons.

In the ovary (Fig. 2C), ELH-ir was strong near the nuclei of most, but not all, follicular cells which surrounded mature oocytes (Ocy). Unlike the mature Ocy, the previtellogenic (POcy) stages exhibited some cytoplasmic ELH-ir.

#### Snow crab, Chionoecetes opilio

ELH-ir was detected in the OL, the VPLC and the ventral nerve cord. In the cerebral ganglion region (Fig. 3A), dense ELH-ir was observed in both the OL and the VPLC. In the OL, the ELH-ir was densely distributed around the nuclei of DGN. However, in the VPLC, ELH-ir was observed in the cytoplasm of neurons in LI-C9. There was a lower level of ELH-ir in the CB (data not shown). In the ventral nerve cord (Fig. 3B, Fig. 5C), dense ELH-ir was found in the axons and perinuclear region of neurons distributed among nerve bundles.

In the ovary (Fig. 3C), ELH-ir was detected in most, but not all, follicular cells which surrounded mature oocytes (Ocy). These oocytes did not show ELH-ir, whereas the early stage oocytes at the previtellogenic stages exhibited some cytoplasmic ELH-ir (Fig. 3C).

#### Blue swimmer crab, Portunus pelagicus

ELH-immunoreactivity was observed in both neural and reproductive tissues of *P*.

pelagisus. In the cerebral ganglion region (Fig. 4A), dense ELH-ir was observed in both the OL and CB, but low density immunoreactivity was found in the VPLC (data not shown). In the OL, ELH-ir was distributed mainly in the cytoplasm of DGN and neurons of the CB. In the ventral

nerve cord (Fig. 4B, Fig. 5D), dense ELH-ir was found within cells in the nerve capsule, but relatively little ELH-ir was found in the cells residing in the nerve bundles.

In the ovary (Fig. 4C), strong ELH-ir was observed around the nuclei of most of the follicular cells surrounding mature oocytes (Ocy). Early stage previtellogenic oocytes were not detected in these ovarian sections.

### **Discussion**

This research shows evidence for the existence for an ELH-like regulatory peptide in four Decapoda species: the Australian fresh water yabbie, *Cherax destructor*, the Australian southern rock lobster, *Jasus edwardsii*, the snow crab, *Chionoecetes opilio*, and the blue swimmer crab, *Portunus pelagicus*. It also reveals similar distribution patterns of ELH-ir in the selected female tissues, i.e. cerebral ganglia, ventral nerve cords and ovaries (Table 1).

Although ELH-ir was observed in the similar tissues and cell clusters within all four species, some differences of signal strength and specific locations were observed and are summarised in Table 1. For example, a strong ELH-ir signal was found in the olfactory lobe (OL) of *C. destructor*, *C. opilio* and *P. pelagicus*, but there was considerably less in *J. edwardsii*. Strong ELH-ir was observed around the nuclei of neural cells and within axons of *C. opilio* ventral nerve cord, but this was not present in the other species. A low level of ELH-ir was observed in *P. pelagicus* ventral nerve cord fibers, compared with a high level in the same structures of the other species. These differences could be due to the fact that animals used in this study were at different stages of gonad maturity (e.g. some previtellogenic oocytes were observed in *J. edwardsii* and *C. opilio* ovaries, but not in *C. destructor* and *P. pelagicus*).

In the ovary, most but not all follicular cells surrounding mature oocytes consistently showed strong immunoreactivity, a feature also characteristic of pre-spawned *P. monodon* which is lost following spawning (Lui et al., 2006). The loss of a putative ELH hormone during spawning could be linked to an active role in the release of oocytes. Previtellogenic oocytes, but not mature oocytes, also exhibited some immunoreactivity, which may indicate the role for the putative ELH hormone in stimulating the development of the early previtellogenic oocytes.

In the black tiger shrimp, *P. monodon*, ELH-ir was identified in the subesophageal-thoracic ganglia region and the supraesophageal ganglion which is known as the brain (Liu et al., 2006). In particular, the ELH-ir in the *P. monodon* brain was within the cytoplasm of the neurosecretory cells and neurons, and a similar pattern was observed in all four species investigated in this study. In eumalacostracan crustaceans, such as crayfish, lobster and crabs, the olfactory neuropil has a principal role in control of mating, feeding and territorial behaviours (Sullivan and Beltz, 2004). In these organisms, outputs from the OL which is the primary olfactory centre, are conveyed to the medulla terminalis and hemiellipsoid body in the lateral protocerebrum, a higher order centre, and this transmission is carried out by a large population of associated neurons (Sullivan and Beltz, 2004). These neurons showed ELH reactivity in the present study.

However, in the present study there were some ELH-ir variations and these are reported in Table 1. For example, some ELH-ir variations were within the OL, DGN, VPLC, LI-C9, DCI-C9, and DCI-C11. These may reflect a status of reproductive maturation as *J. edwardsii* and *C. opilio* appeared to be more sexually mature (see ovary results in Table 1).

In the ventral nerve cords of the four species, the ELH-ir was high, and tended to be denser along the nerve fibers. This may indicate that ELH might be transmitted to the more

caudal region of the CNS and possibly the gonads, thus a cascading mechanism might be involved for spawning control.

ELH was firstly identified in bag cells of the abdominal ganglia of the sea hare, *Aplysia californica*, (Kupfermann, 1967). Expression of ELH genes were later shown to occur, not only in the bag cells, but in an extensive system of neurons distributed in four of the five ganglia of the central nervous system (Scheller et al., 1982; McAllister et al. 1983). These locations are similar to the ELH immunoreactivity in the abdominal ganglia and associated ventral nerve cord of eumalacostracan crustaceans. ELH in *A. californica*, has been characterised as a 36 amino acid peptide (Chiu et al., 1979) acting as a neuromodulator from the abdominal ganglia (Branton et al., 1978), and alerting defined neurons (Mayeri et al., 1985). It is also distributed via the hemolymph throughout the individual, arriving at the target organ which is the female gonad, causing smooth muscle contraction and discharge of the eggs (Rothman et al., 1983). However, in terms of behaviour, ELH and associated peptides, cleaved from a preprohormone, generate a stereotypic repertoire during spawning (Garden et al., 1998), inducing cessation of walking, feeding inhibition, head weaving, and finally, egg expulsion (Scheller et al., 1982).

A seminal fluid protein, Acp26aa, identified in male *Drosophila melanogaster* was found to contain a conserved ELH region to *A. californica* ELH, and features to stimulate female spawning when transferred during mating (Herndon and Wolfner, 1995). This raises interest as to whether a similar process is also involved in crustacean reproduction, utilising a crustacean ELH-like hormone. A crustacean ELH might also be produced in males but requires further testing.

As indicated by the molluscs and insect ELH data, a crustacean ELH might play a multifunctional role in a spawning process. Signaled by either internal or external or both environmental factors for spawning. A crustacean ELH preprohormone might firstly be

expressed in neurosecretory cells located in cerebral ganglia (e.g. OL cells and VPLC cells) and certain neurons in the ventral nerve cord; this immature product was then distributed to the circulation and cleaved into different mature hormones before arriving at individual responsive targets, e.g. smooth muscles in trabaculae and capsule of the female ovaries; and therefore triggered defined activities, one of which is egg-laying. It is also possible that such a preprohormone or certain final product, i.e. ELH, could be produced by male individuals, transferred to and stored by females, which leads to spawning activities as above. Futhermore, the presence of strong ELH immunoreactivity in the follicular cells surrounding mature oocytes and in the cytoplasm of previtellogenic oocytes implies that this hormone may be involved in some way with the process of oocyte maturation.

In summary, a putative ELH in *Decapoda* crustacean has been identified, and as a consequence of its similar distribution in various crustaceans and molluscs, it is likely that the putative crustacean ELH serves as an endocrine factor in the spawning behaviour. Male crustaceans are now being investigated to determine whether they express a putative ELH. We are also investigating the molecular basis of the putative endocrine hormone for better understanding of its function in crustacean reproductive biology. The ability to reliably spawn female crustaceans using an egg-laying hormone, rather than the using eye ablation, would be very important to aquaculture production by having a regulated reproductive cycle. This would then provide for the selection of females with genetically desirable traits, including growth, colour and disease resistance.

# Acknowledgements

We thank Deakin University for a PhD scholarship to Z. Liu, the Thailand Research Fund (TRF) for a PhD scholarship to P. Nuurai and a Senior Research Fellowship to Professor P. Sobhon, and

the Commision on Higher Education (CHE) for a Research Group Development grant to P. Sobhon.

## References

- Branton WD, Arch S, Smock T, Mayeri E (1978) Evidence for mediation of a neuronal interaction by a behaviorally active peptide. Proc Nat Acad Sci USA 75:5732-5736
- Chiu AY, Hunkapiller MW, Heller E, Stuart DK, Hood LE, Strumwasser F (1979) Purification and primary structure of the neuropeptide egg-laying hormone of *Aplysia californica*. Proc Natl Acad Sci USA 76:6656-6660
- Cummins S, Thongkukiatkul A, Hanna PJ (2001) Location of egg-laying hormone in reproductive structures and neurons of *Haliotis rubra* (Leach) using antibodies raised against recombinant fusion proteins. J Shell Res 20:705-710
- Desai UM, Achuthankutty CT (2000) Complete regeneration of ablated eyestalk in penaeid shrimp, *Penaeus monodon*. Curr Sci 79:1602-1603
- Garden RW, Shippy SA, Li L, Moroz TP, Sweedler JV (1998) Proteolytic processing of the *Aplysia* egg-laying hormone prohormone. Proc Nat Acad Sci USA 95:3972-3977
- Herndon L, Wolfner M. (1995) A *Drosophila* seminal fluid protein, Acp26Aa, stimulates egg laying in females for 1 day after mating. Proc Natl Acad Sci USA 92:10114-10118
- Hoang T, Lee ST, Keenan CP, Marsden GE (2002) Observations on growth, sexual maturity and spawning performance of pond-reared *Penaeus merguiensis*. Aquac Res 33:863-873
- Keller R (1992) Crustacean neuropeptides: structures, functions and comparative aspects.

  Experientia 48:439-449
- Kupferman I (1967) Stimulation of egg laying: possible neuroendocrine function of bag cells of abdominal ganglion of *Aplysia californica*. Nature 216:814-815
- Lacombe C, Greve P, Martin G (1999) Overview on the sub-grouping of the crustacean hyperglycemic hormone family. Neuropeptides 33:71-80

- Liu Z, Sobhon, P, Withyachumnarnkul B, Hanna P (2006) Identification of a putative egg-laying hormone in neural and ovarian tissues of the black tiger shrimp, *Penaeus monodon*, using immunocytochemistry. Invert Neurosci 6:41-46
- McAllister LB, Scheller RH, Kandel ER, Axel R (1983) In situ hybridization to study the origin and fate of identified neurons. Science 222:800-808
- Mayeri E, Rothman BS, Brownell PH, Branton WD, Padgett L (1985) Nonsynaptic characteristics of neurotransmission mediated by egg-laying hormone in the abdominal ganglion of *Aplysia*. J Neurosci 5:2060-2077
- Nambu JR, Scheller RH (1986) Egg-laying hormone genes of *Aplysia*: evolution of the ELH gene family. J Neurosci 6:2026-2036
- Palacios E, Carreño D, Rodríguez-Jaramillo MC, Racotta IS (1999) Effect of eyestalk ablation on maturation, larval performance and biochemistry of white pacific shrimp *Penaeus vannamei*, broodstock. J Appl Aquac 9:1-23
- Primavera JH (1978) Induced mauration and spawning in five-month-old *Penaeus monodon*Fabricius by eyestalk ablation. Aquaculture 13:355-359
- Rothman BS, Weir G, Dudek FE (1983) Egg-laying hormone: Direct action on ovotestis of *Aplysia*. Gen Comp Endocrinol 52:134-141
- Roubos EWR, van de Ven AMH (1987) Morphology of neurosecretory cells in basommatophoran snails homologous with egg-laying and growth hormone producing cells of *Lymnaea stagnalis*. Gen Comp Endocrinol 67:7-23
- Saitongdee P, Apisawetakan S, Anunruang N, Poomthong T, Hanna PJ, Sobhon P (2005) Egglaying-hormone immunoreactivity in the neural ganglia and ovary of *Haliotis asinina* Linnaeus. Invert Neurosci 5:165-172

- Salzet M, Verger-Gocquet M, Vandenbulcke F.Minnen JV (1997) Leech egg-laying-like hormone: structure, neuronal distribution and phylogeny. Mol Brain Res 49:211-221
- Scheller RH, Jackson JF, McAllister LB, Schwartz JH, Kandel ER, Axel R (1982) A family of genes that codes for ELH, a neuropeptide eliciting a stereotyped pattern of behavior in *Aplysia*. Cell 28:707-719
- Shyamala M, Nambu JR, Scheller RH (1986) Expression of the egg-laying hormone gene family in the head ganglia of *Aplysia*. Brain Res 371:49-57
- Sullivan JM, Beltz BS (2004) Evolutionary changes in the olfactory projection neuron pathways of Eumalacostracan crustaceans. J Comp Neurol 470:25-38
- Theunis W, Van Minnen J, De Loof A (1990) Immunocytochemical localization in the central nervous system of four different insect species of molecules immunoreactive against peptides present in the causodorsal cells of *Lymnaea stagnalis*. Gen Comp Endocrinol 79:415-422
- Tsutsui N, Kim YK, Jasmani S, Ohira T, Wilder MN, Aida K (2005) The dynamics of vitellogenin gene expression differs between intact and eyestalk ablated kuruma prawn *Penaeus (Marsupenaeus) japonicus*. Fish Sci 71:249-256
- Van Minnen J, Schallin HDFH, Ramkema MD (1992) Identification of putative egg-laying hormone containing neuronal systems in *gastropod molluscs*. Gen Comp Endocrinol 86:96-102
- Vreugdenhil E, Jackson JF, Bouwmeester T, Smit AB, Van Minnen J, Van Heerikhuizen H, Klootwijk J, Joosse H (1988) Isolation, characterization, and evolutionary aspects of a cDNA clone encoding multiple neuropeptides involved in the stereotyped egg-laying behavior of the fresh water snail *Lymnaea stagnalis*. J Neurosci 8:4184-4191

Wang L, Hanna PJ (1998). Isolation, cloning, and expression of a DNA sequence encoding an egg-laying hormone of the blacklip abalone (*Haliotis rubra* Leach). J Shellfish Res 17:789-793

Yahata T (1973) Induced spawning of abalone (*Nordotis discus* REEVE) injected with ganglional suspensions. Bull Jap Soc Sci Fish 39:1117-1122

### Figure legends

Fig. 1 Immunocytochemical detection of ELH in C. destructor tissues. Mouse anti H. rubra ELH polyclonal antibody as primary antibody, biotinylated goat anti mouse IgG monoclonal antibody as secondary antibody, avidin linked horse radish peroxidase (HRP) as tertiary binding, and a NovaRED substrate, were used for visualization of ELH. Reactions at the black arrows indicate ELH immunoreactive cells and the white arrow indicates no ELH detection. High magnification insets are shown. A. Section of the cerebral ganglion showing the olfactory lobe (OL), with ELH immunoreactive dorsal giant neurons (DGN), the ventral paired lateral cluster (VPLC), with ELH immunoreactive local interneurons cluster 9 (LI-C9), and the central body (CB) containing an ELH positive deutocerebral commissure interneurons cell cluster 11 (DCI-C11) and DGN. A high density of ELH is observed within the cytoplasm of LI-C9 in the VPLC (inset 1), and around the DGN nuclear region in OL (inset 2). **B**. A section of the ventral nerve cord showing the ventral nerve capsule (VNC) and the ventral nerve neurofibres (VNF). ELH is mainly distributed in the axon of neurons within the neurofibres, as indicated in the inset. C. An ovarian section showing the ovarian capsule (OC), oocyte (Ocy) and the surrounding connective tissue. High power inset showing ELH immunoreactivity around the nuclei of the positive follicular cells and some connective tissue in the OC. Scale bars are 100 µm in A-C, and 10 µm in insets.

**Fig. 2** Immunocytochemical detection of ELH in *J. edwardsii* tissues, using the same technique as in Fig. 1. Black arrows indicate ELH positive cells and the white arrow indicates an ELH negative cell. High magnifications are shown in insets. **A.** A section of the cerebral ganglion showing the CB and OGTN containing DCI-C9, DCI-C11 and DGN, all of which are

immunoreactive for ELH. Inset shows a high density of ELH around the nucleus in a DCI-C11 cell of the CB. **B.** A section of the ventral nerve cord showing the VNC and VNF. The majority of ELH is located in the axons of neurons within the VNF, and shown by the inset. **C.** An ovarian section showing the trabaculae (Tr) and Ocy. High power inset shows intense ELH immunoreactivity around the nuclei of many follicular cells. Scale bars are  $100 \mu m$  in A-C, and  $10 \mu m$  in insets.

Fig. 3 Detection of ELH in *C. opilio* tissues, using the same immunocytochemistry technique as in Fig. 1. Black arrows indicate ELH positive cells and the white arrow indicates an ELH negative cell. High magnification insets are shown. **A.** A cerebral ganglion section showing the OL and VPLC, containing ELH immunoreactive DGN and LI-C9 cells, respectively. High density of ELH signal is observed around the nuclei of the DGN in the OL (inset 1), and in the cytoplasm of cells in LI-C9 within the VPLC (inset 2). **B.** A section of the ventral nerve cord showing VNC and VNF. Insets show ELH distribution occurs around the nucleus and along the axon of a neuron. **C.** An ovarian section showing the Tr and Ocy. ELH immunoreactivity is identified around the nuclei of many follicular cells which surround each Ocy. Scale bars are 100 μm in A-C, and 10 μm in insets.

**Fig. 4** ELH detection in *P. pelagicus* tissues, using the same immunocytochemistry technique as in Fig. 1. Black arrows indicate ELH positive cells and the white arrow indicates an ELH negative cell. High magnification insets are shown. **A.** A cerebral ganglion section showing the OL and CB, which contain DGN and LI-C9 respectively. Inset shows a high density of ELH signal around the nuclei of DGN in the OL. **B.** A section through the ventral nerve cord showing the VNC and VNF. ELH appears to be located more around the nuclei of the VNC cells than in

neurons of the VNF (see inset). C. An ovarian section showing oocytes (OC) and eggs (E). The inset shows ELH immunoreactivity around the nuclei of the follicular cells surrounding an egg. Scale bars are  $100 \, \mu m$  in A-C, and  $10 \, \mu m$  in insets.

Fig. 5 ELH immunofluorescence confirming the ELH immunoenzyme results represented by nerve cells within the VNC of the four species investigated. Mouse anti *H. rubra* ELH polyclonal antibody was used as the primary antibody and fluorescein isothiocyanate-labelled sheep anti mouse IgG monoclonal antibody used as the secondary antibody, and green fluorescence represents a positive ELH immunoreactive signal. A. C. destructor. B. J. edwardsii. C. C. opilio. D. P. pelagicusis. Scale 10 μm.

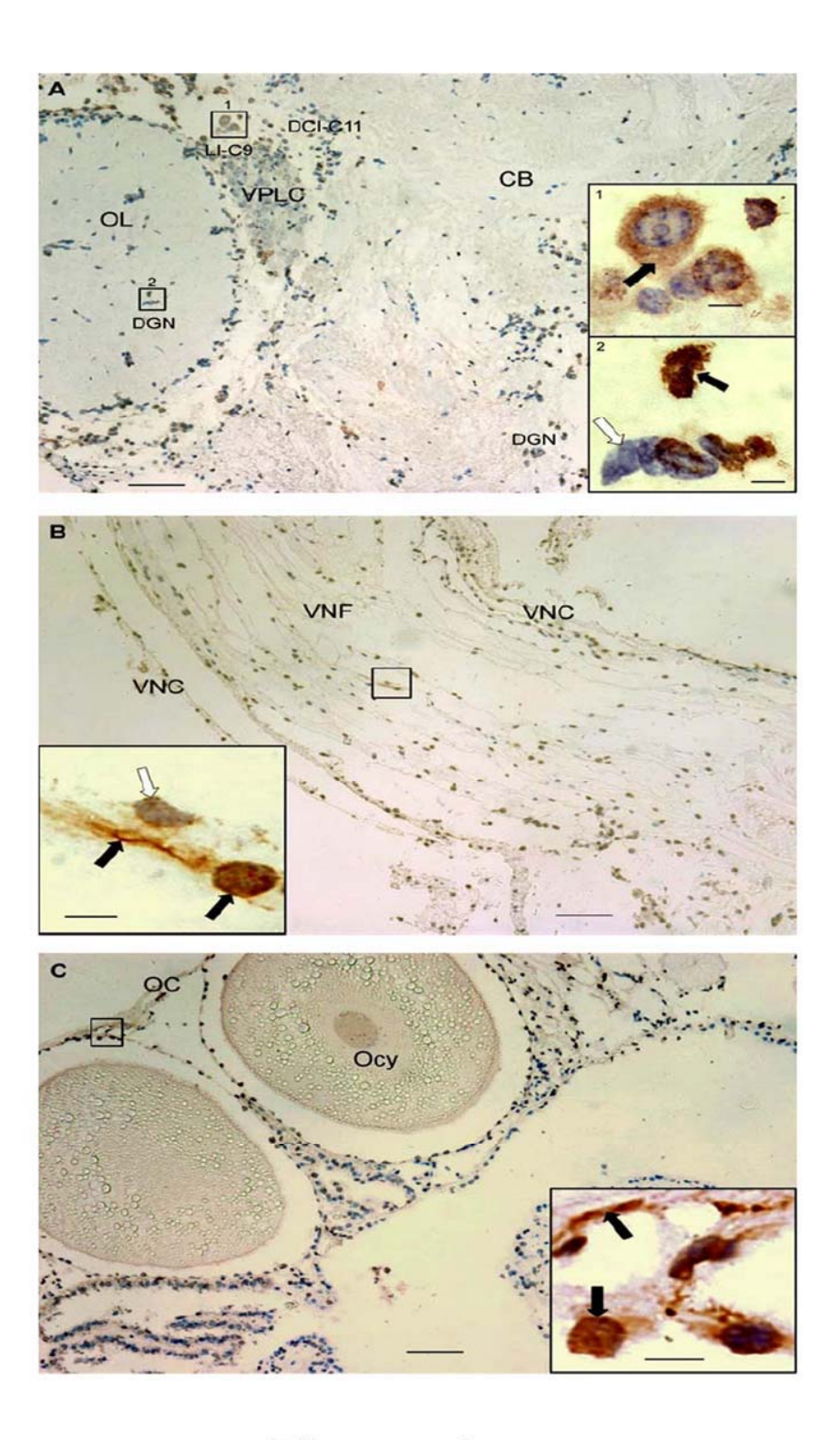


Figure 1

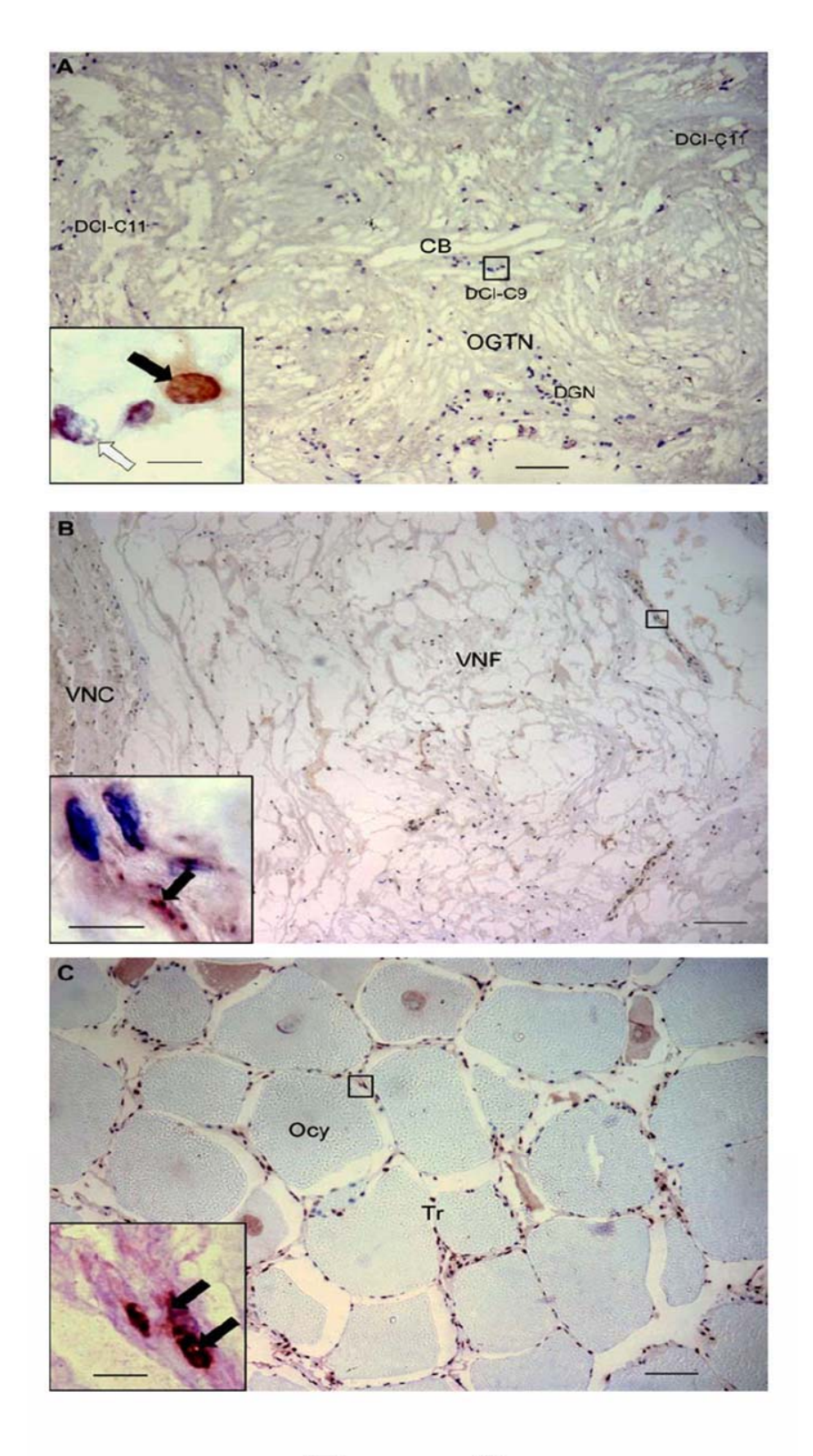


Figure 2

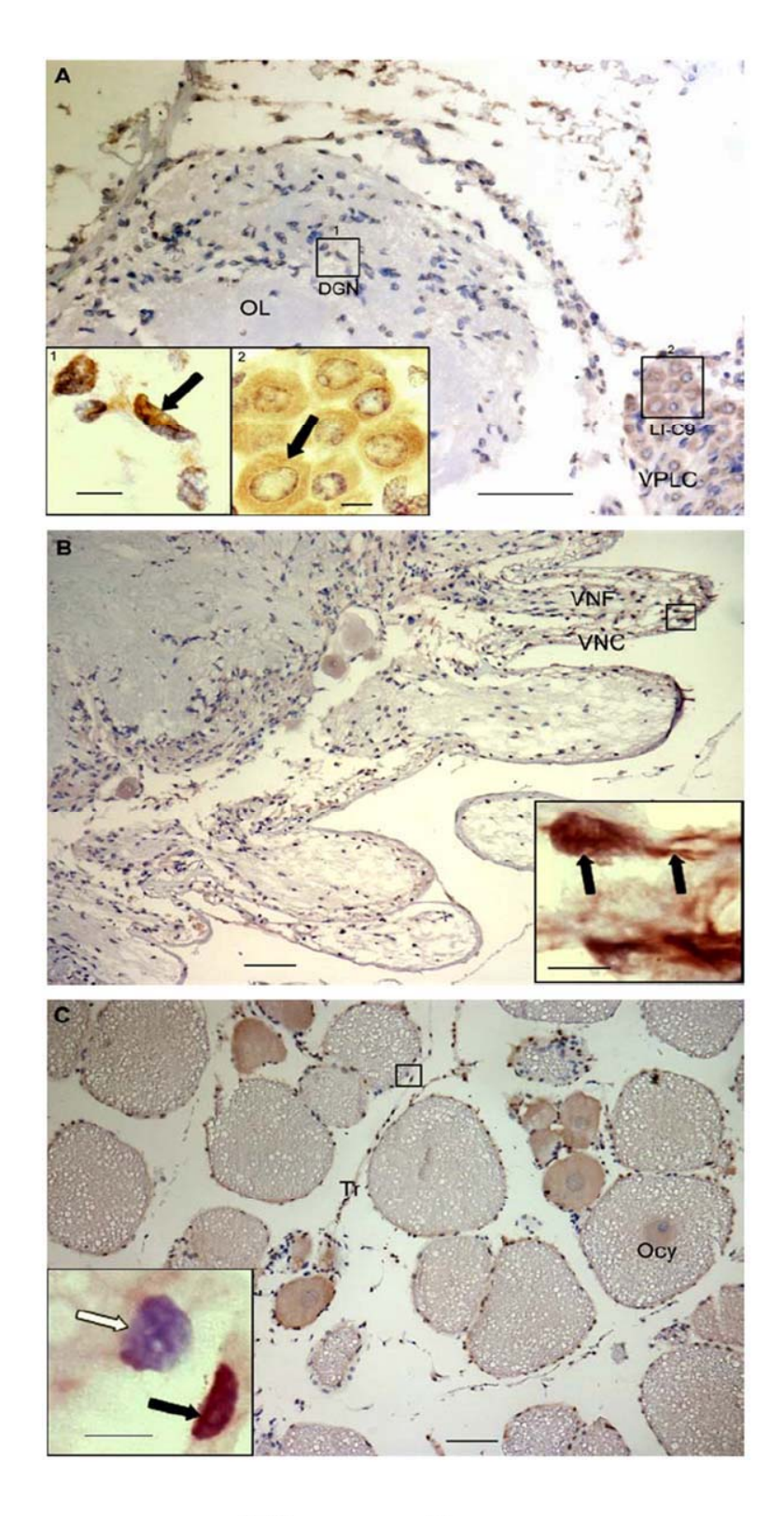


Figure 3

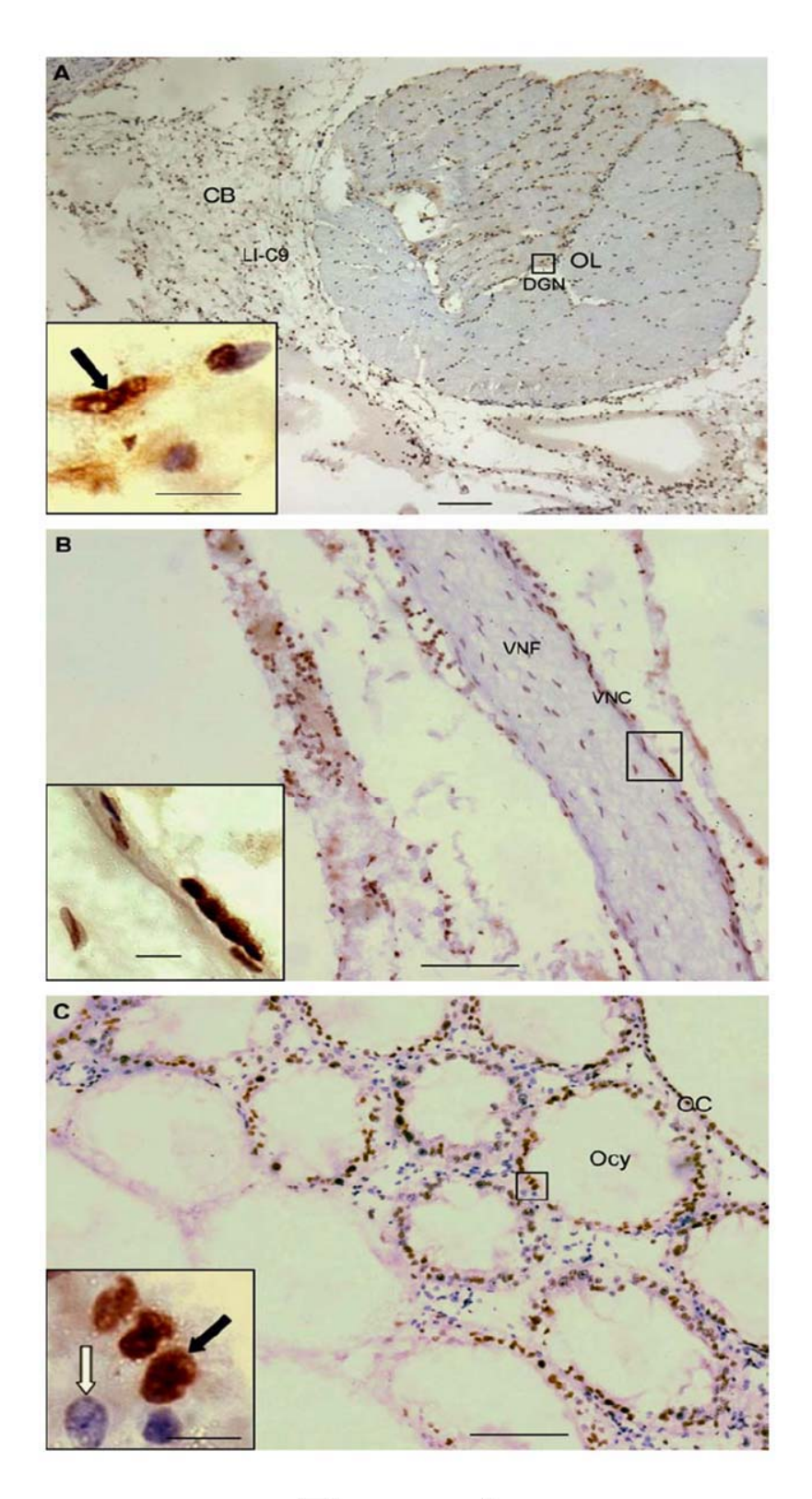


Figure 4

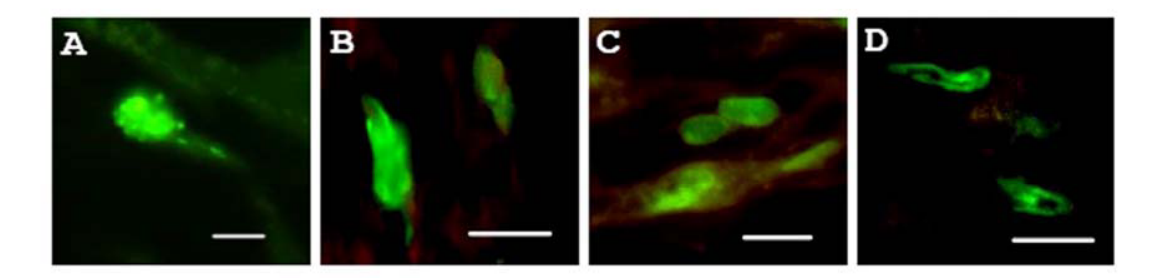


Figure 5

Table 1. Relative density of ELH-immunoreactivity in neural and ovarian tissues.

		Cephalothorax										
Species	Cerebral ganglia						ventral nerve cord			Ovary		
	OL	DGN	VPLC	LI-C9	DCI-C9	DCI-C11	Neurons	Axons	FC	Tr	Pre-Ocy	
Cherax destructor	high	high	high	high	medium	medium	medium	high	medium	medium	NO	
Jasus edwardsii	low	medium	low	medium	high	high	medium	high	medium	medium	high	
Chionoecetes opilio	high	high	high	medium	high	medium	medium	high	high	high	high	
Portunus pelagicus	high	high	low	medium	medium	medium	medium	medium	medium	medium	NO	

Ol, Olfactory Lobe; DGN, Dorsal Giant Neuron; VPLC, Ventral Paired Lateral Cluster; LI-C9, Local Interneurone Cluster 9; DCI-C9,
Deutocerebral Commissure Interneurone Cluster 9; DCI-C11, Deutocerebral Commissure Interneurone Cluster 11; FC, Folicular Cells;
Tr, Trabaculae; Pre-Ocy, Pre-vitellogenic Oocyte (Note: mature Ocy negative), NO, Not Observed.

# Molecular Characterization and Analysis of a Truncated Serotonin Receptor Gene Expressed in Neural and Reproductive Tissues of Abalone.

Sasiporn Panasophonkul<sup>1</sup>, Somjai Apisawettakan<sup>1</sup>, Scott F. Cummins<sup>3</sup>, Patrick S. York<sup>3</sup>, Bernard M. Degnan<sup>3</sup>, Peter J. Hanna<sup>1,2</sup>, Porncharn Saitongdee<sup>1</sup>, Prasert Sobhon<sup>1</sup>, Prapee Sretarugsa<sup>1\*</sup>

1 Department of Anatomy, Faculty of Science, Mahidol University, Bangkok, 10400, Thailand

Deleted: St. Lucia

Abbreviated Title (40 characters or less): Truncated 5-HT Receptor in Abalone

\*Correspondence author and requests for reprints: Dr. Prapee Sretarugsa, Department of Anatomy, Faculty of Science, Mahidol University, Bangkok, 10400, Thailand. Email: <a href="mailto:scpsr@mahidol.ac.th">scpsr@mahidol.ac.th</a>

Three Key Words: Serotonin receptor, Abalone, Reproduction

Supporting Grants: This work was supported by the Thailand Research Fund (Royal Golden Jubilee Ph.D. Program, Grant No. PHD/0150/2543 to S. Pansophonkul and P. Sretarugsa), the Commission on Higher Education with a grant to P. Sobhon, a University of Queensland Fellowship to S. Cummins and ARC grants to BMD.

 $\textbf{Deleted:}\ s$ 

Deleted: and

<sup>2</sup> School of Life & Environmental Sciences, Deakin University, Geelong, VIC 3217, Australia

<sup>3</sup> School of Integrative Biology, University of Queensland, <u>Brisbane</u>, QLD 4072, Australia

In molluscs, the neurotransmitter serotonin (5-HT) has been linked to a variety of biological roles including gamete maturation and spawning. Physiological functions associated with 5-HT, are mediated through binding to 5-HT receptors. A cDNA encoding a putative 5-HT receptor consisting of 359 amino acids was isolated from the tropical abalone Haliotis asinina, termed 5-HT<sub>1Hal</sub>. The 5-HT<sub>1Hal</sub> seems like an odd naming convention – how about Has-5HT1 shares Gprotein-coupled receptor motifs with metazoan 5-HT receptors, including predicted transmembrane domains, active sites for protein kinase action, and N-linked glycosylation sites. However, the third intracellular loop of 5-HT<sub>1Hal</sub> is relatively short, and only six transmembrane domains are predicted, implying a truncated receptor. Phylogenetic analysis with known 5-HT receptor genes suggests that 5-HT<sub>1Hal</sub> belongs to the type 1 5-HT receptor family. Expression analysis by RT-PCR showed that 5-HT<sub>1Hal</sub> mRNA was present in all tissues examined, including the neural ganglia and gonad tissues. Immunocytochemistry revealed the presence of 5-HT<sub>1Hal</sub> specifically within the soma of neuronal cells located in the outer cortex of both cerebral and pleuropedal ganglia. In ovarian and testicular tissues,  $5\text{-HT}_{1\text{Hal}}$  immunoreactivity was observed in epithelial cells of the outer capsule and connective tissue of the trabeculae to which the gamete follicles adhere. The possible involvement of 5-HT in oocyte and sperm release was demonstrated by a dose-dependent increase in Haliotis rubra gonad contractile bioactivity following 5-HT stimulation.

vertebrate

Deleted: invertebrate and

Deleted: homolog

*Abbreviations*: AEBSF, 4-(2-Aminoethyl) benzenesulfonyl fluoride; cg, cerebral ganglia; ppg, pleuropedal ganglia; fgo, female gonad; mgo, male gonad; GAFS, Gomori's aldehyde-fuchsin staining; 5-HT, 5-hydroxytryptamine, serotonin; 5-HT<sub>1Hal</sub>, abalone serotonin receptor; 5-HT<sub>1Hal</sub>-ir, 5-HT<sub>1Hal</sub> immunoreacitivity; TM domains, transmembrane domains; RT-PCR, reverse transcription-polymerase chain reaction.

SEROTONIN (5-HT, 5-hydroxytryptamine) has been established as a major neurotransmitter in vertebrates and invertebrates. In molluscs, bioassays, as well as electrophysiological, immunocytochemical and genetic studies, have implicated it in behaviours and physiological processes such as sensitisation, feeding, development, and locomotion (Rathouz and Kirk, 1988, Croll, 1988; Barlow and Truman, 1991, Kuhl *et al.*, 1992, Satterlie *et al.*, 1995). Serotonin also plays an important role in reproduction through the biosynthesis and release of active egg-laying peptides precursor proteins, gamete maturation, and the control and initiation of gamete release in several molluscan species (Ram *et al.*, 1992, Krantic *et al.*, 1993; Fong *et al.*, 1994; Vaca and Alfaro, 2000, Ouimet and Castellucci, 1997, Zatylny *et al.*, 2000). Administration of 5-HT has been shown to induce spawning in bivalves (Matsutani and Nomura, 1982; Gibbons and Castagna, 1984; Hirai *et al.*, 1988; Ram *et al.*, 1992). However, the interaction of 5-HT with its receptors, particularly in the reproductive process, is not yet fully understood.

In vertebrates, the effects of 5-HT are mediated by a large family of receptors, either ionotropic or coupled to second messenger cascades. Thus, 5-HT receptors are known to display diverse functions and play a critical role in modulating cognitive and behavioural functions. Numerous invertebrate 5-HT receptor genes have also been characterised and are known to mediate a variety of functions (reviewed by Tierney, 2001). In molluscs, most is known from the gastropods *Aplysia californica* and *Lymnaea stagnalis*. In *L. stagnalis*, a cDNA sequence encoding a mature 509 amino acid 5-HT receptor (5-HT<sub>1lym</sub>) was cloned from the nervous system (Sugamori *et al.*, 1993). It had highest sequence homology with *Drosophila* 5-HTdro<sub>2B</sub> (61%) and mammalian 5-HT<sub>1A</sub>-type (53%) receptors. The 5-HT<sub>1lym</sub> receptor contained seven regions of hydrophobic amino acids representing seven transmembrane (TM) domains. Another *L. stagnalis* 5-HT receptor, designated 5-HT<sub>2Lym</sub>, was identified that resembled members of the mammalian 5-HT<sub>2</sub>-type receptor subfamily (Gerhardt *et al.*, 1996).

Deleted: or

In Aplysia, sensory neurons are known to contain at least three 5-HT receptor subtypes. They include: (1) 5-HT<sub>1ap</sub> which is coupled to a cAMP/protein kinase A pathway (Li et~al., 1995); (2) Ap5-HT<sub>B1</sub> and Ap5-HT<sub>B2</sub> that are coupled to an inositol triphosphate/protein kinase C pathway and thereby induce a dose-dependent increase in phospholipase C in response to 5-HT (Angers et~al., 1998); and (3) 5-HT<sub>1ap</sub> which is localised in a variety of tissues, including the ganglia of the nervous system and is negatively coupled to adenylate cyclase. The 5-HT<sub>1ap</sub> receptor has significant amino acid sequence identity with 5-HT<sub>1lym</sub> (62%) (Angers et~al., 1998) and, therefore, also closely resembles the mammalian 5-HT<sub>1</sub> receptor subfamily.

In the present study, we aimed to identify and analyse an abalone 5-HT receptor (5-HT<sub>1Hal</sub>). We discovered that the tropical abalone *Haliotis asinina* contains a truncated 5-HT receptor that is most homologous to *Aplysia* 5-HT<sub>1ap</sub>. Reverse transcription-polymerase chain reactions (RT-PCR) revealed mRNA expression in numerous tissues, including the ganglia and gonad tissues. An antibody generated to the predicted third intracellular loop of 5-HT<sub>1Hal</sub> was used to localize receptor expression to cells of the neural and gonad tissues. The functional significance of 5-HT in abalone reproduction is shown by *in vitro* organ bath gonad contraction assays in the related abalone species, *Haliotis rubra*.

#### **Materials and Methods**

#### Animals

*H. asinina* used for gene identification were collected from Heron Island reef, Australia. *H. asinina* used for immunocytochemical localization were provided by the Coastal Aquaculture Development Center, Prachup Khiri Khan, Thailand. Tissues were dissected and immediately prepared for nucleic acid extractions, protein extractions and serial sectioning. *H. rubra* (Leach) were collected from Pt. Cook, Port Phillip Bay, under a Fisheries Victoria research permit (97/R/049A).

#### Oligonucleotide Primers

The sequences of oligonucleotide (OL) primers used to clone 5-HT<sub>1Hal</sub> (OL1-OL11), to perform RT-PCR expression studies (OL4, OL7), and for recombinant expression (OL12-OL13) are listed as follows:

OL1, AAGCAGTGGTATCAACGCAGAGTGAATTCT<sub>17</sub>

OL2, GC(C/T)AT(A/C/T)GC(A/C)ATGGA(C/T)AG(A/G/T)TACTGG

OL3, (A/G/C)AT(A/G/T)A(A/T/G/C)GAAAGC(C/T)CCAGTGATGAT

OL4, GGCGTGTGCGTTATTAGCCAAGACCAT

OL5, CGGAAAGCAGCCAGAACTCTCG

OL6, GTCGTCGTCGTTGCGTCCTCTTTAACC

OL7, GCACCCATTGCAGTTGGACACACACT

OL8, ATCCGTTTAGCACTGCGGTTACG

OL9, GCTCTAATACGACTCACTATAGG

OL10, AAGCAGTGGTATCAACGCAGAGT

OL11, CACATGAGCGATGTTCGTCTTAACGTG

OL12, GTCAATGGATCCTGTTCCCCAGAAAA

OL13, TTGACGAATTCCTTCCGAGACATGG

cDNA cloning of an abalone 5-HT receptor gene - 5-HT<sub>1Hal</sub>

Total RNA was extracted from juvenile (40 day old) *H. asinina* using a Tripure<sup>®</sup> Isolation Reagent (Roche). Any contaminating genomic DNA was removed by treatment with DNase I (Sigma). First strand cDNA synthesis was performed using 1 μg of total RNA in a 20 μl reverse transcription mixture containing OL1 and 200 U SUPERSCRIPT<sup>TM</sup> III RNase H<sup>-</sup> reverse transcriptase (Invitrogen), following the manufacturer's instructions.

H. asinina juvenile cDNA (1 μl) was used as template in PCRs. Each PCR was performed in a final concentration of 1x PCR Buffer, 2.0 mM MgCl<sub>2</sub>, 200 μM dNTPs, 1.0 μM of sense (OL2) and antisense primer (OL3), 0.25 units of Taq Ti polymerase (Fisher Biotec, Australia) and ddH<sub>2</sub>O, to a final volume of 25 μl. Sterile water was substituted for DNA in negative control reactions. The PCR consisted of 35 cycles, with 2 min denaturation at 94°C, 1 min annealing at 50°C, and a 1 min extension at 74°C. PCR products were detected using 2% agarose gel electrophoresis, and appropriate size bands were extracted and TA cloned using a TA Cloning Kit (Promega), following the manufacturer's instructions. Recombinant plasmid DNA was purified from positive clones, as determined by colony PCR, and inserts then sequenced in both directions and analysed using ClustalW.

The 3' and 5'-end gene sequences were identified by rapid amplification of cDNA ends (RACE). In both cases, PCR was performed using gene-specific primers, and confirmed by DNA sequence analysis. For 5'-RACE, antisense primers OL6-8 were used in combination with the 5'-RACE sense primer OL9. For 3'-RACE, sense primers OL2 and OL5, respectively, were used in combination with the 3'-RACE antisense primer OL10. Due to the apparent truncation of the 3'-RACE transcript, a further RT-PCR was performed using an antisense primer (OL11) with OL5, to ensure transcript entirety. A Kyte-Doolittle hydropathy profile of the deduced amino acid sequence was performed using TMbase (Hofmann and Stoffel, 1993).

Sequence alignment and phylogenetic analysis

Sequences were aligned using Clustal X, 8.1 (Thompson et al., 1997). Phylogenetic trees were constructed from respective multiple alignments using MEGA3 software (Kumar et al., 2004). The unrooted tree was generated with 1000 bootstrap trials using the neighbor-joining method (Saitou and Nei 1987) and presented with a cut-off bootstrapping value of 50.

#### Identification of 5-HT<sub>1Hal</sub>mRNA expression in tissues using RT-PCR

Tissue-specific expressions of 5-HT<sub>1Hal</sub> mRNA were examined by RT-PCR, and expected to have product sizes of 246-bp. Total RNA was extracted from cerebral ganglia (cg), pleuro-pedal ganglia (ppg), female gonad (fgo), male gonad (mgo), 40 day juvenile, mantle, cephalic tentacle, eye stalk, gill, and foot muscle tissues of *H. asinina* using a Tripure<sup>®</sup> Isolation Reagent (Roche). Any contaminating genomic DNA was removed by treatment with DNase I. First strand cDNA synthesis was performed using 1 μg of total RNA in a 20 μl reverse transcription mixture containing oligo d(T)<sub>12-18</sub> (Invitrogen) and 200 U SUPERSCRIPT<sup>TM</sup> III RNase H reverse transcriptase, following the manufacturer's instructions. PCR was performed using 1 μl of cDNA and the following sequence-specific primers were designed from existing 5-HT<sub>1Hal</sub> cDNA sequence (see Results section): OL4 and OL7. Each reaction was performed in a final concentration of 1 x PCR Buffer, 2.0 mM MgCl<sub>2</sub>, 200 μM of each dNTP, 1 μM of sense and antisense primer, 0.25 units of *Taq* Ti polymerase and ddH<sub>2</sub>O to a final volume of 25 μl. Recombinant plasmid containing the 5-HT receptor gene sequence was used as positive controls, and negative controls are substituting cDNA with water or RT absent samples. PCR consisted of 36 cycles, including a 2 min denaturation at 94°C, a 30 sec annealing at 58°C, and a 1 min extension at 74°C. Following PCR, 15 μl of reaction mix was fractionated on 2% agarose gel containing ethidium bromide (0.5 μg/ml).

### Production of a recombinant 5-HT<sub>1Hal</sub> fusion protein

A 5-HT<sub>1Hal</sub> cDNA sequence encoding 51 amino acids of the predicted third intracellular loop corresponding to Cys<sup>265</sup>-Glu<sup>315</sup> (see RESULTS, **Fig. 1A**), was PCR amplified using the following primers which incorporated terminal restriction sites for *Bam* HI and *Eco* RI sequences, OL12 and OL13. PCR consisted of 36 cycles, including a 2 min denaturation at 94°C, a 1 min annealing at 40°C, and a 2 min extension at 72°C. A PCR product of expected 173-bp size was gel extracted, double digested,

directionally ligated into pGEX-2T (Pharmacia), and then transformed into  $\it E.~coli$  strain DH5 $\alpha$  (Stratagene). Positive recombinant clones were subjected to plasmid purification and sequencing of inserts, prior to sub-culture in LB medium, expression of a glutathione S-transferase (GST)-5-HT $_{1Hal}$  fusion protein using 0.1 mM IPTG inducer, and protein purification, according to the manufacturer's instructions. The integrity of the expressed protein was verified by 12% SDS-PAGE and Coomassie blue staining.

Antisera production against recombinant 5-HT<sub>1Hal</sub> fusion protein

Two 6-weeks old female BALB/c mice were injected intraperitoneally with 100 µg fusion protein as an emulsion in Freund's complete adjuvant (Sigma). Booster injections were done with the same immunogen in Freund's incomplete adjuvant (Sigma) three times at intervals of 2 weeks. Retro-orbital plexus blood was collected and then centrifuged to collect antiserum, which was then preabsorbed with GST overnight at 4°C, and subsequently stored at -20°C.

#### *Immunocytochemistry*

*H. asinin*a cerebral and pleuropedal ganglia, ovaries, and testes were fixed in Bouin's solution and processed routinely for paraffin embedding. The sections were deparaffinized, rehydrated, immersed in 70% ethanol containing 1% saturated LiCO<sub>3</sub> and 1% H<sub>2</sub>O<sub>2</sub>, and subsequently immersed in 0.1 M glycine and 0.4% Triton X-100 in order to remove picric acid, endogenous peroxidase, free aldehyde groups, and for tissue permeabilization, respectively. Sections were rinsed three times in PBS, and then incubated for 1 h at room temperature in antisera diluted 1:1,000 in PBS. After three washes in PBS, and incubation with HRP-conjugated goat anti-mouse IgG for 1 h, detection was performed with Nova Red substrate solution. The sections were then dehydrated, cleared, mounted with mounting medium, observed under a Nikon ECLIPESE E600 light microscope, and images captured by a Nikon ECIPESE 2000 CCD camera. The experiments were repeated at least three times for each tissue.

#### Gomori's aldehyde-fuchsin staining (GAFS)

GAFS was used to identify neurosecretory cells in the neural ganglia (Cameron and Steele, 1959), but modified to study both immunoperoxidase staining and GAFS within the same section. After taking images of immunoreactivities within sections following immunoperoxidase staining, the sections were rehydrated in a graded series of ethyl alcohol. They were then oxidized in potassium permanganate solution (0.3% potassium permanganate and 0.3% concentrated sulfuric acid) for 1 min and rinsed in distilled water. The sections were bleached in 2.5% sodium bisulfite solution until permanganate colour was removed and then washed in running tap water for 5 min before transferring into 70% ethanol for 2 min. For neurosecretory cell detection, the sections were stained in aldehyde-fuchsin solution (0.5% basic fuchsin, 1% concentrated hydrochloric acid, 1% paraldehyde solution) for 10 min, then rinsed in 95% ethyl alcohol and further differentiated in fresh 95% ethanol until no more aldehyde-fuchsin was removed. The sections were transferred to 70% ethyl alcohol for 2 min, rinsed in distilled water for 1 min, and then stained in Halmi solution (0.2% light green SF, yellowish, 1% orange G and 0.5% chromotrope 2R). They were then differentiated in 95% ethyl alcohol containing 0.2% acetic acid for 3 min, rinsed in fresh 95% ethanol, dehydrated in absolute alcohol, cleared in xylene, and mounted with permount.

H. asinina ganglia were fixed in 4% paraformaldehyde containing 5% sucrose for 12-16 h. After three washes, the tissues were immersed in 30% sucrose-PBS overnight. The specimens were embedded in Tissue Tek (Sakulra Finetek, U.S.A.) and directly frozen in liquid nitrogen. Cryosections of approximately 15 µm were cut and mounted on poly-L-lysine (Sigma) coated slides. After rinsing in PBS, the sections were incubated in glycine for 5 min and pre-incubated in blocking buffer (4% BSA and 2% normal goat serum in PBS containing 0.1% Tween 20) for 30 min before incubation overnight with a mixture of rabbit anti-5-HT and mouse anti-5-HT<sub>1Hal</sub> diluted 1: 200 and 1: 50, respectively, in blocking buffer. Sections were washed three times in PBS and incubated with goat anti mouse antiserum conjugated to the Alexa 568 fluorochrome and anti-rabbit antiserum conjugated to Alexa 488 fluorochrome diluted 1: 200 in blocking buffer for 1 h. After three washes in PBS, the sections were nuclear stained with TO-PRO-3 (MolecularProbes, U.S.A.), diluted 1: 1000 in PBS, for 5 min. They were then rinsed in PBS and mounted with Vectashield (Vector Lab). Negative controls included the omission of primary antibody, replaced with blocking buffer. Immunolabeled sections were examined by an Olympus FV1000 confocal laser scanning microscope (Tokyo, Japan). Serial optical sections were taken at interval of 0.5 µm, and confocal stacks (3-6 images) were reconstructed using Olympus Fluoview software. All specimens were examined within 24 h of immunolabeling.

In vitro organ bath gonad contraction bioassays

A previous molecular study has demonstrated the existence of 5-HT-like receptor in *H. rubra* (unpublished) that is highly homologous (96%) to *H. asinina* 5-HT<sub>1Hal</sub>. Physiological experiments were performed on gonad tissue of mature *H. rubra*. After the animal was anesthetized by injection of isotonic MgCl<sub>2</sub> (25-50% body weight), freshly dissected gonad rings were prepared for analysis. Transverse cuts were made 1 cm from the tip of the gonad to release a ring of tissue. Hooks were inserted between the hepatopancreas capsule and the capsule of the gonad, which consists of dense collagenous fibres mixed with muscle cells that surround both the testis and ovaries (Apisawetakan *et al.*, 1997).

Preparations were placed into organ baths containing 15 ml of molluscan Ringer's solution (Tucker, 1970) at 23°C, and suspended between a force transducer (Grass-FT03) and a fixed steel hook using cotton thread. Prior to assay, tissues were given a 15 min relaxation and acclimation period, and were allowed 10 min to recover initial tonus after washing. In males, bioactivities were tested using  $10^{-4}$  to  $10^{-6}$  M 5-HT solutions, diluted in 50 µl of molluscan Ringer's solution, and contractions monitored with a force-displacement transducer which was linked to a PowerLab<sup>TM</sup> data collection system. Mean rate of contractility was calculated over a 2 min period and statistical differences between the values were determined using Student's t-test for paired comparisons with significance assumed at a  $P \leq 0.05$ . In females, bioactivity was measured using a  $10^{-6}$  M 5-HT solution.

#### Results

Cloning and characterization of an abalone 5-HT receptor gene

PCR amplification of juvenile *H. asinina* cDNA using degenerate primers generated an amplification product of 633-bp. The amplification product was successfully cloned and sequenced. Subsequently, the full-length gene was identified by 5' and 3' RACE, containing 1633-bp and encoding a protein of 359 amino acids (Fig. 1A). The sequence data has been submitted to the GenBank database under the accession number EU342382. Partial 5-HT receptor sequences of approximately 785 bp, covering predicted TM domains 3 to 7, were obtained previously from *H. rubra* (GenBank accession number AY237917) and *Haliotis laevigata* (GenBank accession number AY237918). These were 96% identical at the nucleotide level???, but the data may reflect sequencing of genomic DNA as DNase I treatments

Deleted: homologous

Formatted: Not Highlight

were not implemented in the earlier mRNA extractions prior to cDNA synthesis (data not shown). <u>Not sure of relevance of this statement</u>

Protein sequence analysis using the Protein Families database of alignments and hidden Markov models, revealed that the deduced amino acid sequence has characteristics common to mammalian and invertebrate G-protein-coupled 5-HT receptors. It possesses a G-protein coupled motif, represented by a conserved triplet in the region A<sup>121</sup>SILHLVAIAMDRYWAV<sup>137</sup>, and spanning the TM3 and carboxyl end of the second intracellular loop. Four potential phosphorylation sites for protein kinase C (S<sup>147</sup>AK, S<sup>251</sup>PK, S<sup>270</sup>MK and S<sup>312</sup>RK) and a single cAMP phosphorylation site (K<sup>149</sup>RIS) were identified. The sequence has four potential sites for N-linked glycosylation (N<sup>3</sup>QT, N<sup>18</sup>VT, N<sup>145</sup>RS and N<sup>277</sup>SS) within the predicted N-terminal region and intracellular loop domains.

Kyte-Doolittle hydropathy profiles of the deduced 5-HT<sub>1Hal</sub> amino acid sequence (**Fig. 1B**) showed that it contained 6 hydrophobic TM segments that were composed of between 20 to 25 residues. A phylogenetic tree of molluscan and selected vertebrate 5-HT receptors, based on amino acid identity, is shown in **Fig. 1C**. The abalone (*Haliotis*) 5-HT receptor is most closely related to molluscan homologs and to human 5-HT Type 1 receptors, and is therefore named 5-HT<sub>1Hal</sub>.

Sequence alignment of *H. asinina* 5-HT<sub>IHal</sub> with *Aplysia* and *Panulirus* (Lobster) homologs show 40% and 41% identity, respectively, with most similarity observed within the TM regions (**Fig. 2**). Most divergence is found within the N-terminus, the third intracellular loop, prior to the first TM domain, and the C-terminus. Within the predicted third intracellular loop of 5-HT<sub>IHal</sub>, there are only 111 amino acids, compared to 154 amino acids for 5-HT<sub>Iap</sub>. However, the relatively short domain is consistent with the size of the equivalent domain of the *Panulirus* 5-HT receptor. The deduced 5-HT<sub>IHal</sub> obtained did not appear to contain the predicted seventh TM domain and intracellular C-termini which is common to other known 5-HT receptors.

Production of a recombinant 5-HT<sub>1Hal</sub> fusion protein and antisera

A 153-bp PCR product, encoding the 51 amino acid sequence of the third intracellular loop (see underlined amino acids in **Fig. 1A**) was directional cloning into a pGEX-2T expression vector following double digestion of the *Bam* HI and *Eco* RI terminal restriction sites. A GST-5-HT<sub>1Hal</sub> fusion protein of 34.5 kDa was then expressed in *E. coli* cells and used to produce murine 5-HT<sub>1Hal</sub> antisera.

Tissue specific expression of 5-HT<sub>1Hal</sub> mRNA

In RT-PCR using template cDNAs produced from *H. asinina* cg, ppg, fgo, mgo, 40 day juvenile, mantle, cephalic tentacle, eye stalk, gill, and foot muscle tissues, predicted 246-bp amplicons were obtained in all tissues (**Fig. 3 upper panel**). Control PCRs using recombinant plasmid 5-HT<sub>1Hal</sub> sequence as template gave a positive result (PCR +), and those using no cDNA template gave a negative result (PCR -), indicating no contaminating genomic DNA. Controls where PCR was performed upon respective samples without the RT reactions were also negative (**Fig. 3 lower panel**).

Immunoperoxidase and Gomori's aldehyde fuschin (GAF) staining

The 5-HT<sub>1Hal</sub>-immunoreactivity (5-HT<sub>1Hal</sub>-ir) was detected in the soma of neuronal cells located in the outer cortex of both cerebral and pleuropedal ganglia (**Fig. 4**). Based on histological characteristics, the immunoreactive cells could be classified as type I (NS1) and type II neurosecretory cells (NS2) according to Upatham et al. (1998) and Kruatrachue et al. (1999). The NS1 was the largest in size, containing cytoplasmic granules and a euchromatic nucleus, whereas the NS2 was smaller with a round nucleus having patches of heterochromatin. NS1 and NS2 in the cerebral and pleuropedal ganglia were positively stained with GAF, especially their secretory granules which exhibited a dark-violet color (**Fig. 4A1, A2, B1, C1**). In addition, 5-HT<sub>1Hal</sub>-ir was also detected in the fibers distributed within the medullar of cerebral and pleuropedal ganglia (**Fig. 4A1**).

In the ovarian tissue, 5-HT<sub>1Hal</sub>-ir was observed in epithelial cells of the outer capsule and connective tissue of the trabeculae to which the ovarian follicles adhered (**Fig. 5A, A1**). Additionally, 5-HT<sub>1Hal</sub>-ir was also expressed in the cytoplasm of late stage oocytes (Oc4, Oc5) (**Fig. 5A2, B**). In the testis, 5-HT<sub>1Hal</sub>-ir was also present in the outer capsule and connective tissue of the trabeculae (**Fig. 5C, C1**).

Colocalization of 5-HT-ir and 5-HT<sub>1Hal</sub>-ir in neural tissues by immunofluorescence

Fluorescence staining showed that 5-HT<sub>1Hal</sub>-ir and 5-HT-ir were present in separate cells of both cerebral and pleuropedal ganglia, i.e. they were not co-localized (**Fig. 6**). Strikingly, numerous 5-HT-ir fibers were present in the medulla region of both ganglia whereas 5-HT<sub>1Hal</sub>-ir fibers were fewer than that of 5-HT-ir fibers (**Fig. 6B, D**). Furthermore, some 5-HT-ir fibers appeared to innervate the 5-HT<sub>1Hal</sub>-ir neuronal cells, both in cerebral and pleuropedal ganglia (**Fig. 6B, D**).

The 5-HT<sub>1Hal</sub> receptor was also found to be expressed in several other tissues (data not shown). In particular, it was observed in the vascularized connective tissues of the eye, epipodial and cephalic tentacles (i.e. connective tissue beneath the surface epithelium and muscle fibers within the central region), and pedal muscle (i.e. around the epithelial cells of foot epithelium, but not in the muscle fibers).

In vitro gonad contraction bioassays

Abalone gonad muscle tissue was monitored for contraction bioactivity following stimulation with 5-HT (10<sup>-4</sup> to 10<sup>-6</sup> M; (Fig. 7). Application of 5-HT typically led to the increase of irregular phasic contractions and relaxations in male *H. rubra* gonad preparations compared to control (Fig. 7A). The use of 0.018 % v/v H<sub>2</sub>O<sub>2</sub>, commonly used to induce spawning in abalone, had no effect on contractility (data not shown). Also, control experiments where molluscan Ringer's solution was substituted for test solution, did not affect basal contractility (negative control).

A dose-response of gonad contraction induced by 5-HT was determined at concentrations of  $10^4$  M to  $10^{-6}$  M (**Fig. 7A**). At each concentration, 5-HT induced a dose-dependent increase in irregular rhythmic contraction, compared with control preparations. The most dramatic effect was observed at  $10^{-6}$  M (P<0.05, n = 6), in which the rate of phasic contraction and relaxation increased more than 200% and continued for at least 10 min, after which the rate decreased. A significant increase in the rate of gonad contraction and relaxation (P<0.05, n = 6) was also demonstrated upon application of  $10^{-4}$  M and  $10^{-5}$  M 5-HT. Application of  $10^{-6}$  M 5-HT also led to the increase of irregular phasic contractions and relaxations in female *H. rubra* gonad preparations compared to control (**Fig. 7B**).

#### Discussion

A putative abalone truncated 5-HT receptor

This study has identified a putative abalone 5-HT receptor, termed 5-HT<sub>1Hal</sub>. Using RT-PCR with degenerate primers, followed by 5' and 3' -RACE, we initially cloned the full-length gene from 40-day *H. asinina* juveniles. Comparative analysis of known nucleotide and predicted amino acid 5-HT receptor sequences, as well as the identification of associated protein motifs, suggests that 5-HT<sub>1Hal</sub> is a homologue to the molluscan *Aplysia* CNS 5-HT<sub>1ap</sub> (Angers *et al.*, 1998) and the crustacean *Panulirus* CNS 5-HT<sub>1Pan</sub> (Sosa *et al.*, 2004). Furthermore, phylogenetic analysis established that the 5-HT<sub>1Hal</sub> belongs to the 5-HT type 1 receptor cluster and represents the first 5-HT receptor transcript identified in 'prosobranchs'.

Pharmacological, ligand-binding and site-directed mutagenesis studies have defined structural and functional properties required for G-protein coupled receptors (GPCRs). Many of these are present in 5-HT<sub>1Hal</sub>. First, serine residues present within cytoplasmic domains can be phosphorylated by protein kinases (Strosberg, 1996). It was notable that the 5-HT<sub>1Hal</sub> had one less potential phosphorylation site for protein kinase C in the third intracellular loop, possibly relating to function. The serine residue within

TM5 domain, may be part of a binding site, already defined for 5-HT (Li et al., 1995). Second, the highly conserved "DRY" motif is present and is located at the C-terminal end of the TM3. The aspartic acid (D) residue is important for the maintenance of the three-dimensional structure of GPCRs. Finally, studies involving site-directed mutation and receptor antibodies have shown that the second intracellular loop is important in receptor G-protein interaction (Ostrowski et al., 1992; Hedin et al., 1993). Specifically, a conserved threonine residue in this loop is involved in G-protein coupling for calcium mobilisation, and to inhibition of calcium channel activation (Lembo et al., 1997). It is also thought to play a minor role in the inhibition of cAMP accumulation (Lembo et al., 1997). In addition, regions of the third intracellular loop are known to dictate the specificity of interaction with different G proteins (Kobilka et al., 1987). A large third intracellular loop is typical of GPCRs coupled to G-inhibitory subunits (Sugamori et al., 1993) as has been demonstrated in the 5-HT<sub>1ap</sub> (Angers et al., 1998). Comparative sequence analyses show that 5-HT<sub>1Hal</sub> demonstrates significant divergence in the third intracellular loop compared with other known molluscan 5-HT receptors. We have found that this loop is considerably shorter by 40 amino acids in the internal portion, which may have important secondary signalling implications. However, it has been established that the primary regions of receptor G-protein interaction are the amino and carboxyl terminal portions of the loop (Ostrowski, et al., 1992), thus the removal of this internal region may not be of significant functional importance. In fact, the amino and carboxyl regions of this loop are largely conserved when compared with 5-HT<sub>1ap</sub>. So although we do not yet know the effector mechanisms associated with the putative 5-HT<sub>1Hal</sub> receptor, we do know that the 5-HT receptor type 1 family signals through pertussis toxin-sensitive Gi/Go proteins to mediate a range of actions that include the ubiquitous inhibition of cAMP formation via Gi, as well as cell-specific G-mediated effects. Future pharmacological analysis is necessary to verify these assumptions.

Interestingly, analysis of the 5-HT<sub>1Hal</sub> transcript showed that the deduced protein appears to be truncated following the TM6 domain. Repeated 3'-RACE did not reveal a larger transcript that may encode a predicted seventh TM and C-terminal intracellular domain. DNase I treatment of isolated RNA ensured that contaminating genomic DNA, which could potentially contain introns leading to mispriming, was not an issue. The published sizes of 5-HT1 homologs vary with the species, typically ranging from around 50–92 kDa. Variation is largely the result of differences in the third intracellular loop as well as differences in the lengths of the N-termini, but rarely the C-termini. However, Sosa et al (2004) have demonstrated in *Panulirus* the expression of a 40 kDa 5-HT<sub>1Pan</sub>, and this may contain a similar truncation to that observed with the abalone 5-HT<sub>1Hal</sub> (predicted to encode a protein of 40 kDa). Western blots have suggested that crustacean 5-HT receptors are alternately spliced and/or differentially modified posttranslationally.

Truncated GPCRs appear to modulate the function of the full-length version of the receptor as shown for the α1A-adrenergic receptor (Cogé *et al.*, 1999), the dopamine D3 receptor (Karpa *et al.*, 2000), the gonadotropin receptor (Grosse *et al.*, 1997), the prostaglandin E2 EP1 receptor subtype (Okuda-Ashitaka et al., 1996), the secretin receptor (Ding et al., 2002), the V2 vasopressin receptor (Zhu and Wess, 1998), and the ghrelin receptor (Gnanapavan *et al.*, 2002). The human wild-type ghrelin receptor consists of 366 amino acids with seven TM domains and has a truncated splice variant consisting of 289 amino acids with only five predicted TM domains which fails to bind ghrelins. It has been demonstrated that the truncated form mRNA exceeds that of wild type in normal human tissues (Gnanapavan *et al.*, 2002). In fact, a 13-fold excess of the truncated ghrelin receptor mRNA compared with its wild-type attenuates trafficking to the cell surface and decreases constitutive activity. The full-length receptor physically interacts with its truncated splice variant and thereby can exist as heterodimers. We hypothesize that the truncated 5-HT<sub>1Hal</sub> may play a similar role in modulation of a full-length serotonin receptor in abalone.

Expression of 5-HT<sub>1Hal</sub> in abalone tissues and its potential role in reproductive processes

Due to the high degree of 5-HT<sub>1Hal</sub> sequence identity with 5-HT<sub>1ap</sub>, we expected a similar expression pattern with 5-HT<sub>1Hal</sub>. In *Aplysia*, 5-HT<sub>1ap</sub> mRNA has been localised to all ganglia tested, and antibody probes have been used to identify widespread receptor protein expression in the gill, heart,

Formatted: Font: 11 pt

Formatted: Left, Right: 1.1 pt, Space After: 4 pt, Adjust space between Latin and Asian text, Adjust space between Asian text and numbers

hermaphroditic duct, kidney and ovotestis (Angers *et al.*, 1998). Indeed, *H. asinina* 5-HT<sub>IHal</sub> mRNA transcripts and protein appeared in all tissues examined. The existence of this receptor in neural and reproductive tissues is of particular significance given existing evidence showing that 5-HT has reproduction-related bioactivity in other molluscs. Like most marine invertebrates, abalone have a well defined annual reproductive cycle culminating in the initiation of spawning (Counihan, R.T., McNamara, D.C., Souter, D.C., Jebreen, E.J., Preston, N.P., Johnson, C.R. and Degnan, B.M. 2001. Pattern, synchrony and predictability of spawning of the tropical abalone *Haliotis asinina* from Heron Reef, Australia. *Mar. Ecol. Prog. Ser.* 213, 193-202.). Upon initiation, detached oocytes undergo germinal vesicle breakdown and start the first meiotic division (Jebreen, E.J., Counihan, R.T., Fielder, D.T. and Degnan, B.M. 2000. Synchronous oogenesis during the semilunar spawning cycle of the tropical abalone *Haliotis asinina*. *J. Shellfish Res.* 19, 845-852). Mature gametes are conveyed to the cavity of the right renal organ, where they escape into the seawater through the respiratory pores of the shell by continual lifting of the shell and rotation of the foot. Our findings suggest that the 5-HT<sub>IHal</sub> may play an important role in this, such as modulating the release of active reproductive peptides precursor proteins, gamete maturation, and/or the control and initiation of gamete release.

This is supported by our *in vitro* organ bath experiments. Application of 5-HT solution was shown to induce an increase in the rate of phasic contraction and relaxation of muscle within male and female abalone gonad capsules. We hypothesize that this neurotransmitter could be required to induce contraction of the gonad in the process of gamete expulsion. Serotonin released from neurones in gonads may bind directly to receptors on muscle cells to induce contractions. In our study, we found examples of colocalization of receptor cells with 5-HT in axons, consistent with the short-term modulatory role of 5-HT in neural and possibly reproductive tissues. Likewise, it has been shown that ovarian muscle contraction is an important process in the movement of gametes prior to egg-laying or spawning (Howard and Talbot, 1992; Henry *et al.*, 1999; Zatylny *et al.*, 2000). For example, in the lobster, 5-HT can induce significant ovarian muscle contraction (Howard and Talbot, 1992). The exact mechanism by which transmitters elicit smooth muscle contraction is unknown, but it may involve a cAMP or Ca<sup>2+</sup> secondary messenger system (Howard and Talbot, 1992).

It is also possible that 5-HT released may function in a similar way to that in the zebra mussel. In zebra mussel, prior to spawning, 5-HT from the gonadal nerve endings acts via a 5-HT receptor to initiate oocyte maturation, including germinal vesicle breakdown (Fong *et al.*, 1994). These events could also be artificially induced by administration of 5-HT to surf clams, ultimately leading to spawning (Hirai *et al.*, 1988). Other research groups have implicated 5-HT in the induction of molluscan oocyte maturation via a single class of 5-HT receptor (Matsutani and Nomura, 1982; Krantic *et al.*, 1993). Based on ligand-binding and pharmacological studies, this receptor appears to be most similar to the 5-HT<sub>1A</sub> type receptor, although it has certain properties that makes it novel (Krantic *et al.*, 1993).

#### Summary

Advances in biotechnology have meant that molecules such as hormones and neurotransmitters may be used for aquaculture purposes to enhance market potential. The results from the current study contribute to our understanding of abalone reproduction and suggest 5-HT and 5-HT receptors may interact in a complex way to control reproduction. Multiple genes encoding 5-HT receptors in vertebrates and invertebrates have been described, and therefore it would be of interest to identify whether this type of complexity also exists in abalone.

#### Acknowledgments

We are grateful to Mr. Tanes Poomtong and staff at the Coastal Development Center, Klongwan, Prachaubkirikhun, and Mr. Tony Smith at the Bay City Seafarm, Geelong, Australia, for provision of animals.

Formatted: Font: Times New

Roman

Formatted: Font: Times New

Roman

Formatted: Font: 11 pt
Formatted: Font: Times New

Roman, 11 pt

Formatted: Font: 11 pt

#### References

- Rathouz MM, Kirk MD 1988 Localization of catecholamines in the buccal ganglia of Aplysia californica. Brain Res 458:170-175
- 2. **Croll RP** 1988 Distribution of monoamines within the central nervous system of the juvenile pulmonate snail, *Achatina fulica*. Brain Res 460:29-49
- Barlow LA, Truman JW 1991 Patterns of serotonin and SCP immunoreactivity during metamorphosis of the nervous system of the red abalone, *Haliotis rufescens*. J. Neurobiology 23:829-844
- Kuhl D, Kennedy TE, Barzilai A, Kandel ER 1992 Long-term sensitization training in Aplysia leads to an increase in the expression of BiP, the major protein chaperone in the ER. J Cell Biol 119:1069-1076
- Satterlie RA, Norekian TP, Jordan S, Kazilek CJ 1995 Serotonergic modulation of swimming speed in the pteropod mollusc *clione limacina*. J Exp Zool 198:895-904
- Bruehl C, Berry R 1985 Regulation of synthesis of the neurosecretory egg-laying hormone of Aplysia: Antagonistic roles of calcium and cylic adenosine 3':5'-monophosphate. Soc Neuroscience 5:1233-1238
- 7. Ram JL, Fong PP, Croll RP, Nichols SJ, Wall D 1992 The zebra mussel (*Dreissena polymorpha*), a new pest in North America: reproductive mechanisms as possible targets of control strategies. Inv Reprod Dev 22:77-86
- 8. **Krantic S, Dube F, Guerrier P** 1993 Evidence for a new subtype of serotonin receptor in oocytes of the Surf Clam *Spisula solidissima*. Gen Comp Endocrinol 90:125-131
- 9. Fong PP, Kyozuka K, Abdelghani H, Hardege JD, Ram JL 1994 *In vivo* and *in vitro* induction of germinal vesicle breakdown in a freshwater bivalve, the zebra mussel *Dreissena polymorpha* (Pallas). J Exp Zool 269:467-474
- Vaca AA, Alfaro J 2000 Ovarian maturation and spawning in the white shrimp, *Penaeus vannamei*, by serotonin injection. Aquaculture 182:373-385
- Ouimet T, Castellucci VF 1997 Gene expression and regulation of Aplysia californica prohromone convertases aPC1B and aPC2. J Neurochem 68:1031-1039
- 12. Zatylny C, Durantou F, Boucaud-Camou E, Henry J 2000 Evidence of 5-hydroxytryptamine synthesis in the follicles of *Sepia officinalis* and direct involvement in the control of egg-laying. Mol Reprod Dev 55:182-188
- 13. **Matsutani T, Nomura T** 1982 Induction of spawning by serotonin in the scallop, *Patinopecten yessoensis* (Jay). Mar Biol Lett 3: 353-358
- 14. **Gibbons M, Castagna M** 1984 Serotonin as an inducer of spawning in six bivalve species. *Aquaculture* 40:189-191
- 15. **Hirai S, Kishimoto T, Kadam AL, Kanatani H, Koide SS** 1988 Induction of spawning and oocyte maturation by 5-hydroxytryptamine in the Surf Clam. J Exp Zool 245:318-321.
- Tierney AJ 2001 Structure and function of invertebrate 5-HT receptors: a review. Comp Biochem Physiol A 128:791-804
- 17. Sugamori KS, Sunahara RK, Guan H, Bulloch AGM, Tensen CP, Seeman P, Niznik HB, Van Tol HM 1993 Serotonin receptor cDNA cloned from *Lymnaea stagnalis*. Proc Natl Acad Sci USA 90: 11-15.
- 18. Gerhardt CC, Leysen JE, Planta RJ, Vreugdenhil E, and Van Heerikhuizen H 1996 Functional characterisation of a 5-HT<sub>2</sub> receptor cDNA cloned from *Lymnaea stagnalis*. Eur J Pharmacol 311:249-258
- Li X, Giot J, Kuhl D, Hen R, Kandel ER 1995 Cloning and characterization of two related serotonergic receptors from the brain and the reproductive system of *Aplysia* that activate phospholipase C. J Neurosci 15(11):7585-7591.

- Angers A, Storozhuk MV, Duchaine T, Castellucci VF, DesGroseillers L. 1998 Cloning and functional expression of an *Aplysia* 5-HT receptor negatively coupled to adenylate cyclase. J Neurosci 18(15):5586-5589.
- Hofmann K, Stoffel W 1993 TMbase A database of membrane spanning proteins segments. Biol Chem Hoppe-Seyler 374,166.
- 22. **Thompson JD, Gibson TJ, Plewniak F, Jeanmougin F, Higgins** DG 1997 The CLUSTAL\_X windows interface: flexible strategies for multiple sequence alignment aided by quality analysis tools. Nucl Acids Res 25:4876-4882.
- 23. **Kumar S, Tamura K, Nei M** 2004 MEGA3: Integrated software for molecular evolutionary genetics analysis and sequence alignment, Briefings in Bioinformatics 5:150-163.
- 24. **Saitou N, Nei M** 1987 The neighbor-joining method: a new method for reconstructing phylogenetic trees, Mol Biol Evol 4:406-425.
- Cameron ML, Steel JE 2001 Simplified aldehyde-fuchsin staining of neurosecretory cells. Stain Technology 34:265-266.
- 26. Apisawetakan S, Thongkukiatkul A, Wanichanon C, Linthong V, Kruatrachue M, Upatham ES, Poomthong T, Sobhon P 1997 The gametogenic processes in a tropical abalone, *Haliotis asinina* Linnaeus. J Sci Soc Thailand 23:225-240.
- 27. **Tucker LE** 1970 Effects of external salinity on *Scutus breviculus* (Gastropoda, Prosobranchia) II. Nerve conduction. Comp Biochem Physiol 37:467-480.
- 28. Upatham ES, Thongkukiatkul A, Kruatrachue M, Wanichanon. C, Chitramwong YP, Sahavacharin S, Sobhon P 1998 Classification of neurosecretory cells, neurons and neuroglia in the cerebral ganglia of *Haliotis asinina* Linnaeus by light microscopy. J Shellfish Res 17:737-742.
  - 29. Kruatrachue M, Thongkukiatkul A, Sobhon P, Upatham ES, Wanichanon. C, Sretarugsa P 1999 The ultrastructure of neuron and neuroglia in the cerebral and pleuro-pedal ganglia of *Haliotis asinine* Linnaeus. Science Asia 25:134-142.
  - 30. Sosa MA, Spitzer N, Edwards DH, Baro DJA crustacean serotonin receptor: cloning and distribution in the thoracic ganglia of crayfish and freshwater prawn. J Comp Neurol 2004 Jun 7:473(4):526-37.
  - 31. **Strosberg AD** 1996 G protein coupled R<sub>7</sub>G receptors. Cell Signalling. Cold Spring Harbor Laboratory Press. 27:65-83.
  - 32. **Ostrowski J, Kjelsberg MA, Caron MG, Lefkowitz RJ** 1992 Mutagenesis of the β<sub>2</sub>-adrenergic receptor: how structure elucidates function. Annu Rev Pharmacol Toxicol 32:167-183.
  - 33. **Hedin KE, Duerson K, Clapham DE** 1993 Specificity of receptor G-protein interaction: searching for the structure behind the signal. Cell Signal 5:505-518.
  - 34. **Lembo PMC, Ghahremani MH, Morris SJ, Albert PR** 1997 A conserved threonine residue in the second intracellular loop of the 5-hydroxytryptamine 1A receptor directs signaling specificity. Molecular Pharmacology 52:164-171.
  - 35. Kobilka BK, Frielle T, Collins S, Yang-Feng TL, Kobilka TS, Francke U, Lefkowitz, RJ, Caron MG 1987 An intronless gene encoding a potential member of the family of receptors coupled to guanine nucleotide regulatory proteins. Nature 329:75-79.
  - 36. Cogé F, Guenin SP, Renouard-Try A, Rique H, Ouvry C, Fabry N, Beauverger P, Nicolas JP, Galizzi JP, Boutin JA, Canet E 1999 Truncated isoforms inhibit [<sup>3</sup>H]prazosin binding and cellular trafficking of native human α<sub>1A</sub>-adrenoceptors. J. Biochemistry, 343:231-239
  - 37. **Karpa KD, Lin R, Kabbani N, Levenson R** 2000 The dopamine D3 receptor interacts with itself and the truncated D3 splice variant d3nf: D3-D3nf interaction causes mislocalization of D3 receptors. Mol Pharmacol 58:677-683
  - 38. **Grosse R, Schultz G, Gudermann T** 1997 Inhibition of gonadotropin-releasing hormone receptor signaling by expression of a splice variant of the human receptor. Mol Endocrinol 11:1305-1318
  - 39. Okuda-Ashitaka E, Sakamoto K, Ezashi T, Miwa K, Ito S, Hayaishi O 1996 Suppression of prostaglandin E receptor signalling by the variant form of EP1 subtype. J. Biol. Chem. 271:31255-31261.

**Formatted:** English (Australia)

- 40. **Ding WQ, Cheng ZJ, McElhiney J, Kuntz SM, Miller LJ** 2002 Silencing of secretin receptor function by dimerization with a misspliced variant secretin receptor in ductal pancreatic adenocarcinoma. Cancer Res 62:5223-5229
- 41. **Zhu X, and Wess J** 1998 Truncated V2 vasopressin receptors as negative regulators of wild-type V2 receptor function. Biochemistry 37:15773-15784.
- 42. Gnanapavan S, Kola B, Bustin SA, Morris DG, McGee P, Fairclough P, Bhattacharya S, Carpenter R, Grossman AB, Korbonits M 2002 The tissue distribution of the mRNA of ghrelin and subtypes of its receptor, GHS-R, in humans. J Clin Endocrinol Metab 87(6):2988.
- 43. **Howard DR, and Talbot P** 1992 *In vitro* contraction of lobster (*Homarus*) ovarian muscle: Methods for assaying contraction and effects of biogenic amines. J Exp Zool 263:356-366.
- 44. **Henry J, Zatylny C, Boucaud-Camou E** 1999 Peptidergic control of egg-laying in the cephalopod *Sepia officinalis*: involvement of FMRFamide and FMRFamide-related peptides. Peptides 20:1061-1070.

- FIG. 1. Molecular identification of a 5-HT receptor in the abalone, H. asinina. A, Nucleotide sequence (1633-bp) and deduced amino acid sequence (359 aa) of a H. asinina 5-HT<sub>1Hal</sub> receptor. Boxed grey areas indicate predicted TM domains (TM1-6; http://www.enzim.hu/hmmtop/html/submit.html). The 50 amino acids (underlined) of H. asinina are those which were expressed as a recombinant peptide to make an antibody probe. Inset: RT-PCR using primers (double underlined) spanning the coding and untranslated regions, followed by agarose gel electrophoresis visualization. PCR - represents a negative control with RT absent. B, Kyte-Doolittle hydropathy profile of the deduced H. asinina 5-HT receptor sequence. C, Phylogenetic tree of molluscan 5-HT receptors compared with selected non-molluscan 5-HT receptors. A tree was constructed from deduced amino acid sequences by using the neighbor-joining method. The number at each branch point represents the bootstrap probability that two lineages join together to form a cluster. Genbank accession numbers: Lymnaea (Q25414), Heliothis (AY395746), Aplysia 1a (AAM46088), Haliotis (EU342382), Mizuhopecten (AB209935), Aplysia 1b (AAC28786), Panulirus (AY528822), Takifugu 1a (CAA65175), Oreochromis (AAP83427), Takifugu 1b (CAA65176), Mus (NP 032334), Homo 1A (NM 000524), Oreochromis (AAP83428), Homo 1D (NM 000864), Homo 1B (NM 000863), Homo 2C (NM 000868), Homo 2A (NM 000621), Xenopus 2B (NP 001082744), Homo 2B (NM 000867), Homo 7 (NM 000872), and Homo 5A (NM 024012).
- **FIG. 2.** Comparative analysis of deduced 5-HT receptor sequences. Comparison of deduced amino acid sequences from *H. asinina* 5-HT<sub>1Hal</sub> receptor, with *Aplysia* CNS (5-HT<sub>1ap</sub>; AF041039) and *Panulirus interruptus* (5-HT<sub>1Pan</sub>; AY528822). The identical residues are shaded in black, similar residues are shaded in grey, represents gaps in the alignment. A schematic diagram shows the relative length of deduced 5-HT receptor proteins and dark boxes represent transmembrane domains.
- **FIG. 3.** Tissue-specific expression of the 5-HT $_{IHal}$  mRNA using gene specific primers OL5 and OL7 in PCRs with cDNAs prepared from different tissues. Amplification products were separated on 2% agarose gels and stained with ethidium bromide. Amplification products were 246-bp. All tissues tested were positive for 5-HT $_{IHal}$  mRNA: cerebral ganglia (CG), pleuro-pedal ganglia (PPG), female gonad (FGO), male gonad (MGO), 40 day juvenile (40 day), mantle, cephalic tentacle (Ctent), eye stalk (Eye), gill, and foot muscle tissues. PCR + represent the positive control using recombinant plasmid containing the 5-HT receptor gene sequence, PCR represents the negative control using water instead of cDNA, and Control includes respective samples without RT reaction.
- FIG. 4. Immunoperoxidase staining of the 5-HT<sub>1Hal</sub> in cerebral ganglion (A) and pleuropedal ganglion (B and C), together with Gomori's aldehyde-fuschin staining (GAFS) (A2, B1, lower). A, Cross-section of cerebral ganglion showing the distribution of 5-HT<sub>1Hal</sub> immunoreactivity (5-HT-ir) in cells within the cortical region (arrows). A1. High power micrograph of boxed 1 area in A showing 5-HT<sub>1Hal</sub>-ir in type1 neurosecretory cells (NS1) and fibers (arrow heads). A2. High power micrograph of boxed 2 area in A showing NS1 stained with immunoperoxidase method (upper), and GAFS (lower), repectively. B and C, Low power micrographs of a section of the pleuropedal ganglion showing the distribution of 5-HT<sub>1Hal</sub>-ir in the cells (arrows). B1, High power micrograph of boxed 1 area in B showing NS1 stained with immunoperoxidase (upper), and GAFS (lower), respectively. C, Cross-section of lower pleuropedal horn showing 5-HTR-ir in cells located at the peripheral region. C1, High power of boxed area 1 in C showing both NS1 and NS2 contain 5-HT<sub>1Hal</sub>-ir in the cytoplasm. Scale bars: 100 μm (A, B, C); 10 μm (A1, A2, B1, C1)
- **FIG. 5.** Immunoperoxidase staining of 5-HT<sub>1Hal</sub>-ir in the gonads. **A,** Low power of ovary showing the distribution of 5-HT<sub>1Hal</sub>-ir in the outer capsule (arrows), trabeculae (arrow heads) and late stage oocytes (asterisks). **A1 and A2.** High power inset of boxes 1 and 2 in A, showing 5-HT<sub>1Hal</sub>-ir in the trabeculae (arrow heads) and the cytoplasm of stage 4 oocyte (Oc4), respectively. No immunostaining of 5-HT<sub>1Hal</sub> occurs in previttellogenic oocytes (Oc2, Oc3). **B,** High power of Oc5 showing immunostaining of 5-HT<sub>1Hal</sub> in the cytoplasm. **C.** Medium power of testis showing the distribution of 5-HT<sub>1Hal</sub> in the outer

capsule (arrows) and the trabeculae (arrow heads). C1, high power from box 1 in C showing 5-HT<sub>1Hal</sub>-ir in trabeculae (arrow heads). Scale bars: 50 μm (A, C); 10 μm (A1, A2, B, C1)

- FIG. 6. Immunofluorescent staining of cerebral (**A and B**) and pleuropedal ganglia (**C and D**) illustrating the distribution of 5-HT $_{1Hal}$  immunoreactivity (red) and 5-HT immunoreactivity (green), and nuclear staining (blue). **A and C**, Medium power micrographs of cerebral (**A**) and pleuropedal ganglia (**C**) showing 5-HT neurons (S) and neurosecretory cells (NSs) containing 5-HT $_{1Hal}$  (R) localized in the cortex. Abundant 5-HT positive fibers are present in the medulla of both ganglia. **B and D**, High power micrograph of cerebral and pleuropedal ganglia demonstrating the 5-HT fibers innervating the NSs (red) (**B**, inset; **D**, inset) respectively. Some fibers of NSs are observed (**B**, **D** arrows). Scale bars: 40 µm (**A**); 10 µm (**B**, **B** inset, **D**); 20 µm (**C**, **D** inset)
- **FIG. 7.** Contractility of male and female gonad rings following 5-HT stimulation. **A,** Representative trace of the effect of 5-HT ( $10^{-6}$  M) on male gonad muscle. Time of application of 5-HT is shown by the arrow. Dose-response for the effect of 5-HT on change in rate of gonad contraction (n = 6, mean  $\pm$  S.D.). Asterisks indicate significant different compared to the control (p<0.05). **B,** Representative trace of the effect of 5-HT ( $10^{-6}$  M) on female gonad muscle.

1	Title: Ultrastructure, Compositions and Possible Roles of the Egg Coats in <i>Haliotis</i>
2	asinina
3	
4	Authors: Worawit Suphamungmee <sup>a</sup> , Wattana Weerachatyanukul <sup>a</sup> , Tanes
5	Poomtong <sup>b</sup> , Rapeepun Vanichviriyakit <sup>a</sup> and Prasert Sobhon <sup>a</sup> *
6	
7	Affiliations:
8	<sup>a</sup> Department of Anatomy, Faculty of Science, Mahidol University, Rama VI Road,
9	Bangkok 10400, Thailand
10	<sup>b</sup> The Coastal Aquaculture Research and Development Center, Department of Fisheries,
11	Klong-wan, Prachuabkirikhun 77000, Thailand
12	
13	*Address for manuscipt correspondence:
14	Professor Prasert Sobhon
15	Department of Anatomy, Faculty of Science,
16	Mahidol University, Rama VI Road,
17	Bangkok 10400, Thailand
18	Email: scpso@mahidol.ac.th
19	Tel. (+66) 2-201-5406
20	Fax. (+66) 2-354-7168
21	
22	Short title: Study of abalone egg coats

23 SUMMARY

Spawned egg of a tropical abalone <i>H. asinina</i> has two protective barriers, i.e., the
egg jelly coat (EJ) and the vitelline envelope (VE). At electron microscopic level, EJ is
shown to be composed of a network of large fibers (40-50 nm thick) cross-linked by
smaller fibers (15-20 nm thick) while VE is a thin tough sheet containing pores that
might be channels for sperm contact and entry. Electrophoretically, EJ contains two
major glycoproteins at 107 and 178 kDa, while VE contains a broad spectrum of protein
bands ranging from 15-200 kDa which also includes the corresponding EJ protein bands.
Glycoproteins of EJ and VE exhibit strong cross reactivities and they appear around late
oocytes (Oc4, Oc5). Glucose is the major sugar composition of both EJ and VE
glycoproteins, while a minor proportion of arabinose, fructose, galactose and fucose is
detected in both EJ and VE. Our findings suggest that sperm acrosome reaction could be
induced by isolated VE glycoproteins, whereas acceleration of the sperm motility could
be stimulated by EJ glycoproteins.

Keywords: Haliotis asinina, egg jelly, vitelline envelope, acrosome reaction, motility

#### INTRODUCTION

46

47

48

49

50

51

52

53

54

55

56

57

58

59

60

61

62

63

64

65

66

67

68

Molecules on sperm and egg surfaces that mediate gamete recognition and fertilization in broadcast-spawning marine invertebrates have been extensively studied, especially in sea urchins (Darszon et al., 2001; Hirohashi and Vacquier, 2003; Moy et al., 1996; SeGall and Lennarz, 1979; Vilela-Silva et al., 2002), and in two abalone species, Haliotis rufescens and Haliotis corrugata. It was demonstrated in the latter that the sperm acrosomal lysin binds to the vitelline envelop (VE) receptor and creates a hole through which sperm could pass and fuse with the egg cell membrane, and this is non-enzymatic species-specific mechanism (Kresge et al., 2001; Lewis et al., 1982; Vacquier et al., 1999). Mechanistically, sperm lysin binds to a 1,000-kDa glycoprotein molecule, named vitelline envelope receptor for lysin (VERL) that is a major constituent of the egg VE. This receptor molecule is composed of at least 50% carbohydrate (Swanson and Vacquier, 1997), containing predominantly glucose and mannose residues. Lysin dimers make the tight, species-specific binding to VERL. Upon binding to lysin, the fibrous VERL molecules lose cohesion and are splayed apart, creating hole for sperm passage (Vacquier et al., 1999). However, it was not demonstrated that this VE molecules could induce acrosome reaction (AR). Structurally, the eggs of red abalone, Haliotis rufescens, and Japanese abalone, Haliotis discus, are covered by a coat of fibrous jelly layer (EJ) (Mozingo et al., 1995; Shiroya and Sakai, 1995). The role of EJ has not yet been fully demonstrated, whilst in sea urchins, EJ is thought to be involved in sperm acrosome reaction (AR) induction. Sperm AR is believed to be induced on the sea urchins' egg surface by sulfated fucose polymer (FSP) in the jelly layer (SeGall and Lennarz, 1979). Similarly, AR-inducing

substance (ARIS) and its cofactor molecule (CoARIS) are reported to reside in starfish egg's jelly coat (Gunaratne et al., 2003). In abalone, the agents for AR induction have not exactly been identified.

In this study, we have investigated the ultrastructure of egg surface coatings, namely, the jelly coat (EJ) and vitelline envelope (VE) of a tropical abalone *Haliotis asinina*, using electron microscopies. The glycoprotein compositions of the egg coatings were analyzed for their proteins and carbohydrate compositions. And lastly the roles of EJ and VE in sperm AR induction and enhancing motility were demonstrated.

#### **MATERIALS AND METHODS**

## Ultrastructure of the egg coats

Eggs spawned into seawater were settled down for 5 min and pipetted into fixative solution containing 2.5% glutaraldehyde in 0.1 M cacodylate buffer, pH 7.8 at 4°C, and left for overnight. After washing with 50 mM cacodylate buffer, pH 7.8, the samples were postfixed in 1% osmium tetroxide in the same buffer, at 4°C, for 1 hr. Subsequently, the fixed eggs were washed twice with the same buffer, dehydrated in increasing concentrations of ethanol (from 50% to 100%), and embedded in Araldite 502 resin (Electron Microscopy Sciences, Fort Washington, PA, USA). Semithin and thin sections were cut with ultramicrotome. Semithin sections were stained with 1% methylene blue, and then observed under a light microscope (LM) (Nikon Eclipse E600). Thin sections were placed on 300-mesh copper grids, stained sequentially with uranyl acetate and lead citrate, and then observed under a transmission electron microscope (TEM) (Hitachi H-300), operating at 75 kV. In order to observe the surface features of

the egg's coats, spawned eggs were similarly prepared and fixed as described. Samples were dehydrated in a critical point-drying apparatus (Hitachi HCP-2), sputter-coated with palladium. Finally, they were observed under a scanning electron microscope (SEM) (Hitachi S-2500) operating at 20 kV.

## Molecular composition of the egg coats

About 1,000 spawned eggs were washed and settled in 3 ml filtered seawater. The jelly coat was extracted by dropping 1 N HCl to the egg suspension to lower the pH to 5.0 (Lewis et al., 1982). After thorough mixing, the suspension was incubated for 30 min at 4°C by continuous shaking. Then, drops of 1 M Tris-HCl (pH 8.0) were added to readjust the final pH of the egg suspension to 7.0. Seawater above the settled eggs was pipetted into a tube, leaving the dejellied eggs which were then kept at 4°C for further studies. Egg jelly in seawater was separated from cellular debris by centrifugation at 10,000 ×g, 4°C, for 30 min. Supernatant containing the egg jelly (EJ) proteins was collected and dialyzed (with molecular weight cut off at 10 kDa) against 10 mM Tris-HCl, pH 7.4, containing 150 mM NaCl (TBS) at 4°C for overnight. Later, EJ proteins were concentrated, using microCON (Millipore Corperation, Billerica, MA, USA) with a 10-kDa cut off and kept at 4°C for further experiment.

To isolate proteins from the egg vitelline envelope (VE), the dejellied eggs were washed several times in 3 ml filtered seawater, and then 5 volumes of salt medium (454 mM NaCl, 9.7 mM KCl, 24.9 mM MgCl<sub>2</sub>, 27.1 mM MgSO<sub>4</sub>, 4.4 mM NaHCO<sub>3</sub>, 10 mM Tris base, and 10 mM EGTA, pH 7.0) was added to 1 volume of the dejellied eggs in seawater. This suspension was homogenized by 10 strokes at 4°C and filtered through 3 layers of gauze. The homogenate was spun at  $190 \times g$ , 4°C, for 5 minutes. Then, the pellet

was washed twice by resuspension in the salt medium and subjected to centrifugation (50 xg, 4°C, 5 min). The solution appeared as 2 layers: the lower layer containing pigment granules, and the fainter upper layer containing VE. The upper layer was removed and then transferred to a new tube. After the third wash with the salt medium and centrifugation, VE pellet appeared colorless and free from cytoplasmic contaminants, as observed by light microscopy. To further purify VE, the isolate was overlaid on Percoll gradient (40%-80%) (Sigma-Aldrich Chemical Co., Saint Louis, MO, USA) and subjected to 1,000 xg centrifugation, for 20 min. The intact VE appeared at the interface of 40% and 60% Percoll, and was separated from the debris of nucleus and cytoplasmic granules at the bottom of the tube. Solution containing only intact VE was collected by a Pasture pipette and washed with the salt medium until pure envelopes were obtained. The sample was stored in the salt medium at 4°C until use. To solubilize the vitelline envelope, acetic acid was added to the purified VE for 2 min to adjust pH to 2.8. The reaction was stopped by a dropwise addition of 1 M Tris-HCl, pH 8.0 into the solution for the readjustment of pH to 7.8. Then, the solution was centrifuged at 5,000  $\times g$ , at 4°C, for 3 min, the supernatant containing soluble VE was dialyzed against TBS. VE proteins were concentrated using microCON with 10 kDa cut off, and kept for protein analysis and for inducing the sperm acrosome reaction. The protein quantification was done by Lowry's method using bovine serum albumin (BSA) as the standard (Lowry et al., 1951).

# Analysis of protein and glycoprotein components

115

116

117

118

119

120

121

122

123

124

125

126

127

128

129

130

131

132

133

134

135

136

137

SDS-PAGE was carried out using a stacking gel of 5% acrylamide and separating gel of 10%. Proteins ( $\sim$ 10  $\mu$ g) from both EJ and VE were denatured in sample buffer containing 0.125 mM Tris base, pH 6.8, 4% SDS, 10%  $\beta$ -mercaptoethanol, 20% glycerol,

0.2% bromophenol blue. The broad range molecular weight standard was used as the molecular weight markers (Biorad Laboratories, Ltd., Hercules, CA, USA). Gels were run at constant current (40 mA) for 50 min, and visualized by staining with 0.125% Coomassie brilliant blue R-250. For identification of glycoproteins, the gels were visualized by staining with Periodic acid-Schiff (PAS). A parallel histological experiment was performed by staining semithin sections of ovaries and spawned eggs with PAS to demonstrate whether they were invested with carbohydrate-containing coats.

### Analysis of sugar moieties by HPLC

Isolated EJ and VE proteins were analyzed for the sugar compositions by HPLC. The HPLC system was set at room temperature on a Prevail Carbohydrate Column (15  $\times$  0.46 cm in size) (Alltech Associates, Inc., Deerfield, IL, USA). EJ and VE proteins were prepared at 1 mg/ml in seawater, and were carefully pushed through 0.22- $\mu$ m nylon filter to exclude the particulate contaminants. The samples were chromatographed using a mixture of acetronitrile:deionized distilled water in the ratio of 80:20 as a mobile phase. The refractive index (RI) detector was set at a flow rate of 1 ml/min, for 2.5-30 min. A solution containing a mixture of fucose, fructose, galactose, glucose, sucrose, mannose, arabinose and maltose (50  $\mu$ g for each sugar) was run as the standards. Chromatograms indicated various kinds of sugar and their amount present in the injected samples.

### Production of antibodies against EJ and VE proteins

Polyclonal antibodies against EJ and VE proteins were produced by immunizing isolated EJ or VE proteins into six-week old female ICR mice. Each animal was first subcutaneously injected with the EJ or VE proteins (~300 µg) that were emulsified with an equal volume of Freund's complete adjuvant. Two boosting injections, each

containing the same amount of proteins with Freund's incomplete adjuvant, were given twice at two-week intervals. Immune sera were collected by the tail bleeding and the presence of antibodies was tested by Western blotting, using preimmune sera as the control. The animals, whose antisera were found to be reacting exclusively with the targeted antigens, were sacrificed at the seventh day after the second boosting, and blood was collected from the heart. After centrifugation, the antisera were kept at -20°C until use.

## Cross-reactivities and immunolocalization of EJ and VE proteins

The separated EJ or VE proteins were transferred onto nitrocellulose membrane in an electrophoretic transfer chamber (LKB Bromma, Hoefer Scientific Instruments, San Francisco, CA, USA) using the constant voltage set at 100 V, for 1 hr, in a transfer buffer (0.028 mM Tris base, 0.039 mM glycine, 20% methanol). Following the blocking step with 5% skim milk in TBST (Tris buffer saline containing 0.05% Tween 20), the membrane strips were incubated with mouse antiserum to EJ or VE proteins (at the dilution of 1:100), for 1 hr at room temperature. For the negative control, the membranes were incubated with preimmune serum instead of primary antibody. Then, the membranes were incubated in rabbit anti-mouse IgG conjugated to horseradish peroxidase (Zymed Laboratories, Inc., San Francisco, CA, USA) in TBST at 1:3,000 dilution, for 30 min at room temperature. The specific reaction was visualized by using ECL substrate kit (Amersham Pharmacia, Buckinghamshire, UK).

To investigate the expression of EJ and VE proteins in oocytes and spawned eggs, pieces of ovarian tissue and freshly spawned eggs were immersed in a fixative solution of 0.5% glutaraldehyde, 4% paraformaldehyde in 0.1 M phosphate buffer, pH 7.8 at 4°C, for

2 hr. After washing, the samples were sequentially dehydrated in increasing concentrations of ethanol (from 50% to 100%), and embedded in LR White resin (London Resin Co., Thule, UK). Semithin sections were cut and mounted on the gelatin-coated glass slides. The sections were then incubated in 0.15 M glycine in order to block free aldehyde groups, and then in 4% BSA for blocking non-specific bindings. The sections were incubated in mouse anti-EJ or anti-VE antisera (at dilution 1:80) or preimmune sera (control) in TBST, for 1 hr at 37°C, and then washed by TBST. The sections were further exposed to biotinylated rabbit anti-mouse IgG (Zymed Laboratories, Inc.) in TBST at 1:100 dilution, and then with FITC-conjugated streptavidin (Sigma-Aldrich Chemical Co.) in TBST at 1:100 dilution, 37°C, for 30 min. After washing, samples were mounted with cover glasses, using Vectashield mounting medium (Vector Laboratories, Inc., Burlingame, CA, USA), observed and photographed under a Nikon Eclipse 600 fluorescence microscope equipped with a Nikon DXM 2000 CCD camera.

#### Induction of sperm acrosome reaction and assessment of sperm motility

EJ and VE proteins were prepared at various concentrations, i.e.,  $10 \mu g/ml$ ,  $100 \mu g/ml$ ,  $500 \mu g/ml$  and 1 mg/ml of proteins in filtered seawater. Sperm were incubated in each concentration of EJ and VE proteins, and AR induction was stopped at 2 min by fixing with 1% paraformaldehyde, and the occurrence of AR was observed by a light microscope. Acrosome intact (AI) sperm possess a round-shaped head with smooth anterior while the acrosome reacted (AR) sperm contain a long-extended filament projection at the anterior region. Sperm incubated in filtered seawater were used as the control. Approximately 200 sperm were counted for each data point from four separated experiments.

Sperm motility was assessed by observing under an inverted light microscope. A droplet of 50  $\mu$ l sperm suspension taken from non-treated, EJ or VE treated sperm were plated onto a slide and a 40× objective was used for analyzing the sperm that were motile in the total sperm population.

212 RESULTS

## Ultrastructure of spawned eggs' coatings

When observed at LM level, a normal live egg exhibited round shape with green color due to the presence of its yolk (Fig. 1A, B). There were two covering layers over the egg, i.e., jelly layer (EJ) and vitelline envelope (VE) (Fig. 1B). The space between VE and the egg cell membrane, so called perivitelline space, was filled with fluid. The size of a live egg was approximately 160-200 µm in diameter. The thickness of EJ was about 100 µm, whereas the thickness of VE was about 1 µm. EJ was easily torn off the egg when the eggs were left in seawater for a prolonged period (>1 hr). It could also be separated by mechanical force, such as continuous shaking in seawater for 20-40 min. In this study, EJ was isolated by mild acid (~0.1 N HCl) at pH 5.0 in the seawater, which resulted in the eggs being devoided off EJ (Fig. 1C). After homogenization and several washes, VE could be detached from the eggs (Fig. 1D).

At TEM level, EJ appeared as a network of fibrous structures, while VE was a thin, condensed sheet, comprising two dense lines separated by a light zone about 0.25 µm in width (Fig. 2A-C). The subjacent egg cytoplasm contained numerous mitochondria, yolk granules and lipid droplets (Fig. 2E, F). At the egg cell membrane, there were microvilli projecting outwards into the perivitelline space (Fig. 2B, D). Higher

magnification demonstrated a network of fine fibers linking between neighboring microvilli (Fig. 2D). The spawned egg's EJ (Fig. 2C) exhibited two-sized fibers tightly attached to VE as well as loosely distributed around the egg (Fig. 2B, C). Large fibers were approximate 40-50 nm in thickness, and they were interconnected by smaller fibers, each approximately 15-20 nm in thickness.

When observed by SEM, the spawned egg's EJ exhibited spongy appearance (Fig. 3A, B). After the removal of EJ, VE exhibited smooth surface with small pores distributed throughout its entire surface (Fig. 3C, D). Each pore was measured about 190-200 nm.

## Molecular compositions of EJ and VE

When separated by 10% SDS-PAGE, EJ consisted of the only two major bands of proteins at molecular mass of 107 and 178 kDa, while there were also some proteins larger than 200 kDa left in the stacking gel (Fig. 4A). VE consisted of several proteins ranging from 15 kDa to 200 kDa with the major bands appeared at 29-32, 45, 48 and 82 kDa, while the 107 kDa and 178 kDa and some larger proteins were also found in lesser amount than in EJ. The separated protein bands from EJ and VE were also stained with PAS that identified the carbohydrate-conjugated proteins. In EJ, the intensely PAS-positive bands were at 107 kDa, 178 kDa, and some other bands larger than 200 kDa remaining in the stacking gel. VE showed weak PAS stained bands at the lower molecular weights, whereas larger proteins at 107 kDa, 178 kDa, and over 200 kDa were also strongly PAS-positive (Fig. 4A).

In the ovarian oocytes (Fig. 4B), a thick PAS-positive layer of jelly coat appeared in premature stage 4 oocyte (Oc<sub>4</sub>) and mature stage 5 oocyte (Oc<sub>5</sub>), while the surfaces of

early stage oocytes (Oc<sub>1</sub> to Oc<sub>3</sub>) were not stained (oocyte classification based on Apisawatakan et al., 2001). Very weak PAS staining was also detected in the ovarian trabeculae and inside oocyte cytoplasm. In spawned eggs (Fig. 4C), a weak PAS staining could also be observed at VE and throughout EJ. The histochemical stain and SDS-PAGE results suggested that both EJ and VE were composed of glycoproteins, which were laid down in the late stage oocytes (Oc<sub>4</sub> and Oc<sub>5</sub>).

The carbohydrate compositions of the EJ and VE proteins was quantitatively analyzed by HPLC (Fig. 5). The result revealed that EJ contained a large amount of glucose (~81% per total content), whereas fructose (~6%) and galactose (~1.5%) were barely present. In comparison, VE also contained the highest amount of glucose (~73%) and smaller amount of fucose (2.7%).

## Cross reactions and expression of EJ and VE components

Cross-reactivity of the antibodies raised against EJ and VE proteins was tested by Western blotting (Fig. 6). It was shown that anti-EJ strongly reacted with EJ proteins, specifically at 107 kDa, 178 kDa, and to a small extent with the bands over 200 kDa (remaining in the stacking gel). Anti-EJ showed a slight cross-reactivity with VE proteins at the 107 kDa protein band. In comparison, anti-VE reacted strongly with the 30 kDa VE protein and to a lesser extent with the 48 and 82 kDa proteins. A trace staining could also be observed at a 107 kDa band. When this antibody was applied to EJ protein isolate, some cross reactivity with the 30 and 48 kDa proteins were notable. These results indicated that some isolated proteins from EJ and VE may share common epitopes, though the degree of their cross reactivities varied. It may also be possible that some contamination from the EJ components may be left during VE extraction, dispite a

careful cleaning process was done to wash away EJ proteins. This could be because some EJ fibers were seen tightly adhered to VE under TEM.

Immunofluorescent staining of ovarian sections with anti-EJ showed that the fluorescence was firstly detected in the jelly layer of the mature oocytes at Oc<sub>4</sub>-Oc<sub>5</sub> stages, whereas no fluorescence was observed in immature oocytes at Oc<sub>1</sub>-Oc<sub>3</sub> (Fig. 7A, B). Similarly, anti-VE showed an intense fluorescence in Oc<sub>4</sub>-Oc<sub>5</sub> (Fig. 7C, D). This strong fluorescence was particularly prominent over the entire region of the two layers and seemed to occupy larger area than those detected by anti-EJ. For the spawned eggs, both anti-EJ and anti-VE showed strong fluorescence at the jelly coat and vitelline envelope as in mature ovarian oocytes (Fig.7E, F). In controls, there was no fluorescence signal detected either on VE or EJ. However, some autofluorescence (exhibited a yellow color) was observed in the oocyte cytoplasm in both ovarian sections and the spawned eggs (Fig. 7G, H).

#### Induction of sperm acrosome reaction and motility

Sperm acrosome reaction (AR) and its associated morphological changes were observed by SEM, which revealed that the acrosome of most sperm disappeared from the head after contact with VE region following the incubation of spawned eggs with sperm. These AR-sperm possessed filamentous structure projecting from the anterior region of the head (Fig 8A-C). In contrast, some sperm remaining on EJ had an intact acrosomal integrity showing still smooth anterior end (Fig. 8D).

To confirm the above SEM observations of intact and AR-sperm and study the role of EJ and VE proteins in inducing sperm AR, freshly spawned sperm were treated with proteins isolated from both layers at various concentrations in seawater. At  $10~\mu g/ml$ 

of EJ proteins (Fig. 9, black bars), most sperm still exhibited normal head bearing acrosomal vesicle with no anterior projection. The pattern of their swimming, as observed by LM, did not differ from the normal spawned sperm. Similar characteristics were observed when sperm were treated with EJ proteins at higher concentrations at 100 μg/ml (5.4%), 500 μg/ml (5.6%) and 1 mg/ml (4.5%). However, at 1 mg/ml EJ, the proportion of sperm showing motility was increased from ~60% to >90%, whereas other characteristics of sperm still remained normal. When sperm were treated with VE proteins at concentrations 10 μg/ml and 100 μg/ml (Fig. 9, hatched bars), most sperm still exhibited normal morphological features while the percentage of AR sperm detected at concentrations of 10 μg/ml (5.1%) and 100 μg/ml (5.4%) were comparable to those of the control group (4.7%). At higher concentrations of 500 μg/ml and 1 mg/ml VE, the number of AR sperm was significantly increased to 19.8% and 25.9%, respectively. All VE-treated AR sperm exhibited heads with anterior projections which were subacrosomal filaments, while other characteristics were still normal, and their motility was unaltered.

#### 314 DISCUSSION

#### Ultrastructure of the egg coats

We have recently described oogenesis in *H. asinina* and the formation of EJ in ovarian oocytes (Apisawetakan et al., 2001). EJ surrounding the mature ovarian oocytes at Oc<sub>4</sub> and Oc<sub>5</sub> stages appears to be a thick homogeneous structure. In contrast, EJ of the spawned egg shown in this study appeared as a fibrous meshwork of glycoprotein fibers. High magnification TEM micrographs of the spawned eggs could define the fibrous nature of EJ, which was clearly separated from VE. This EJ fibrous network was formed

by interconnection between the large fibers (40-50 nm) and smaller fibers (~20 nm). Similar filamentous network has been observed around the egg of sea urchin, *Strongylocentrotus purpuratus* (Chandler and Heuser, 1980; Chandler and Kazilek, 1986), red abalone (Mozingo et al., 1995) and Japanese abalone (Shiroya and Sakai, 1995). However, the sizes of both types of fibers are variable according to species. It has also been reported in *H. discus* that the jelly-freed eggs are found to be 90% fertilizable, suggesting that EJ has no direct role in the process of fertilization and gamete fusion (Shiroya and Sakai, 1995). In contrast to EJ, VE was not as clearly defined in the mature ovarian oocyte (Oc<sub>5</sub>) as in the spawned egg, where it appeared as a thin tough sheet. In addition, the surface of VE exhibited pores which could not be easily visualized in TEM micrographs of VE cross sections, partly due to the fact that they were small in size and widely separated. The function of these pores is, at present, not known, but they could be channels for sperm penetration.

#### The compositions of EJ and VE

We found that EJ could be easily isolated and dissolved in buffer, whereas VE was harder to be solubilized, supporting the compact nature of VE composition as a thin tough sheet. These VE proteins could be extracted by acetic acid, which yielded higher amount of proteins than other chemical treatments, such as mercaptoethanol or SDS. Electrophoretic analyzes showed that *H. asinina* EJ contained major glycoproteins with molecular weights at 107 and 178 kDa. VE also contained both proteins and other smaller glycoproteins at the range of 15-82 kDa. Staining with PAS in sections of mature ovary and spawned egg indicated that these glycoproteins started to be deposited around the late vitellogenic oocytes (Oc<sub>4</sub>), in consistent with the previous morphological study showing

that EJ coating started to be visible in Oc<sub>4</sub> (Apisawetakan et al., 2001). The detailed carbohydrate compositions analyzed by HPLC revealed a high amount of glucose in EJ and VE proteins, whereas other sugars were present in much smaller quantities. Highly variable corbohydrate compositions of the egg outer coats have been reported in a broad spectrum of species from invertebrates to vertebrates which are known to serve the functions in gamete recognition and/or AR induction. In the well studied model of invertebrate, sea urchin, the egg's jelly layer is composed mainly of sulfated polysaccharides, i.e., fucose sulfate polymer (FSP) with the various bands of glycoproteins at molecular mass ranging between 120 kDa to 260 kDa and over 10<sup>4</sup> kDa depending on species (Shimizu et al., 1990). It is well established that these egg FSP glycoproteins initiate AR in the species-specific manner in sea urchin (Hirohashi and Vacquier, 2002; SeGall and Lennarz, 1979; Vilela-Silva et al., 2002). In oocytes of amphibians, Bufo arenarum, mannose is the most abundant carbohydrate residue which is involved in recognition of sperm (Omata and Katagiri, 1996), whereas sulfated glycoproteins riched in hexosamines, fucose, and galactose are found in Xenopus laevis EJ and act in a similar manner (Yurewicz et al., 1975). In comparison, mammalian eggs' coating (zona pellucida) has large oligomers of carbohydrate-conjugated proteins, such as β-N-acetylglucosamine (GlcNAc), which is involved in sperm-egg binding (Miller et al., 1993; Wassarman, 1999; Wassarman, 2005). Whether the carbohydrate moieties of EJ and VE of H. asinina involved in sperm binding and AR modulation are still unknown and remain to be investigated.

366

345

346

347

348

349

350

351

352

353

354

355

356

357

358

359

360

361

362

363

364

365

#### Induction of sperm acrosome reaction (AR) and motility

366

367

368

369

370

371

372

373

374

375

376

377

378

379

380

381

382

383

384

385

386

387

AR in abalone sperm involves the exocytosis of the acrosomal vesicle and the polymerization of subacrosomal materials, composed mainly of actin, to form the anterior spike called acrosomal process (Neill and Vacquier, 2004). Abalone sperm can undergo AR after exposing to high concentration of calcium ions and then lysin, which could bind to VE (Lewis et al., 1980). Few studies have shown that egg VE might be responsible for the induction of sperm AR in abalone (Sakai et al., 1982). By contrast, in sea urchin, EJ glycoconjugates rich in fucose sulfate (FSP) has reported to be the AR inducer (Hirohashi and Vacquier, 2002; SeGall and Lennarz, 1979; Vilela-Silva et al., 2002). Interestingly, constituents of FSP that regulates AR in sea urchins were pure polysaccharides, with no associated protein (Mengerink and Vacquier, 2001; Vacquier and Moy, 1997). In fact, the significance of carbohydrate moieties on regulating fertilization has not only been shown in invertebrates but also in mammals including human (Shalgi and Raz, 1997; Wassarman, 2005; Zara and Naz, 1998). Surprisingly, although we showed herein that EJ of H. asinina were enriched in carbohydrate compositions (Fig. 4), they were not involved in initiating sperm AR, but rather in regulating sperm motility. In sea urchins, motility was activated when sperm were spawned into seawater. It is believed that some factors associated with the EJ may function as "chemoattractants" to stimulate sperm motility (Neill and Vacquier, 2004). In red abalone H. rufescens, L-tryptophan has been shown to be released from the eggs into seawater, which serves dual functions in triggering both sperm activation and chemotaxis (Riffell et al., 2002; Riffell et al., 2004). Experimental evidence in the present study also showed acceleration of sperm motility in

388	the presence of high concentration of isolated EJ proteins, though the exact protein	
389	inducer(s) have yet to be identified.	

391	ACKNOWLEDGEMENTS
392	This research was supported by the Thailand Research Funds (Senior Research
393	Scholar Fellowship to PS, Research scholar to WW and RGJ-Ph.D. scholarship to WS)
394	and Mahidol University.
395	
396	

396	REFERENCES
397	Apisawetakan, S., Linthong V., Wanichanon, C., Panasophonkul, S., Meepool, A.
398	Kruatrachue, M., Upatham, E. S., Pumthong, T. and Sobhon, P. (2001).
399	Ultrastructure of female germ cells in Haliotis asinina Linnaeus. Inv Reprod Dev 39
400	67-79.
401	Chandler, D. E. and Heuser, J. (1980). The vitelline layer of the sea urchin egg and its
402	modification during fertilization. A freeze-fracture study using quick-freezing and
403	deep-etching. J Cell Biol 84, 618-32.
404	Chandler, D. E. and Kazilek, C. J. (1986). Extracellular coats on the surface of
405	Strongylocentrotus purpuratus eggs: stereo electron microscopy of quick-frozen and
406	deep-etched specimens. Cell Tissue Res 246, 153-61.
407	Darszon, A., Beltran, C., Felix, R., Nishigaki, T. and Trevino, C. L. (2001). Ion
408	transport in sperm signaling. Dev Biol 240, 1-14.
409	Gunaratne, H. M., Yamagaki, T., Matsumoto, M. and Hoshi, M. (2003). Biochemical
410	characterization of inner sugar chains of acrosome reaction-inducing substance in
411	jelly coat of starfish eggs. Glycobiology 13, 567-80.
412	Hirohashi, N. and Vacquier, V. D. (2002). High molecular mass egg fucose sulfate
413	polymer is required for opening both Ca2+ channels involved in triggering the sea
414	urchin sperm acrosome reaction. J Biol Chem 277, 1182-9.
415	Hirohashi, N. and Vacquier, V. D. (2003). Store-operated calcium channels trigger
416	exocytosis of the sea urchin sperm acrosomal vesicle. Biochem Biophys Res
417	Commun <b>304</b> , 285-92.

- 418 Kresge, N., Vacquier, V. D. and Stout, C. D. (2001). Abalone lysin: the dissolving and
- evolving sperm protein. *Bioessays* **23**, 95-103.
- 420 Lewis, C. A., Leighton, D. L. and Vacquier, V. D. (1980). Morphology of abalone
- spermatozoa before and after the acrosome reaction. J Ultrastruct Res 72, 39-46.
- 422 Lewis, C. A., Talbot, C. F. and Vacquier, V. D. (1982). A protein from abalone sperm
- dissolves the egg vitelline layer by a nonenzymatic mechanism. Dev Biol 92, 227-
- 424 39.
- Lowry, O. H., Rosebrough, N. J., Farr, A. L. and Randall, R. J. (1951). Protein
- measurement with the Folin phenol reagent. *J Biol Chem* **193**, 265-75.
- 427 Mengerink, K. J. and Vacquier, V. D. (2001). Glycobiology of sperm-egg interactions
- in deuterostomes. *Glycobiology* **11**, 37R-43R.
- 429 Miller, D. J., Gong, X. and Shur, B. D. (1993). Sperm require beta-N-
- acetylglucosaminidase to penetrate through the egg zona pellucida. Development
- **118**, 1279-89.
- 432 Mov, G. W., Mendoza, L. M., Schulz, J. R., Swanson, W. J., Glabe, C. G. and
- Vacquier, V. D. (1996). The sea urchin sperm receptor for egg jelly is a modular
- protein with extensive homology to the human polycystic kidney disease protein,
- 435 PKD1. *J Cell Biol* **133**, 809-17.
- 436 Mozingo, N. M., Vacquier, V. D. and Chandler, D. E. (1995). Structural features of the
- 437 abalone egg extracellular matrix and its role in gamete interaction during
- fertilization. *Mol Reprod Dev* **41**, 493-502.
- Neill, A. T. and Vacquier, V. D. (2004). Ligands and receptors mediating signal
- transduction in sea urchin spermatozoa. *Reproduction* **127**, 141-9.

441 Omata, S. and Katagiri, C. (1996). Involvement of carbohydrate moieties of the toad 442 egg vitelline coat in binding with fertilizing sperm. Dev Growth Differ 38, 663-672. 443 Riffell, J. A., Krug, P. J. and Zimmer, R. K. (2002). Fertilization in the sea: the 444 chemical identity of an abalone sperm attractant. J Exp Biol 205, 1439-50. 445 Riffell, J. A., Krug, P. J. and Zimmer, R. K. (2004). The ecological and evolutionary consequences of sperm chemoattraction. Proc Natl Acad Sci USA 101, 4501-6. 446 Sakai, Y. T., Shiroya, Y. and Haino-Fugushima, K. (1982). Fine structural changes in 447 448 the acrosome reaction of the Janpanese abalone, Hailotis discus. Dev Growth Differ 449 **24**, 531-542. SeGall, G. K. and Lennarz, W. J. (1979). Chemical characterization of the component 450 451 of the jelly coat from sea urchin eggs responsible for induction of the acrosome 452 reaction. Dev Biol 71, 33-48. 453 Shalgi, R. and Raz, T. (1997). The role of carbohydrate residues in mammalian 454 fertilization. Histol Histopathol 12, 813-22. 455 Shimizu, T., Kinoh, H., Yamaguchi, M. and Suzuki, N. (1990). Purification and characterization of the egg jelly macromolecules, sialoglycoprotein and fucose 456 457 sulfate glycoconjugate, of the sea urchin Hemicentrotus pulcherrimus. Dev Growth 458 Differ 32, 473-487. 459 Shiroya, T. and Sakai, Y. T. (1995). Filamentous structure of the external surface of abalone eggs revealed by quick-freeze deep-etch technique. Dev Growth Differ 37, 460

461

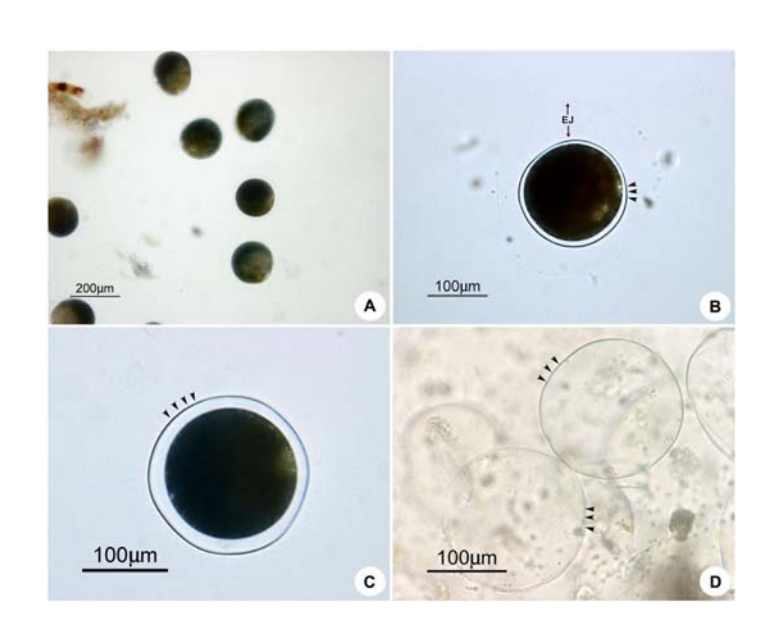
85-91.

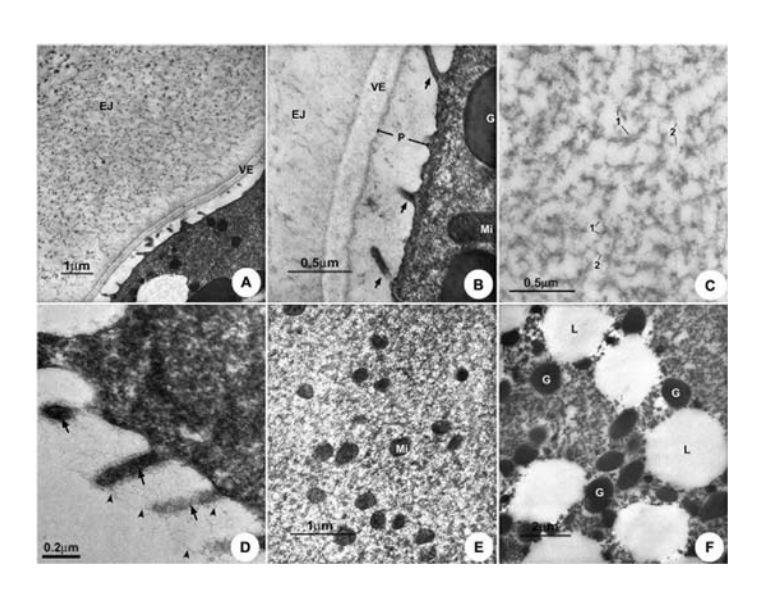
462	Swanson, W. J. and Vacquier, V. D. (1997). The abalone egg vitelline envelope
463	receptor for sperm lysin is a giant multivalent molecule. Proc Natl Acad Sci USA
464	<b>94</b> , 6724-9.
465	Vacquier, V. D. and Moy, G. W. (1997). The fucose sulfate polymer of egg jelly binds
466	to sperm REJ and is the inducer of the sea urchin sperm acrosome reaction. Dev
467	Biol <b>192</b> , 125-35.
468	Vacquier, V. D., Swanson, W. J., Metz, E. C. and Stout, C. D. (1999). Acrosomal
469	proteins of abalone spermatozoa. Adv Dev Biochem 5, 49-81.
470	Vilela-Silva, A. C., Castro, M. O., Valente, A. P., Biermann, C. H. and Mourao, P. A
471	(2002). Sulfated fucans from the egg jellies of the closely related sea urchins
472	Strongylocentrotus droebachiensis and Strongylocentrotus pallidus ensure species-
473	specific fertilization. J Biol Chem 277, 379-87.
474	Wassarman, P. M. (1999). Mammalian fertilization: molecular aspects of gamete
475	adhesion, exocytosis, and fusion. Cell 96, 175-83.
476	Wassarman, P. M. (2005). Contribution of mouse egg zona pellucida glycoproteins to
477	gamete recognition during fertilization. J Cell Physiol 204, 388-91.
478	Yurewicz, E. C., Oliphant, G. and Hedrick, J. L. (1975). The macromolecular
479	composition of Xenopus laevis egg jelly coat. Biochemistry 14, 3101-3107.
480	Zara, J. and Naz, R. K. (1998). The role of carbohydrates in mammalian sperm-egg
481	interactions: how important are carbohydrate epitopes? Front Biosci 3, D1028-38.
482	
483	
484	
485	

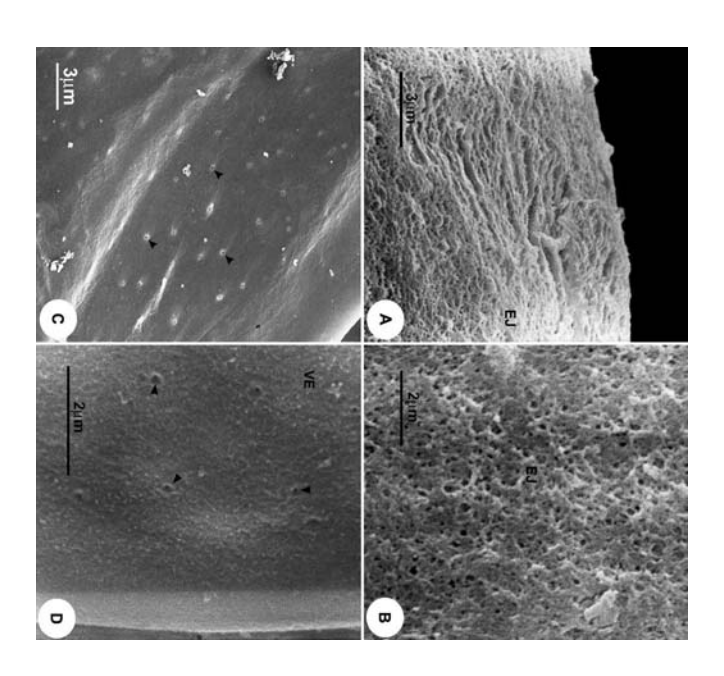
485	FIGURE LEGENDS
486	Figure 1 (A, B) Light micrographs of live H. asinina spawned egg showing two coating
487	layers, jelly coat (EJ) and vitelline envelope (arrow head). After acid treatment, jelly coat
488	is detached from the egg (C), and then its vitelline envelope is isolated using
489	homogenization (D).
490	
491	Figure 2 (A, B) Ultrastructure of the coatings of the spawned egg displaying a fibrous
492	network in the jelly coat (EJ) and thin dense double lines of vitelline envelope (VE). (C)
493	In EJ, large, 40-50 nm thick (1) and small, 15-20 nm thick (2) fibers are interconnected.
494	(D) At the egg cell membrane, microvilli (arrows) are present over the entire surface, and
495	they are linked by small fibers (arrow heads). (E, F) Egg's peripheral cytoplasm contains
496	abundant lipid droplets (L), yolk granules (G) and small mitochondria (Mi). P -
497	perivitelline space
498	
499	Figure 3 (A, B) The jelly coat (EJ) exhibits a network of thick and thin fibers that give
500	spongy appearance. (C, D) The vitelline envelope (VE) exhibits smooth surface with
501	numerous pores (arrow heads).
502	
503	Figure 4 (A) Electrophoretograms of egg jelly (EJ) and vitelline envelope (VE) proteins
504	separated on 10% SDS-PAGE, stained by Coomassie blue (CB) and Periodic acid-Schiff
505	(PAS). PAS-stained mature ovarian oocytes (Oc <sub>4</sub> , Oc <sub>5</sub> ) (B) and spawned egg (C) showing
506	strong-PAS positive jelly coat (EJ) and vitelline envelope (VE). Oc - developing oocyte
507	stage, Tr - connective tissue trabeculae

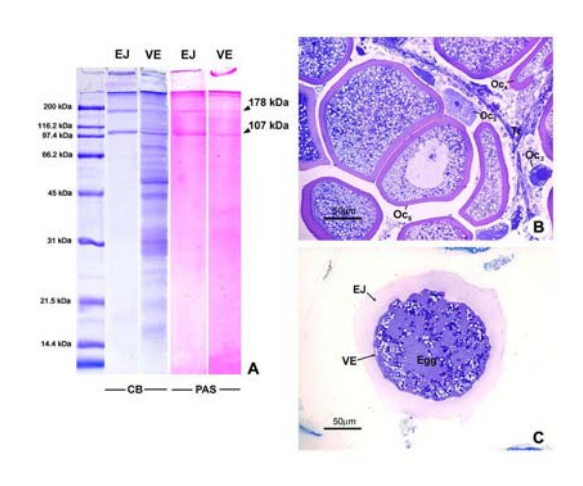
508	Figure 5 HPLC chromatograms exhibiting percentages of the constituent sugars in the
509	extracted EJ and VE glycoproteins. The numbers on arrows indicate types of sugar that
510	are used as standards for HPLC: 1) = fucose, 2) = fructose, 3) = mannose, 4) = glucose, 5)
511	= galactose, 6) = sucrose, 7) = maltose
512	
513	Figure 6 Western blottings of extracted EJ and VE proteins, probed with anti-EJ and
514	anti-VE, showing the cross-immunoreactivities among both groups of separated proteins.
515	
516	Figure 7 Indirect immunofluorescent staining of ovarian sections (A-D) and spawned
517	eggs (E, F) using mouse anti-EJ and anti-VE anti-sera, demonstrating strong
518	immunoreactivities in both jelly coat and vitelline envelope. Control slides were
519	incubated with mouse preimmune sera instead of primary antibodies (G, H). Cp - ovarian
520	capsule, Oc5 - stage 5 oocyte, EJ - jelly coat, VE - vitelline envelope
521	
522	Figure 8 (A-C) SEM micrographs of sperm undergoing acrosome reaction (AR) on VE
523	(arrows) after 2-min incubation with the spawned eggs, compared to acrosme intact (AI)
524	sperm on EJ (D). Extension of acrosomal filament (C) is clearly observed in AR sperm in
525	contact with VE surface, while the heads of AI sperm on EJ appear smooth (D).
526	
527	Figure 9 Histogram displaying percents of acrosome-reacted (AR) sperm after incubating
528	sperm in various concentrations of EJ (black bars) and VE (hatched bars) proteins in
529	seawater. Numbers of AR sperm with acrosomal filament (inset, arrowheads) are counted

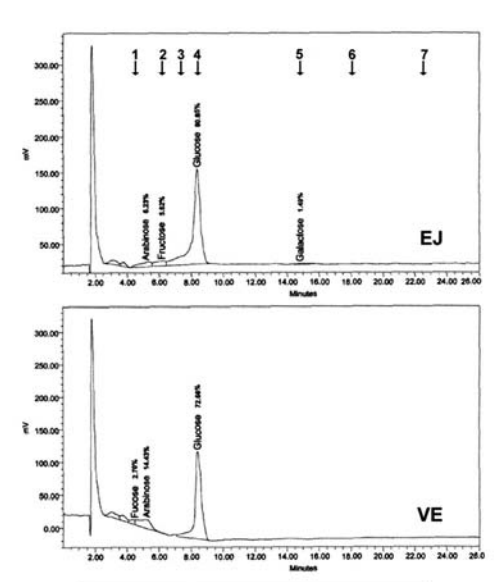
530	from at least 200 sperm. Control represents sperm incubated in filtered seawater. The
531	experiments are repeated four times, and bars indicate standard errors.
532	











	Percent sugar composit	
	EJ elute	VE elute
Glucose	80.85	72.66
Arabinose	6.23	14.43
Fructose	5.62	ND*
Galactose	1.49	ND*
Fucose	ND*	2.70

\*ND = non detectable

